ÉCOLE DE TECHNOLOGIE SUPÉRIEURE
UNIVERSITÉ DU QUÉBEC

DISSERTATION PRESENTED TO
ÉCOLE DE TECHNOLOGIE SUPÉRIEURE

IN PARTIAL FULFILLMENT OF THE REQUIREMENTS FOR
A MASTER'S DEGREE IN MECHANICAL ENGINEERING
M.Eng.

BY
César Augusto Corrêa ALBA

IMAGE ACQUISITION AND PROCESSING IN AN ATTEMPT TO AUTOMATE THE FLUORESCENT PENETRANT INSPECTION

MONTREAL, MAY 6 2011

BOARD OF EXAMINERS

THIS THESIS HAS BEEN EVALUATED

BY THE FOLLOWING BOARD OF EXAMINERS:

Mr. Martin Viens, Thesis Supervisor
Departement de génie mécanique à l'École de technologie supérieure

Mr. Jean-Luc Fihey, President of the Board of Examiners
Departement de génie mécanique à l'École de technologie supérieure

Mr. Xavier Maldague, External Examiner
Departement de génie électrique et de génie informatique à l'Université Laval

THIS THESIS WAS PRESENTED AND DEFENDED

BEFORE A BOARD OF EXAMINERS AND PUBLIC

ON JUNE 15, 2011

AT ÉCOLE DE TECHNOLOGIE SUPÉRIEURE

ACKNOWLEDGEMENTS

I would like to express my gratitude to many people who have provided assistance and inspiration during my master study. First of all, I am very grateful to my supervisor, Dr. Martin Viens. His contribution to my project has been essential for achieving my research goals. I would like to thank as well Dr. Xiao-Wei Tu. He has been always prompt to provide me immediate assistance. I would like to acknowledge all other members of the project CRIAQ MANU418. These people have been adding significant contribution to my research.

It is a pleasure to thank the members of my examining committee: Dr. Jean-Luc Fihey and Dr. Xavier Maldague, who have kindly agreed in reading, analyzing this dissertation.

Many thanks also to my friends in the LIVIA (Laboratoire d'imagerie, de vision et d'intelligence artificielle) who have helped me providing an initial guidance in my master studies. I am very grateful to Dominique Rivard, Eduardo Vellasques, Éric Thibodeau, George Eskander, Jean-François Connoly, Jonathan Bouchard, Idrissa Coulibaly, Luana Batista, Marcelo Kapp, Paulo Cavalin, Philippe LaMontagne, Vincent Doré, and Wael Khreich. Special thanks to Dr. Robert Sabourin and Dr. Éric Granger. Their ideals have had a notorious influence on this work.

I would like to acknowledge my friends in the LIPPS (Laboratoire d'ingénierie, des produits, procédés et systèmes). Abbasali Saboktakin and Louis-Alexandre Généreaux became great friends during my graduate study.

I would like to express my thankfulness to all members of AIESEC located worldwide (especially in Canada and in Brazil) who have helped to adapt to this country. People from this organization have become very good friends since my arrival in Montreal.

I would like to give thanks to César Gemelli, Danielle Van der Kay, Diego Mattos, Douglas Moreira, Eduardo França, Francesca Capitanio, Francisco Fincheira, Gustavo Spanholi, Jean-Maxime Lemerise, Jennifer Vachon, Juliana Davi, Lisiane Saraiva, Louis Phillip Choquette, Luís Vitório Cargnini, Marie-Catherine Dremers, Marie-Hélène Le Rossignol, Maryse Rabeau,

Rabih Majzoub, Shulabh Gupta, Tiago Monteiro, Raïmé Drouin, Teju Alliu, Thiago Linares and many others. All these friends have been providing support to me.

I am so grateful to Mario Corbin, Michel Drouin, Patrick Sheridan, Radu Ramenica and Sylvain Brisebois. I definitely would not have completed this project without their contribution. They have provided all necessary equipment for conducting my research, giving advices as needed.

I manifest my gratefullness to M.Sc. Christian Belleau, Dr. Éric David, Dr. Véronique François, Chantal Gamache and Nicole Brasseur. They have never hesitated to give assistance.

I am pleased to acknowledge Dr. Berenice Dedavid and Dr. João Carlos Beck. They have been encouraging me to pursue the graduate studies. Since my bachelor degree in Engineering, they have had a valuable influence on my career.

I would like to demonstrate my infinite gratitude to my parents, Plínio and Raquel. They have been always encouraging and inspiring me with their hardwork and love. Thanks to my sisters, grandparents, godmother, godfather, niece and other relatives who have been loving me. I dedicate this work to all of them.

Furthermore, I am glad to thank the École de Technologie Supérieure for supporting me financially. This assistance has been important for the conclusion of this work.

Last, I express all my thankfulness to God for giving me endless motivation, providing me energy to work hard during these three years. You surely have been generous, giving me plenty of opportunities.

ACQUISITION ET TRAITEMENT NUMÉRIQUE DES IMAGES POUR L'AUTOMATISATION DU RESSUAGE

César Augusto Corrêa ALBA

RÉSUMÉ

Une défaillance mécanique dans les pièces d'aéronefs est susceptible de se produire s'il y a des discontinuités de surface qui comprennent des régions de concentration de contraintes. Le ressuage (*FPI*) est une méthode de contrôle non destructif (*NDE*), sensible qui permet de vérifier la présence des indications dans la surface des matières premières ou des pièces soumises à des efforts de service.

En général, une fois que l'inspection FPI est en cours, l'inspecteur effectue l'évaluation d'une surface traitée en fonction de ses connaissances et de son expérience en contrôle non destructif, la détection des défauts étant une décision qualitative selon jugement de l'inspecteur. Dans ce cas, l'acuité de sa vision, son attitude et sa motivation peuvent compromettre l'analyse en matière d'inspection. L'automatisation de l'inspection peut améliorer la reproductibilité de cette méthode *NDE*, en ce qui concerne le classement des pièces par le système de vision industrielle, compte tenu de l'analyse quantitative des données objectives. Les algorithmes d'extraction des caractéristiques sont exécutés pour offrir des donnés à une procédure d'analyse de données qui classifie les indications détectées comme des indications pertinentes ou non, selon les spécifications ou le code. Par conséquent, les systèmes de vision par ordinateur, lorsqu'ils sont appliqués au ressuage, améliorent la fiabilité technique globale, garantissent le stockage automatique des données, la récupération et le retour des informations de contrôle de la fabrication et de la maintenance des équipements.

Dans la littérature, il existe plusieurs exemples de systèmes de vision industrielle: Par exemple, le système de balayage laser, tel que proposé dans Tracy et Moore (2001), est une bonne approche pour l'automatisation et l'inspection. Dans ce système, un *spot* laser focalisé est déplacé sur la surface de l'échantillon et un photodétecteur mesure la quantité de fluorescence dans la zone éclairée, dont la puissance est directement proportionnelle à la quantité de pénétrant piégé dans des cavités de surface (Tracy et Moore (2001)). Une autre approche, proposée par Armstrong (1986), est d'éclairer un échantillon traité avec une lampe UV standard dans une cabine sombre et d'obtenir des images formées par indications fluorescentes à l'aide d'une caméra.

Dans ce travail, un système ultraviolet de détection d'indications a été développé pour automatiser l'inspection en FPI. Seules les indications de surface peuvent être détectées par le système. Il mesure la distance euclidienne maximum, mesure l'aire de surface et classifie la forme des indications. Ces caractéristiques peuvent être évaluées selon les normes de qualité prédéfinies. Les courbes de probabilité de détection ont été tracées et ont montré leur capacité de 21.6 microns de profondeur avec 100% de fiabilité.

Keywords: FPI, systèmes de vision, automatisation

IMAGE ACQUISITION AND PROCESSING IN AN ATTEMPT TO AUTOMATE THE FLUORESCENT PENETRANT INSPECTION

César Augusto Corrêa ALBA

ABSTRACT

Mechanical failure in aircraft workpieces is likely from happening, if open to surface discontinuities which comprise stress concentration regions are present. The fluorescent penetrant inspection (*FPI*) is a sensitive nondestructive evaluation (*NDE*) method capable to verify the presence of indications in surface of raw materials or of processed parts or parts submitted to service charges.

In general, when *FPI* inspection is being conducted, an inspector performs an evaluation of a treated surface based on his knowledge and experience in nondestructive testing, being the defect detection a qualitative decision according to his/her judgment. In this case, the inspector's vision acuity, attitude and motivation can compromise the analysis in inspection. The automation in inspection may improve the repeatability of this *NDE* method, regarding that machine vision systems classify parts considering quantitative analysis of objective data. Algorithms for the feature extraction are run, providing features for a data analysis procedure which classifies the detected indications as relevant or irrelevant indications according to specification or code. Therefore, the machine vision systems, when applied to fluorescent penetrant inspection, improve the overall technique reliability, guaranteeing automatic storage, retrieval and feedback of data for controlling the manufacturing and maintenance of equipments.

In the literature, there are several examples of machine vision systems: For example, the laser scanning systems, as proposed in Tracy and Moore (2001), is a good approach for the inspection automation. In this system, a focused laser beam spot is translated over the specimen surface and a photodetector measures the amount of fluorescence in that illuminated area whose power is directly proportional to the quantity of penetrant trapped in surface cavities (Tracy and Moore (2001)). Other manner which was proposed by Armstrong (1986) is to illuminate a treated sample with a standard UV lamp in dark booth and acquire images formed by fluorescent bright indications using a camera.

In this work, an ultraviolet indication detection system was developed for the automation of the inspection stage in *FPI*. Only open to surface indications are capable to be detected through the system. It measures the area and maximum euclidean distance and classifies the shape of indications. They are feasible to be evaluated according to predefined quality standards. Metrics such as the probability of detection curves were traced, obtaining a capability of 21.6 microns of depth with 100% of reliability.

Mot-clés: FPI, machine vision, automation

TABLE OF CONTENTS

LIST OF TABLES

Page

LIST OF FIGURES

Page

LIST OF ABBREVIATIONS

AC	Alternating Current
ASM	American Society for Materials
ASNT	American Society for Nondestructive Testing
Avg	Average
CC	Continuous Current
CCD	Charge-Coupled Device
CGSB	Canadian General Standards Board
CINDE	Canadian Institute of Nondestructive Evaluation
Disc.	Discontinuity
ET	Eddy Current Testing
FPI	Fluorescent Penetrant Inspection
HAZ	Heat Affected Zone
IDS	Indication Detection System
ISP	Indication Starting Point
L	Linear Indication
LIPPS	Laboratoire d'Ingénierie des Produits, Procédés et Systèmes
LIVIA	Laboratoire d'Imagerie, de Vision et Intelligence Artificielle
LOF	Lack of Fusion
LOP	Lack of Penetration

MT	Magnetic Particle Testing
NASA	National Aeronautics and Space Administration
NDE	Nondestructive Evaluation
NDI	Nondestructive Inspection
NDT	Nondestructive Testing
NRCan	Department of Natural Resources Canada
OW	Oil and Whiting Method
POD	Probability of Detection
PSM	Penetrant System Monitor
PT	Liquid Penetrant Testing
PU	Precision Uncertainty
R	Rounded Indication
ROI	Region of Interest
SD	Standard Deviation
UT	Ultrasound Testing
UV	Ultraviolet
RT	Radiography Testing

LIST OF SYMBOLS

A	Distance between the camera focusing lens and specimen
Ad	Adhesive Force
α	Illumination Angle
B	Magnetic Flux Density
C	Distance between the UV lamp and the specimen
ϕ	Magnetic Flux
g	Acceleration of gravity
γ_{ab}	Surface tension among a and b interface
H	Magnetic Force
h	Meniscus height
L	Self Inductance
M	Mutual Inductance
μ	Magnetic permeability
r	Meniscus radius
$r(x,y)$	Gradient magnitude at (x,y)
ρ	Liquid density
SP	Set containing the indication starting points
θ	Contact angle or wetting ability
$\theta(x,y)$	Orientation at (x,y) obtained through gradient extraction

INTRODUCTION

From 1930 to 1940, the techniques called nondestructive testing, due to the development of aerospace industries, became notorious as an important tool for the quality control. The cost in production and maintenance of aircrafts, if evaluated in terms of requirements for ensuring the safe service started to have a lesser importance at that time (Betz (1963)).

In 1920, the radiography was the only NDT employed for the verification of soundness in workpieces. It became an excellent method for the evaluation of internal discontinuities. In a casting, forging and machined parts, fine surface cracks, seams were not detected at that time with this technique (Betz (1963)). Around 1930's the magnetic particle was introduced in the market with the trade name Magnaflux and immediately became important for the analysis of surface discontinuities in ferromagnetic workpieces. However, due to the increasing number of parts made of nonmagnetic materials, the necessity for the development of a cost-effective, instantaneous analysis, portable and easy NDT technique for ensuring the integrity of surfaces became obvious (Betz (1963)).

Before liquid penetrant, several etching methods were applied for the analysis of nonmagnetic surfaces. The inspected workpiece was often damaged by the application of acid and alkali solutions and only large size discontinuities were successfully detected through it (Betz (1963)). The oil and whiting method *(OW)* was the actual forerunner of the current liquid penetrant inspection (Betz (1963)). The main purpose of *OW* was to detect open to surface cracks using penetrating elements (Betz (1963)). The penetrant was a high density lubricating oil whose trade name was "600 W" (Betz (1963)). This chemical fluid was thinned with kerosene or any other low-density oil resulting into a dark light solution (Betz (1963)). The developer was a mixture containing white chalk and denaturated alcohol (Betz (1963)). Even though the technique allowed significant progress, the lack of control related to the amount and concentration of involved materials, cleaning and excess removal leaded to bad performances in detection of shallow and thin cracks (Betz (1963)). The brightness ratio between the penetrant and whiting mixture often did not offer good contrast for perfect seeability of indications (Betz (1963)).

In 1938, the research laboratory of Magnaflux Corporation developed color-contrast penetrants (Betz (1963)). The results were not satisfactory. Robert C. Switzer from the enterprise Switzer Brothers, Inc. began the development of fluorescent dyes with ultraviolet spectrum (Betz (1963)). On October 14^{th} of 1941, a patent was issued in his name referring to his research of fluorescent and color-contrast penetrant methods for detecting indications in solid materials (Betz (1963)). In February 1942, under his approval, Magnaflux obtained full rights of the Switzer Brothers patent. Together, Magnaflux Corporation staff including Greer Ellis Taber de Forest, F. Catlin and R. Ward with the Switzer Brothers made significant improvements to the research regulated in the patent. In July 1942, the fluorescent penetrant inspection started to be an option in the market, once the product whose trade name was Zyglo became manufactured in large scale by Magnaflux Corporation. The patent of Zyglo was only issued in July 30^{th} of 1946 to Mr. R. Ward (Betz (1963)).

Before the release of Zyglo, several manufacturing enterprises that demanded surface inspection of nonmagnetic parts attempted to execute a technique called hot oil which was based on leaked information from Magnaflux and Switzer Brother's research. This method employed hot lubricating oil as penetrant, quick excess penetrant removal aided with solvent and analysis under black light illumination. The glare of the indications was observed by the inspector's eyes. Some aircraft and marine engine companies, under the pursuit of quality caused by War, were satisfied with the hot oil performance. Nonetheless, some companies did not achieve satisfactory inspection results. When Zyglo came out for purchasing, it immediately replaced the hot oil method.

Nowadays, the penetrant testing evolved. It is widely used for ensuring high quality in aerospace production and maintenance. It became a cost-effective, simple, fast and powerful nondestructive testing (NDT) method capable to detect the presence of open to surface discontinuities which are either already in the raw material or resulted from the fabrication/service. The utilization of fluorescent penetrants was consolidated. The fluorescent penetrant inspection (FPI) is largely performed for guaranteeing the airworthiness of aircrafts.

Problem Statement

A large portion of aerospace parts are made of nonmagnetic materials. In these workpieces, the PT is the most convenient NDT method capable to detect surface discontinuities which are high stress concentration areas and possible initiation sites for part failure. Due to this reason, the correct PT inspection is essential for the airworthiness of aircrafts.

Even though the materials which are involved in PT such as penetrant, developer, and emulsifier evolved over the past years, in manual inspection, the performance is still extremely dependent on the human inspectors. He/she pre/post cleans the specimen and applies the required chemical products manually (Betz (1963)), analyzes the detected indications, being influenced by his/her experience, vision acuity, attitude and motivation (Larson (2002)). Such process, in these circumstances, is prone to erroneous interpretation. Once the aerospace industry demands outstanding quality, the sensitivity, capability and repeatability are important concerns. The automation provides more reproducible results, eliminating inconvenients inherent to human inspectors.

Research Goals and Contributions

This research comprises a preliminary investigation which is part of the CRIAQ MANU418 project. This main study aims at automating the fluorescent penetrant inspection (FPI), eddy current testing (ET) and infrared thermography, improving the sensitivity, reliability and repeatability of the methods. The aerospace industries L-3 MAS and Pratt & Whitney Canada are the partners involved in this research and will benefit from the development of the automated system.

For this master project, an indication detection system is developed for automating the inspection stage in FPI in an attempt to eliminate the influence of the inspector's attitude, motivation and vision acuity which are intrinsic to the manual process. Steps prior and posterior such as precleaning, postcleaning, part drying & cool-off, liquid penetrant and developer application, penetrant excess removal are not automated, being conducted manually in the experiments.

The system acquires images of treated surfaces, detects indications, measures its maximum euclidean distance and area and identifies their shape with the objective to provide discriminant data for a classifier which accepts/rejects workpieces according to defined standards or codes. The probability of detection curve is traced in order to verify the capability and reliability of the system. The precision uncertainties related to the measurement of maximum euclidean distance and area of indications are evaluated for analyzing the variability of the automated inspection.

Organization of the dissertation

This dissertation consists of seven chapters. In chapter 1, the discontinuities which are likely to be detected through liquid penetrant testing are described. They are analyzed in terms of causes (e.g. manufacturing processes and/or service which generated them) and the corresponding effects in workpieces.

In chapter 2, a general overview of nondestructive evaluation techniques that are most applied in the aerospace industry is explained. Techniques such as liquid penetrant, magnetic particles, eddy current, ultrasound and radiography are briefly described. A maintenance program for the aircraft fleet is exemplified.

In chapter 3, we investigate the liquid penetrant testing in details. The physical phenomena which are responsible for the penetrant entrapment into discontinuities are explained. The types of penetrant, emulsifier and developer and most used methods for applying these chemicals are presented. The metrics and reference panels for evaluating the performance in PT inspection are introduced.

The automation of the fluorescent penetrant inspection, in terms of hardware, is analyzed in chapter 4. Stations in automated systems for loading, cleaning and drying parts and applying the PT chemicals to them are described. Diverse configurations of inspection systems with ultraviolet illumination are explained, providing introduction background for the system that has been developed for this work.

Important factors for the FPI automation related to software for detecting indications are outlined in chapter 5. It introduces 3 image acquisition techniques and indicates two image segmentation approaches for extracting relevant objects of the image. A feature extraction procedure is suggested for obtaining characteristics such as maximum euclidean distance, area and shape of indications.

The experimental protocol is described in chapter 6. The samples, the adopted procedure for preparing them and the respective experiments are indicated. The steps for tracing probability of detection curves and evaluating the system performance in terms of measurement and classification of indications are related. The results are reported in chapter 7. Finally, our conclusions are exposed and guidelines for future work are suggested.

CHAPTER 1

MANUFACTURING METHODS, DISCONTINUITIES AND SERVICE DEGRADATION

The nondestructive testing methods aims at detecting and interpreting indications with certified personnel and specialized equipment classifying them as *relevant*, *non-relevant* or *false* indications (American Society for Materials (2002b)). The *false indications* comprise all formed due to incorrect practice of NDT technique (American Society for Materials (2002b)). For instance, in penetrant testing, it would be represented by any region where the excess of penetrant has not been well removed after the *dwell time* (American Society for Materials (2002b)). The *non-relevant indications* consist of discontinuities that do not involve the rejection of a part. This group includes surface roughness, sealing joint, fasteners, etc. The *relevant indications* are discontinuities that may be evaluated by an inspector or machine vision system. Based on technical specification or quality code, the part is accepted or rejected (American Society for Materials (2002b)).

In NDT, it is important to know beforehand the history of the workpiece being inspected (i. e. the manufacturing processes that are involved for the part production and the service to which it was submitted). This provides useful information for verifying critical areas and typical discontinuities that may be detected. Several are formed during the casting process either in the molten metal (e. g. inclusions) or during solidification (e. g. shrinkage). An analysis of casting ingots is important, once several imperfections and service problems found in forged, rolled, drawn, extruded parts are attributed to conditions that already existed in the ingot, sometimes even before the its primary reduction. In addition, the discontinuities can be formed through all fabrication operation from the casting of the raw material to the finishing of a part. Depending on its type and size, it can result in serious consequences (Shull (2002)). For instance, an ingot with chemical segregation is characterized by composite structures with fragile elements. In metals, the presence of localized regions that deviate from nominal composition can deteriorate the corrosion, mechanical and fatigue resistances as well as fracture toughness, compromising

the forming, machining and welding operations (American Society for Materials (2002b)). In heat-treatable alloys, it may result in unexpected responses to heat treatments, causing the hardening of soft spots, quench cracks and other discontinuities (American Society for Materials (2002b)).

Among the NDT techniques that are dedicated to the verification of the surface integrity (which includes PT), open to surface cracks are important to be localized. The cracks are long narrow discontinuities which are found internally or on the surface of materials (Shull (2002), Callister Jr (2007), American Society for Materials (2002b)) as illustrated in figure 1.1. The presence of open to surface discontinuities is the startup of the failure of a mechanical part, once they act as stress concentrators sometimes leading to fracture. As long as cyclic stresses are maintained, the cracks tend to be enlarged in the direction and orientation of the stress concentration. If it grows at a critical level, the part must be discarded, assuming that the final failure is reached (Callister Jr (2007)). Otherwise, if safety is an important issue, disasters as the picture in figure 1.2 may happen (Callister Jr (2007)). Stress concentration areas in a part could be exemplified by sharp fillets, keyways, threads, dents, scratches, roughness, corrosion, laps, bursts, laminations, seams, stringers, the flash line, undercut, heat affected zone (HAZ), porosities, shrinkage, etc (Callister Jr (2007), American Society for Materials (2002b)). Thermal cycling during the welding and machining results in high residual stresses. During the service, if cyclic load is applied to these regions, extremely small cracks on the surface may be generated due to these initiation sites. Inadequate conditions of manufacturing operations like casting, forming (see figure 1.3), machining, joining may result into cracks as well. The application of stresses in corroded areas may also initiate these discontinuities (American Society for Materials (2002b)).

In this chapter, some fabrication techniques and service degradation processes are explained. The comprehension of them is crucial for the analysis of discontinuities caused during the manufacturing and service of parts. Several types are analyzed in terms of causes and effects. At the end, there is a summary of the main topics which are discussed in this chapter.

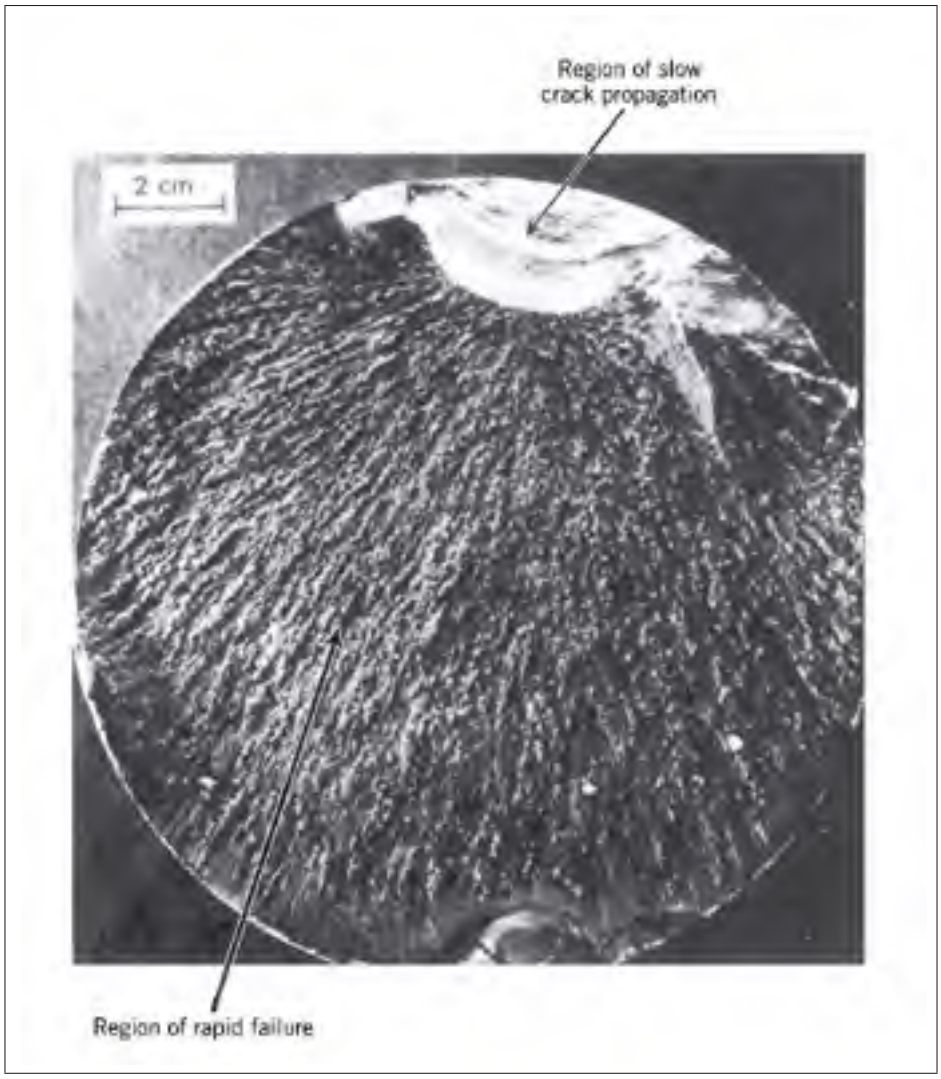

Figure 1.1 Typical case of part failure due to crack propagation. A crack formed on the top of the surface propagated slowly and a rapid fracture happened.
Reproduced from the book Callister Jr (2007)

1.1 Casting

The casting is a manufacturing process in which a fully molten metal fills, through a pouring technique, a mold cavity that provides the shape of final part after solidification. The casting is chosen as fabrication method, if a quite large or very complicated geometry part must be produced, and/or if the material is an alloy whose ductility is extremely low for forming. The most common casting techniques are the sand casting, die casting, investment casting, lost

Figure 1.2 Oil tanker which suffered a fracture due to crack propagation.
Reproduced from Callister Jr (2007)

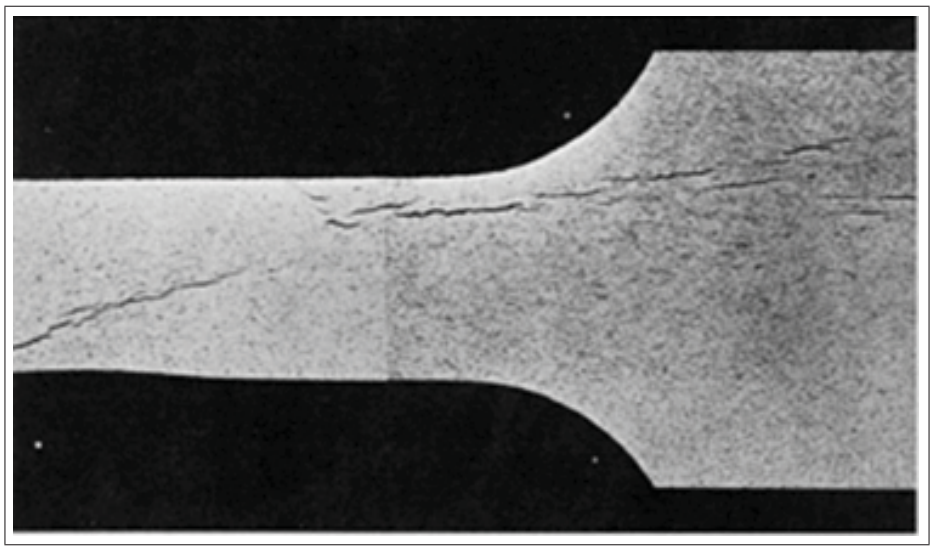

Figure 1.3 Forged alloy 7075-T6 part which contains shrinkage cavities and internal cracks formed during the solidification during the casting.
Reproduced from American Society for Materials (2002b)

foam casting and continuous casting. In figures 1.4, 1.5 and 1.6, there are examples of casting molds containing important compounds (American Society for Nondestructive Testing (1981)).

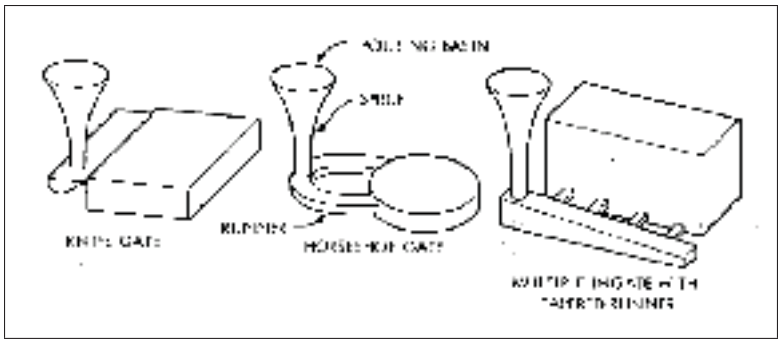

Figure 1.4 Example of gating systems typically used in casting molds.
Reproduced from American Society for Nondestructive Testing (1981)

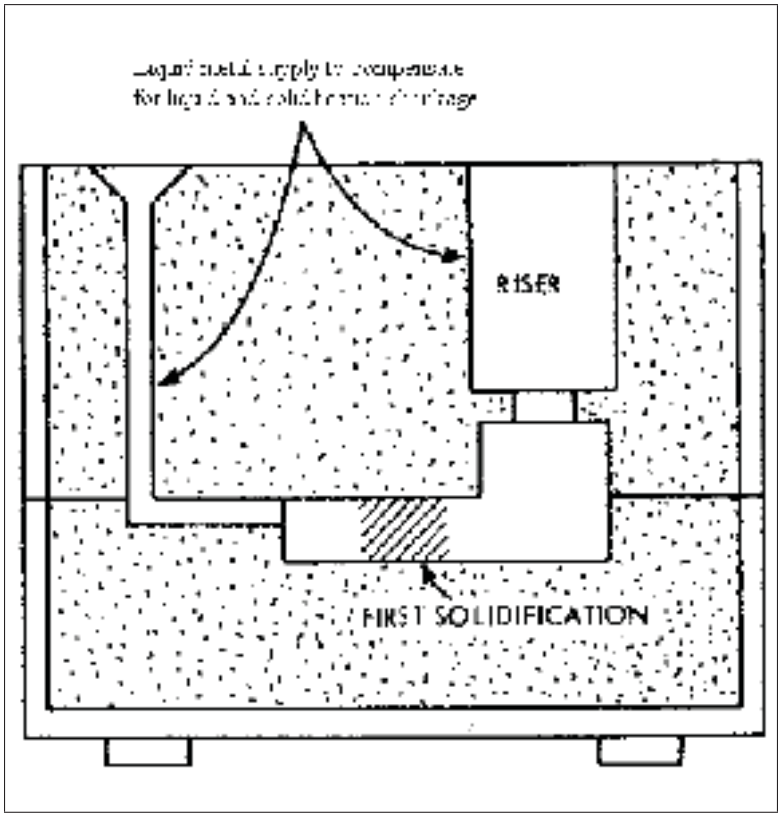

Figure 1.5 Casting mold containing risers for controlling shrinkage.
Reproduced from American Society for Nondestructive Testing (1981)

In a casting mold, the riser is a reservoir located outside the casting which aims at supplying molten metal as necessary, compensating the shrinkage before the end of solidification. The runner is a channel that allows the liquid metal to be distributed over receptacles. The gate is a region of the runner that connects with the mold cavity. The sprue is a channel that is linked

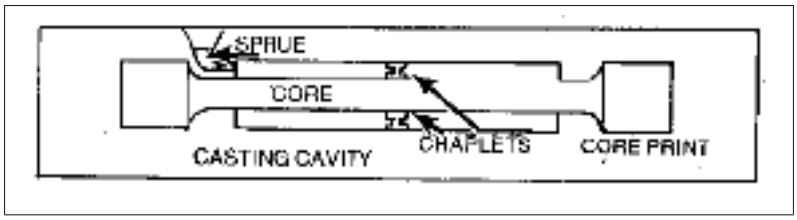

Figure 1.6 Casting mold containing a core which is supported by chaplets.
Reproduced from American Society for Nondestructive Testing (1981)

to the runner. The core is an element whose function is to generate an internal cavity in the casting. The chill is a metallic component which is designed for increasing the cooling rate of certain walls in the casting. The chaplets constitute metallic supports used for the sustentation of the core during the pouring. They must be made by the same metal as the one filled, because, as it is exposed to the poured metal temperature, it should melt and become part of the same casting (American Society for Materials (2010b)).

The regular nondestructive inspection results in detection several inappropriate casting conditions. For instance, the bridging and piping as depicted in figure 1.7 is usually due to high solidification velocity or to insufficient quantity of molten metal to feed the whole mold cavity. Another important example which indicates an incorrect casting process is the presence of cold shut (also known as cold lap) as illustrated in figure 1.8 (b). It is a smooth, generally half-moon shaped discontinuity which happens when two streams of molten metal do not fuse properly. It occurs more often when there is more than an unique gating system which causes an interrupted pouring technique. One metal stream solidifies before the second and consequently, there is a lack of fusion. A third indication of improper casting technique is the presence of a surface inclusion usually coated with oxides known as cold shot being represented in figure 1.8 (c). This is due to the extremely quick pouring and to its very small amount of base metal that does not fuse with the casting part. Other evidence of lack of casting control is the detection of a crack-like shaped discontinuities on the surface named as hot tears as shown in figure 1.8 (d). This indicates that the part walls were cooled at different rates. It is likely from happening, if the mold wall thickness varies along its extension. It is the only type of crack observed in castings. The detection through NDT of internal porosities called blowholes (depicted in figure

1.8 (e)) and even the explosion of the casting mold, indicates that it contains elements such as chaplets, chills, inserts, etc made with contaminant materials. Other types of porosities in the casting are due to entrapped gases in the solidifying metal and must be unacceptable in high safety workpiece (American Society for Materials (2002b)).

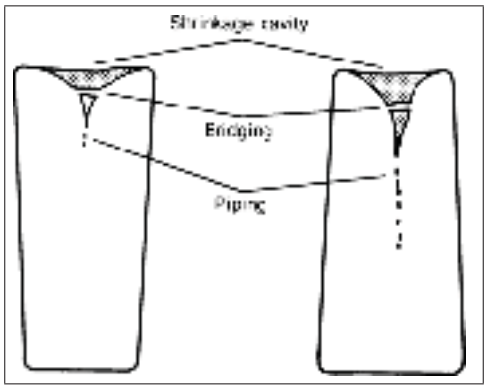

Figure 1.7 Sketch demonstrating the shrinking cavity, bridging and piping which can occur under inappropriate solidification conditions.
Reproduced from American Society for Materials (2002b)

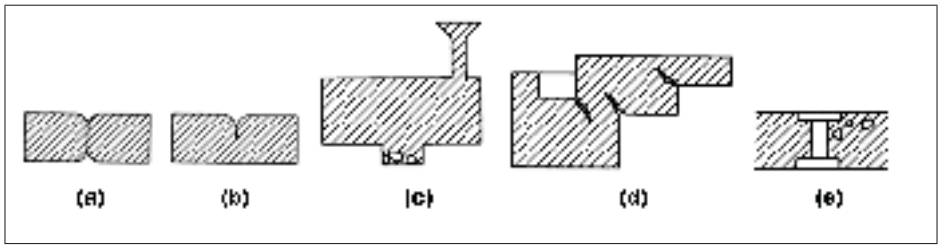

Figure 1.8 In (a), there is a representation of lack of fusion in a casting; in (b), of cold shut; in (c), of cold shot; in (d), of hot tears and in (e), of blowholes.
Reproduced from American Society for Materials (2002b)

1.2 Forming (plastic deformation shaping)

The forming operations comprise all techniques which deform plastically a part through induced forces or stresses without exceeding the strength of the part material. In general, metals can be, with certain control, deformed by these techniques due to its ductility without fracture or crack generation. This group includes manufacturing processes like forging, rolling, drawing and extrusion. If the forming is conducted under hot temperatures (setting often specified

as hot working), larger repeated deformations can be executed, once the metal is kept ductile and soft. However, material is often lost and occasional surface oxidation deteriorates the microstructure properties. On the other hand, if the same operations are performed at room temperature (setting referred as cold working), a better material strength, mechanical properties, surface finish, and dimension control are achieved. This is explained by smaller ductility levels caused by the higher metal strain hardness (Callister Jr (2007), American Society for Materials (2010a)).

The forging is a process which modifies plastically a metallic piece either by successively blowing or continuously squeezing it with localized compressive hammers and/or presses for obtaining a desired shape. It is mostly conducted under hot temperatures. This operation is divided into closed or open-die forging. In the former, (see figure 1.9 (a)) a force is imposed on several dies halves whose shape contains a cavity which will deform the part into the desired shape. In the latter, in general applied in large parts, two dies whose geometry is quite simple are compressed (Callister Jr (2007), American Society for Materials (2010a)).

The rolling is an operation which reduces the thickness of a metallic part using pairs of rotating rollers as depicted in figures 1.10 and 1.9 (b) . A series of roller pairs gradually reduces the size through compressive stresses. After the last rolling step, a piece with the desired cross-sectional area is obtained (Callister Jr (2007), American Society for Materials (2010a)).

The extrusion is a process in which a billet, using a ram, is pressed against a die orifice whose cross-sectional outline is smaller than the original billet diameter (or height and width) as shown in figures 1.11 and 1.9 (c). It is usually employed when the desired cross-section is uniform along the billet length. Similarly to extrusion, the drawing reduces the stock of a larger geometry pulling the part against a die orifice as illustrated in figure 1.9 (d) (Callister Jr (2007), American Society for Materials (2010a)).

If safety is an important concern, an adequate program which establishes a regular NDT inspection of forging, rolling, extrusion and drawing operations, must be executed in the industry. For example, a burst which is depicted in figure 1.12 determines that the forming is being con-

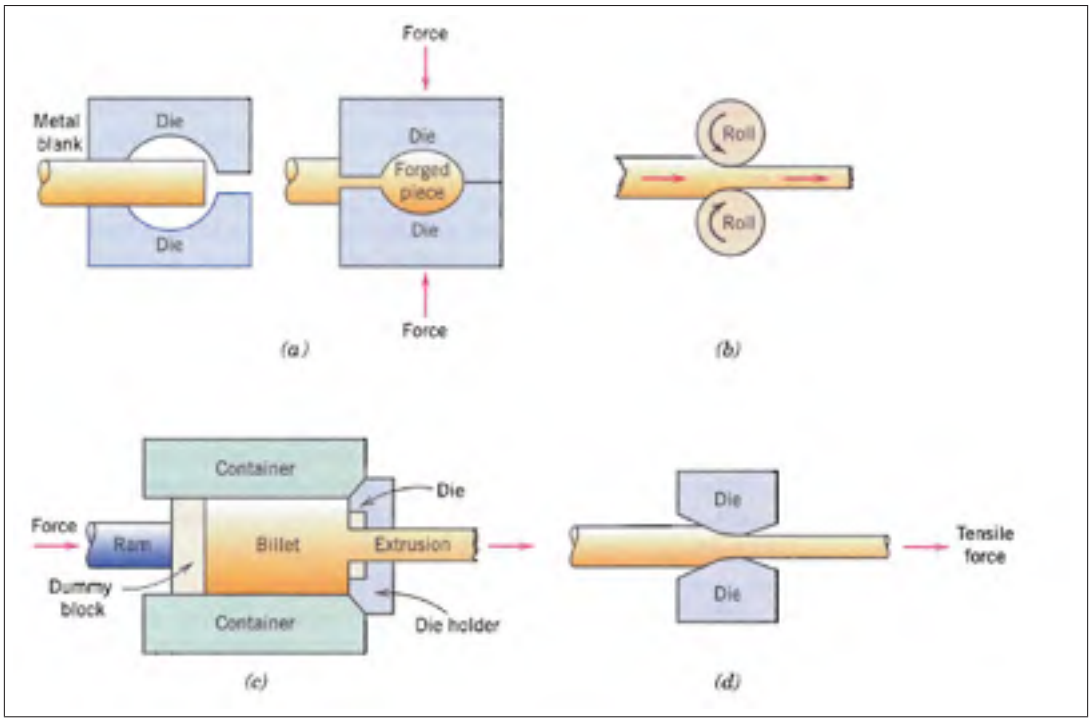

Figure 1.9 The most common forming tasks. In (a), forging; in (b), rolling; in (c), extruding; and in (d), drawing.
Reproduced from Callister Jr (2007)

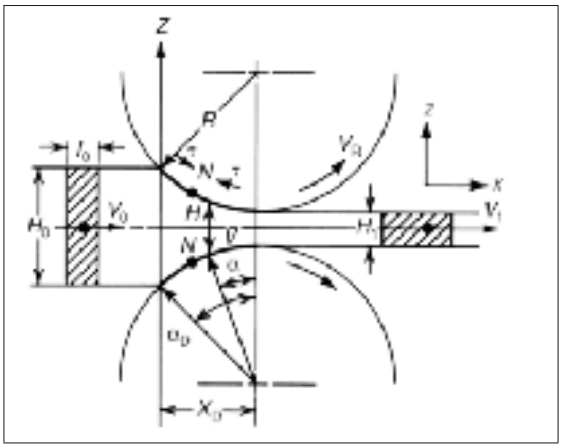

Figure 1.10 This picture depicts the rolling operation. The hatched volume illustrated on the left of the figure is flattened to the volume on the right.
Reproduced from American Society for Materials (2010a)

ducted with a force above the workpiece load capacity or at a temperature below the required. If a forged part contains a folded surface (as illustrated in figure 1.13, there is misalignment of the die halves in the forging operation, characterizing a discontinuity known as lap. In ad-

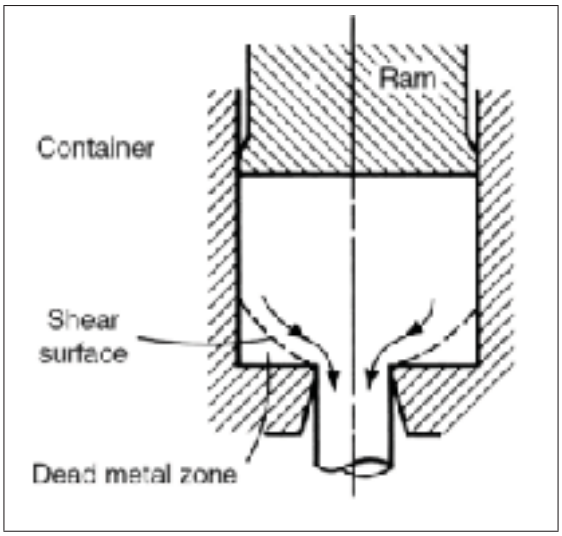

Figure 1.11 This picture depicts the extrusion process. The hot billet is inserted into a container and it is pressed by a ram against a die opening. Reproduced from American Society for Materials (2010a)

dition, after any forming operation, the NDT may be efficient for revealing indications which were not detected immediately after the solidification of ingots or billets. For instance, if a part contained internal cracks, pipes, inclusions, segregations, blowholes or porosities, etc prior to plastic deformation shaping, these discontinuities are flattened out becoming thinner and parallel-aligned with the surface material, being referred as laminations. Through the same manner, discontinuities called seam and stringer can be formed (American Society for Materials (2002b)). The former is located on the surface of the processed part. It is long and similar to a crack. The latter is originally just below the surface, but it can be brought to the surface, if machining is executed. It is short and found in groups (American Society for Materials (2002b)).

1.3 Machining

Machining processes designate the material removing operations aided with sharp cutting tools generating particles of swarf, resulting into parts with diverse shapes and dimensions (American Society for Materials (2002a)). To conduct these operations, relative motion between the tool and the part subjected to them is mandatory (American Society for Materials (2002a)). This displacement, the shape of the cutting tool and its penetration generates a machined part

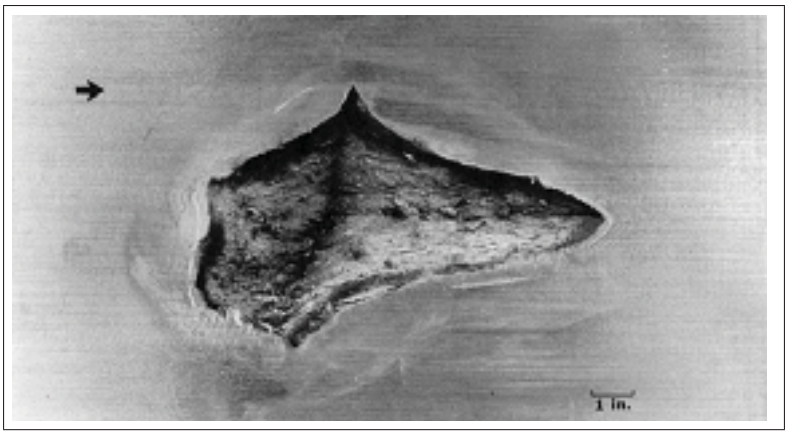

Figure 1.12 Picture of a burst located in a forged bar.
Reproduced from American Society for Materials (2002b)

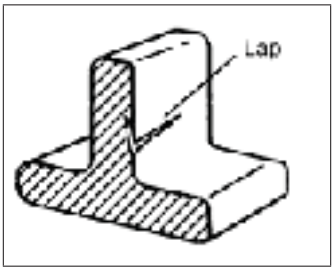

Figure 1.13 Schematics of a lap formed during the forging operation.
Reproduced from American Society for Materials (2002b)

with the desired shape (American Society for Materials (2002a)). The most important machining operations are explained below (American Society for Materials (2002a)):

1. The lathe modifies the shape of a dowel, rotating it around its own axis and translating a sharp cutting tool which removes material at the same time. The final product is a part whose shape is either conical or cylindrical (American Society for Materials (2002a)).

2. The milling changes any piece geometry using a rotating cutting tool (called milling cutter) with diverse number of cutting teeth. It allows the manufacturing of different shaped parts. The piece remains static in this process (American Society for Materials (2002a)). In figure 1.14, there is an sketch of a milling cutter removing material.

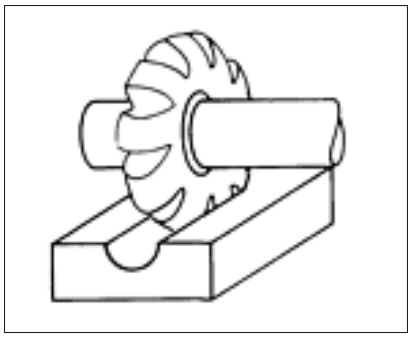

Figure 1.14 This sketch depicts the milling in the fabrication of a part.
Reproduced from American Society for Materials (2002a)

3. Through the drilling, a tool with one or several flutes called drill perforates a cylindrical cavity in the part. The tool is rotated and it is moved in the direction of the axis of hole which is being generated (American Society for Materials (2002a)). The figure 1.15 replicates one example of a drilling machine.

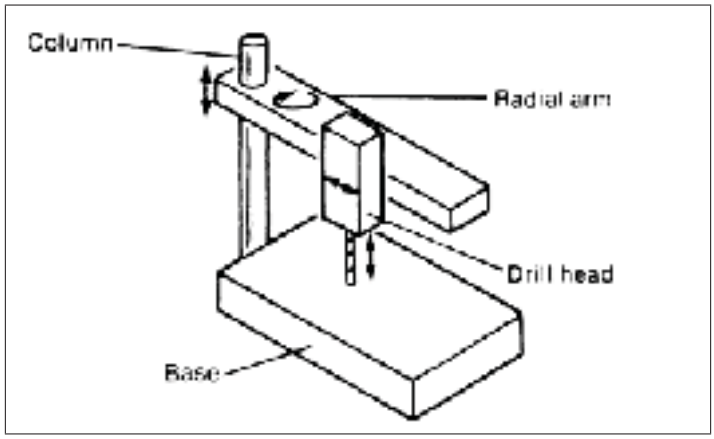

Figure 1.15 This schematics illustrates a radial drilling machine with the compounds.
Reproduced from American Society for Materials (2002a)

4. The broaching is a machining operation in which material is removed through the translation of a multiple cutting edges tool. The machined part remains static in most cases (American Society for Materials (2002a)). It provides a good finishing quality, but it is costly due to the price of the cutting tool. The broaching can be external and internal as exposed in figure 1.16 (American Society for Materials (2002a)).

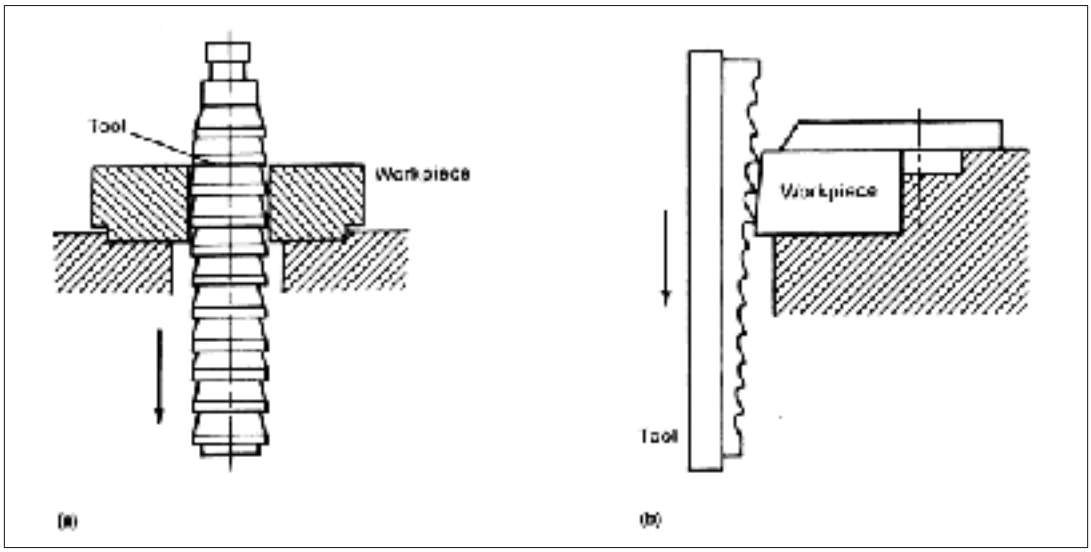

Figure 1.16 These figures illustrates the broaching. In (a), the broach is removing material internally; in (b), the broaching is executed on an external surface. Reproduced from American Society for Materials (2002a)

The discontinuities most likely from happening during the machining operations are the cracks. The incorrect choice of tool, tools with blunt edges and wrong machining parameters (cutting speed, feed and depth of cut) are the main causes for their generation.

1.4 Welding and Thermal Processing

Welding is the most wordwidely used operation for joining materials such as metals in manufacturing and maintenance of parts, equipments and structures. Applications of this process go from the assembly of electronic components to complex metallic structures of ships, tube vessels, vehicles, bridges, etc. Theorically the welding is conducted by the approximation of at least two parts at a short distance allowing chemical bonding between atoms. For some materials and parts, the welding becomes complicated due to factors like roughness, oxide layers, moisture, grease, dust and other contaminants. Arc and gas welding require the melting of filler and base metal around the joint, resulting in a single joint around them. After cooling and solidification of the heated metals, both workpieces are permanently fused together. Due to this thermal cycle, the mechanical properties of the material in the adjacent area may have been affected. This region is known as the *heat-affected zone (HAZ)*, being represented in

figure 1.17. To describe the discontinuities caused by improper setup in the welding process, several features of a weld joint must be explained beforehand. In figure 1.18, in the face is the weld metal which comes out on the side where the welding was executed; the toe is the intersection between the face and the base metal surface; the leg and throat are respectively the minimum distance among the toe and the root and between the face to root in joints such as fillets and laps; the size of a weld (known as penetration in a butt weld) is the depth of the root penetration (in other words, the vertical distance from the toe to the root, disregarding the root reinforcement) (Callister Jr (2007), American Society for Materials (2002c)).

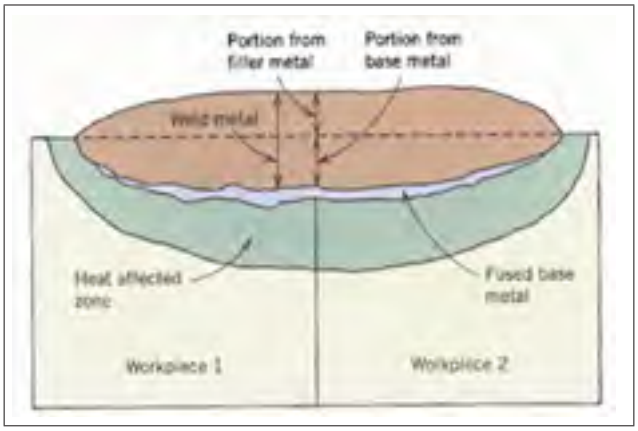

Figure 1.17 This figure represents the heat-affected zone.
Reproduced from Callister Jr (2007)

Figures 1.19, 1.20 and 1.21 show typical discontinuities that may result from incorrect welding procedure. As illustrated in figure 1.19, the lack of fusion (LOF) indicates that the base metal did not melt in order to fuse with the filler metal for obtaining a safe weld joint. In the case of lack of penetration (LOP), there was not enough fusion between filler and base metals in the root of the joint. As demonstrated in figure 1.20, the undercut is characterized as groove melted on the base metal surface adjacent to the weld toe or root. The overlap is an excess of filler material which has not been fused with the base metal located beyond the toe or face of a weld. The underfill is a depression of the weld joint due to lack of filler material, being found on the face or on the root of a weld. All of these discontinuities indicate that the welding has not been conducted with proper electrode handling, filler metal or power parameters (American Society for Materials (2002b)).

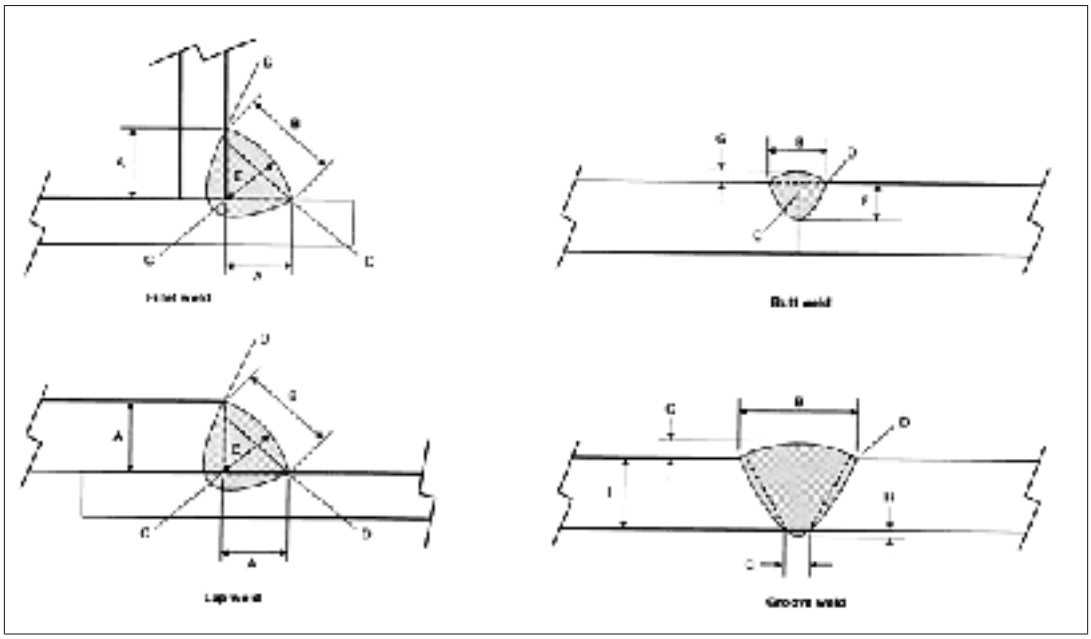

Figure 1.18 Weld joint most important features. The letter A represents the leg; B, the face; C, the root; D, the toe; E, the throat; F, the penetration; G, the face reinforcement; H, the root reinforcement; I, the size of weld.
Reproduced from American Society for Materials (2002c)

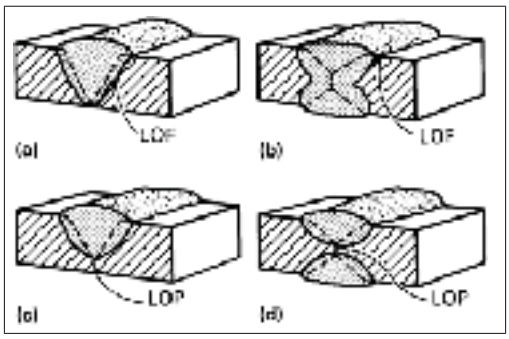

Figure 1.19 Lack of fusion in a single-V-groove and double-V-groove weld joints and lack of penetration in a single-V-groove and double-V-groove weld joints are represented in (a), (b), (c) and (d) respectively.
Reproduced from American Society for Materials (2002b)

Once the welding process demands hot temperatures for melting the weld metal followed by its cooling and solidification, the joint suffers from residual stresses caused by hot shortness. This phenomenon, if not properly controlled, may result in cracks in the weld metal or along the base metal near the HAZ. There are several types of welding cracks. The most common are: transverse, longitudinal, crater, hat, underbead, toe, root, HAZ and cold cracks. The figure

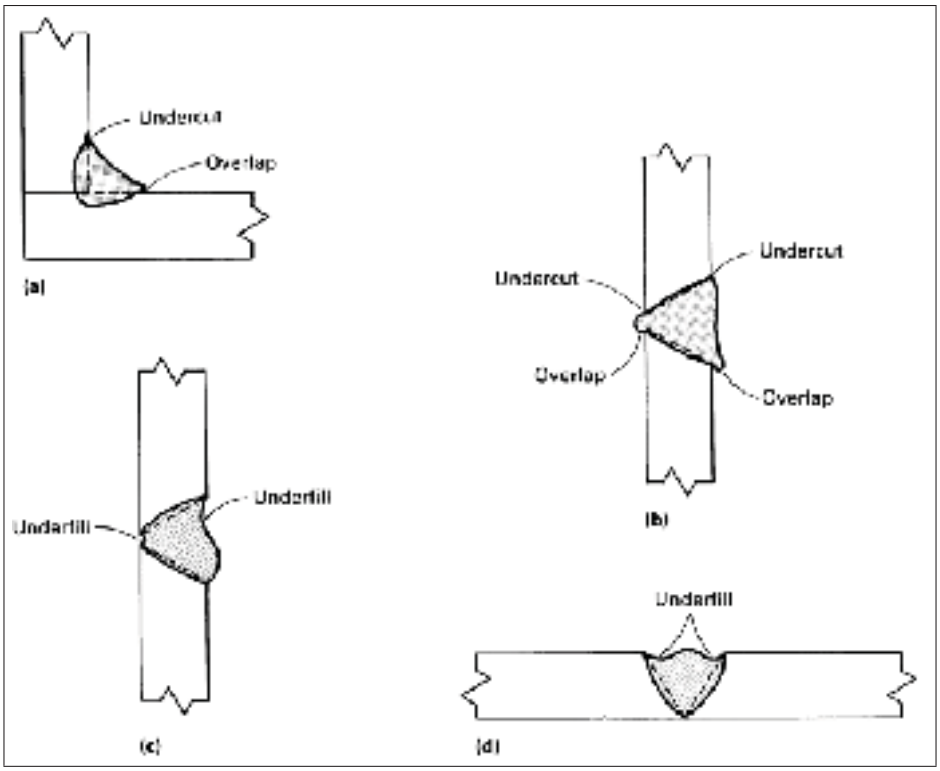

Figure 1.20 In a fillet weld, undercut and overlap are represented in (a). In (b), undercut and overlap are depicted in a groove weld. In (c) and (d), there is an illustration of underfill in groove welds.
Reproduced from American Society for Materials (2002b)

1.21 exemplifies sorts of crack which may be found in welding joints (American Society for Materials (2002b)).

Transverse cracks are due to stress contraction in the direction of the weld axis. They are perpendicular to the axis of the weld, often open to the surface, extending to the base metal near HAZ. They propagate into the weld or beyond the HAZ in order to relieve the residual stresses. The underbead cracks are caused the same way, but they are located in the base metal. The longitudinal cracks are found on the surface, extending from the root to the face, being also consequence of stress contraction (American Society for Materials (2002b)).

Crater crack happens when the joint is not properly formed, resulting into joint craters. Regarding that a crater is shallow and thinner, it has a faster cooling rate than the remaining joint. Consequently, tensile stresses appear, originating a crack. The hat cracks, as the name says,

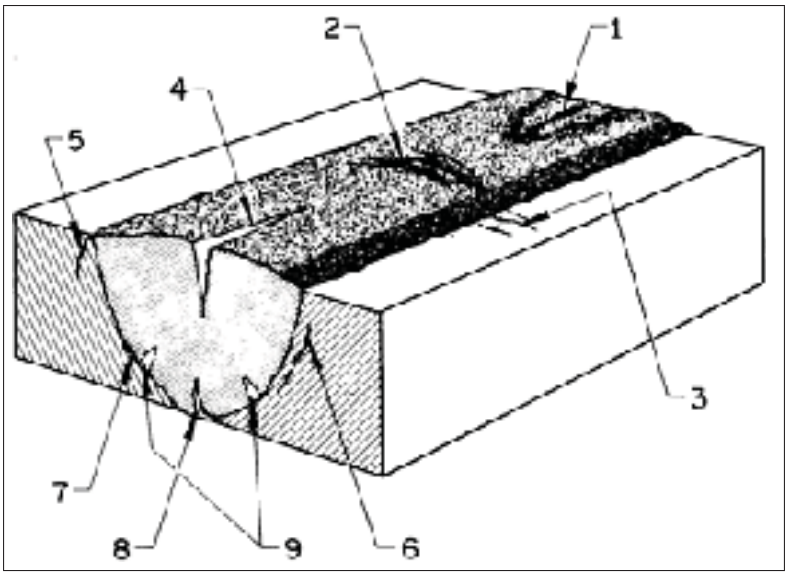

Figure 1.21 Crack types which may be found in a weld joint. 1) is a crater crack in weld metal; 2), transverse crack in weld metal; 3) transverse crack in HAZ; 4) longitudinal crack in weld metal; 5) toe crack in base metal; 6) underbead crack in base metal; 7) fusion-line crack; 8) root crack in weld metal; 9, hat cracks in weld metal. Reproduced from American Society for Materials (2002b)

have the shape similar to an inverted hat. This defect is located close to the weld face (about halfway up) and extends into the weld metal. It is caused by excessive electrode voltage or welding speed. Toe and root cracks may occur in high residual stresses welding locations. These cracks primarily propagate through the HAZ and may extend to more ductile regions of the base metal. The HAZ cracks are formed due to inadequate prior heating of the parts being joined. Due to it, during the cooling of the joint, the unmelted material shrinks which implicates in contraction stresses in the HAZ, forming cracks (American Society for Materials (2002b)).

In addition, several material properties may be adjusted through thermal processing methods. Annealing consists in submitting a part to high temperature (below the fusion temperature) for a long period and letting it cool slowly. It can be an efficient method for adapting the material microstructure according to the working requirements, relieving stresses, increasing the ductility and toughness. In steels, most of the heat treatments are for hardness improvement. In

this case, different levels of hardness are achieved according to the chosen quenching medium (Callister Jr (2007)). In heat treatments, cracks are likely found in stress rising areas.

1.5 Service Degradation of Mechanical Parts

Aircraft components which are regularly in service are subjected to degradation. The assessment of the integrity of parts must be conducted preventively. Otherwise catastrophic failure will happen suddenly and without any warning. The fatigue is a sort of failure which is observed in structures submitted to dynamic and fluctuating stresses, occurring after long periods of cyclic load (Callister Jr (2007)). Under these conditions, fatigue cracks are formed and the failure of a part may be developed at stress levels below the tensile or yield strength for a static load (Callister Jr (2007)). Open to surface discontinuities aggravate these effects, once comprise stress raising sites.

Furthermore, the corrosion deteriorates mechanical properties of workpieces, compromising their service as well (American Society for Nondestructive Testing (1981), Callister Jr (2007)). It consists of a degradation of metals due to the chemical action of a medium (which can be a liquid, gas or both) that is likely from developing along the service (American Society for Nondestructive Testing (1981), Callister Jr (2007)). The impact of the corrosion depends on the combination of metals and the involved corrosive agents (American Society for Nondestructive Testing (1981), Callister Jr (2007)). Accompanied by corrosion, the fretting is one type of wear which compromises drastically the serviceability of workpieces (American Society for Nondestructive Testing (1981)). It is caused by movements of mating surfaces under load (American Society for Nondestructive Testing (1981)). The stress corrosion cracks are susceptible to be formed if the they are submitted to cyclic and small amplitude movements, leading to mechanical failure (American Society for Nondestructive Testing (1981)).

1.6 Summary

This chapter was an introduction to defects that are likely to occur due to improper manufacturing parameters and hostile service condition. Even though some internal discontinuities

were briefly described, only surface indications are revealed through liquid penetrant testing. For verifying the integrity of workpieces internally, radiography and ultrasound are the most recommended methods. Therefore, PT testing is capable to detect the cold shot, laps, flash line tears, LOP, seam and stringers. Cracks, cold shuts, porosities, inclusions, hot tears, bursts, blowholes and LOF, if open to surface, can be observed through PT. Table 1.1 contains causes and effects of discontinuities feasible to be detected through penetrant testing.

Table 1.1 Summary of the main defects which can be detected through PT

Discontinuity	**Causes**	**Effects**
Porosity	Gases which are entrapped either in the mold or in the molten metal	Low density part, more fragile structure, stress rising area generation
Cold Shut	Metal streams and poured at different velocities, interrupted pouring	Stress raising area
Cold Shot	Extremely quick pouring technique	Fragile casting structure, stress raising area
Hot Tear	Inadequate cooling of the mold, bad mold design	Stress raising area
Lap	It is likely from happening, if misalignment of hammers or die halves (forging) or rollers (rolling)	Stress raising area
Burst	Forming executed over the strength capacity of the material and over the recommended temperature	Stress raising area
Seam and Stringer	Any forming operation is conducted in a part which contains an internal discontinuity	Stress raising area
Crack	Any manufacturing operation or service condition that induce stresses in the workpiece	Stress raising area
LOF, LOP, Overlap, Underfill and Undercut	Incorrect electrode handling, lack of filler metal and bad power parameters	Stress raising area

CHAPTER 2

METHODS OF NONDESTRUCTIVE EVALUATION

The nondestructive evaluation techniques (*NDE*) also referred as nondestructive inspection (*NDI*) and nondestructive testing (*NDT*) comprise physical methods for analysis of material properties without causing any sort of damage to the service and integrity of mechanical parts. The *NDE* may be employed as a powerful tool for increasing reliability, guaranteeing the safety of workpieces. The *NDT* equipment can be purchased in stationary/laboratory or portable configurations. Due to it, the inspector is capable to execute analysis on site with a kit, if workpieces are complicated to be transported to a laboratory (Shull (2002), Canadian Institute for NDE (2010)).

The inspectors must be certified according to rules specified in the standards of country where the inspection is being conducted. The *Canadian General Standards Board (CGSB)* is responsible for the standard *CGSB-48.9712* which is applicable in Canada. In the United States of America, the adopted standard is *SNT-TC-1A*. A code which is valid for one country is, in general, not accepted in other. The *CGSB* delegates to the *Canadian Institute of Nondestructive Evaluation (CINDE)* the task of providing training according to *CGSB-48.9712* for personnel seeking certification. Minimum periods of experience are mandatory, varying between NDT methods and level of certification (Canadian Institute for NDE (2010)).

In Canada, the *Department of Natural Resources Canada* (*NRCan*) is the certifying agency which elaborates written and practical certification exams on behalf of *CGSB*. *NRCan* is responsible for judging if candidates match with all CGSB certification requirements. Only people with successful scores in examination, minimum training and practical experience is allowed to be certified. The certification in *NDT* is regarded as a privilege delegated to qualified personnel (Canadian Institute for NDE (2010)).

In this chapter, a general overview of the main nondestructive techniques is described. In section 2.1, a general program for aircraft fleet maintenance is analyzed. The techniques of

liquid penetrant, magnetic particle, eddy current, ultrasound and radiography are respectively explained in sections 2.2, 2.3, 2.4, 2.5 and 2.6.

2.1 Nondestructive Testing in Aircraft Fleet Maintenance

The airworthiness of a plane depends mostly on maintenance conditions to which it is submitted. Commercial airlines must pursue a trade-off among safety, continuous serviceability, cost-effectiveness and comfortable transportation to passengers. Preventive programs must be emphasized in aircrafts. However, sometimes, only corrective intervention is feasible (Tracy and Moore (2001)). The maintenance of an aircraft fleet must primarily guarantee the soundness of a structure, ensuring long and safe service life. Special attention must be given to critical structure, joint areas which suffer cyclic loads (regions prone to fatigue) (Tracy and Moore (2001)). The frequency and level of inspection must be defined in order to provide continuous knowledge of the current state of vital structure of a plane in a fleet. Any sort of deterioration which may result into near future failure (the most common are fatigue cracks and corrosion) must be detected in a very early formation stage (Tracy and Moore (2001)). According to Tracy and Moore (2001), an efficient airline maintenance program is composed by the following stages:

1. The *preflight check* includes visual verification of engines, flight controls, airframe prior to aircraft take-off;

2. The *line servicing* consists of, in general, detailed inspections between every 100 or 125 flight hours of aircraft components and structures;

3. The *base overhaul* comprises a meticulous examination of removable airframe structure components within intervals varying from 2000 to 5000 hours of aircraft flight. Initially, the removable components are replaced and the inspection is conducted on them. If necessary, these workpieces are modified or repaired for ensuring the service safety. In this phase of aircraft maintenance, the NDE techniques are largely employed. Among these methods, in the aircraft maintenance, from a simple visual inspection to high complexity

scientific analysis, a wide range of techniques is performed. The most used are the radiography, fluorescent penetrant inspection, magnetic particle and ultrasound (Tracy and Moore (2001)).

Between the discontinuities, the fatigue cracks presents the highest relevance in detection (Tracy and Moore (2001)). The presence of corrosion, once it is normally occurring prior to fatigue cracks, is defining the life cycle of a workpiece. Nonetheless , the aircrafts (especially the wings and fuselage) are designed based on concept of fail safe (Tracy and Moore (2001)). It means that a plane, even if it contains cracked, warped, stretched, fractured, sheared or snapped structures, it is capable to land with complete safety. This is achieved because its structure is designed to support unexpected loads, stresses, fatigue and corrosion (Tracy and Moore (2001)). Programs of inspection are adopted for monitoring and controlling critical structure workpieces of a plane.

2.2 Liquid Penetrant Testing (PT)

The liquid penetrant testing is a NDT method largely employed for revealing surface indications. It is a very simple method, but it requires cleanliness. In general, if the specimen is ferromagnetic, instead of PT, the inspector prefers the application of magnetic particles (Shull (2002), American Society for Materials (2002b), NDT Resource Center (2010)).

The technique consists of the application of penetrant to a specimen which is drawn into any open to surface discontinuity through capillary forces. After the dwell time, the excess of penetrant is removed from the surface , the developer is applied and the part will bleed out in regions where surface indications are located. The use of ultraviolet source in a variation called *Fluorescent Penetrant Inspection* enhances the seeability of indications (Shull (2002), American Society for Materials (2002b), NDT Resource Center (2010)). In the next chapter, the PT is discussed in a deeper level.

2.3 Magnetic Particle Inspection (MT)

The MT method consists of applying a magnetic field to a part for its inspection. In the magnetized part, the presence of a discontinuity causes a field leakage and the generation of a magnetic dipole. If magnetic particles are applied to such a magnetized part, they will agglomerate around the field leakage area. This agglomeration indicates the contour of the field leakage, allowing the detection of the shape and the length of the indication (American Society for Materials (2002b), Shull (2002), NDT Resource Center (2010)).

The magnetic permeability is the ability of a material to be magnetized. It is represented by the letter μ, being mathematically defined as the ratio between the absolute magnetic permeability of the material with respect to the one in vacuum. Based on the magnetic permeability, the materials can be separated into three classifications (American Society for Materials (2002b), Shull (2002), NDT Resource Center (2010)):

1) Ferromagnetic Materials: $\mu > 1$

   Comprise all materials strongly attracted by a magnet such as iron, cobalt, nickel and almost all sorts of steel. These materials are ideal for MT inspection (American Society for Materials (2002b), Shull (2002), NDT Resource Center (2010)).

2) Paramagnetic Materials: $\mu \approx 1$

   This group contains materials which are slightly attracted by a magnet. It contains materials such as aluminium, chrome, stain, potassium, platinum, being not recommended for MT inspection (American Society for Materials (2002b), Shull (2002), NDT Resource Center (2010)).

3) Diamagnetic Materials: $\mu < 1$

This category is formed by materials which are slightly repelled by a magnet such as silver, zinc, lead, copper and mercury. MT is not employed for testing (American Society for Materials (2002b), Shull (2002), NDT Resource Center (2010)).

The magnetic permeability may vary among parts made of the same material. It is dependant of the magnetic flux density B and the magnetic force H. In general, when the literature indicates this property, μ is obtained under magnetic saturation. This condition is reached, increasing the H into a level at which B remains constant. In figure 2.1, there is an hysteresis curve which indicates the level of the magnetic flux density where the saturation condition is achieved (American Society for Materials (2002b), Shull (2002), NDT Resource Center (2010)).

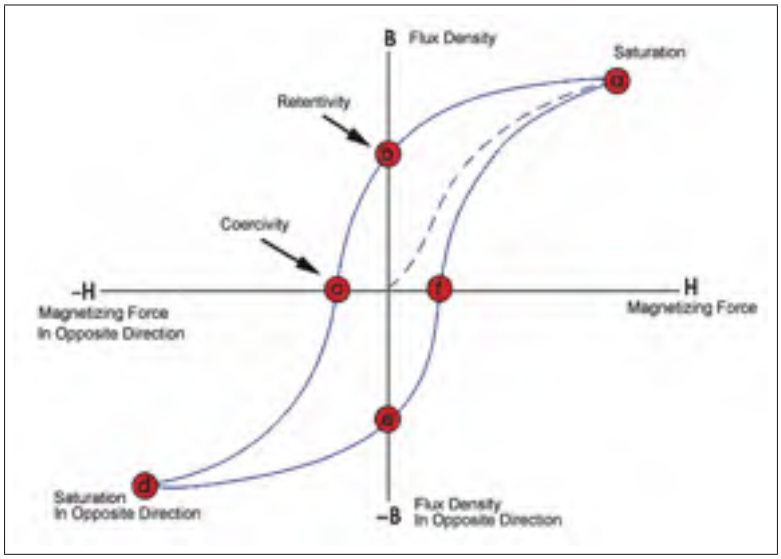

Figure 2.1 Hysteresis cycle. In the state (a), the saturation condition of B is reached. Reproduced from NDT Resource Center (2010)

The magnetic particle is the most reliable method for revealing open to surface discontinuities, especially fine and shallow cracks (Shull (2002)). The MT is a technique easy to conduct, not requiring much training to inspectors. It is capable to inspect parts with diverse shapes and sizes even if the surface is covered with a nonmagnetic coating. Nonetheless, only ferromagnetic materials can be analyzed through MT. The method often burns and generates electrical arc in the contact points (Shull (2002)). Typical mechanical parts inspected with magnetic particles include steel coil springs, welds and railroad wheels (Shull (2002)). Even though the technique

is capable to detect indications below the surface, when the inspection is verifying the presence of them, ultrasound and radiography are the preferred techniques (Shull (2002)).

2.4 Eddy Current Testing (ET)

The *NDT* method called eddy current was developed based on several technological principles such as electromagnetic induction of coils, the change of impedance of the inspection coil caused by small defects and metallurgy (American Society for Materials (2002b), Shull (2002), NDT Resource Center (2010)). To understand this technique, two physical phenomena must be explained: 1) Whenever an alternating current is employed to a conductor A, a magnetic field a is produced in and around the conductor, being proportional to the alternating current which provoked it. 2) In case a second conductor B is approached to the surrounding area where A is placed, a is modified and current is induced in B. The eddy current is, thus, a circular path current which is induced in a second conductor (NDT Resource Center (2010)). Regarding the circuit 1 in figure 2.2, the magnetic field generates induced current in the circuit 2. The current flow in the circuit 2 causes its own magnetic field which, as well, influences subsequently the magnetic field of the circuit 1. Therefore, the net magnetic field in the circuit in the right is partially generated by the current of both circuits, being proportional to them (NDT Resource Center (2010)). In these circuits, the self inductance L_1 and L_2 are dependent on the number of coil turns and the material conductivity, permeability and dimension. The mutual inductance M of both circuits consequently varies according to this geometrical feature, being identical for both circuits. The fluxes ϕ_1 and ϕ_2 are then given by NDT Resource Center (2010):

$$\phi_1 = L_1 * i_1 + i_2 * M \tag{2.1}$$

$$\phi_2 = L_2 * i_2 + i_1 * M \tag{2.2}$$

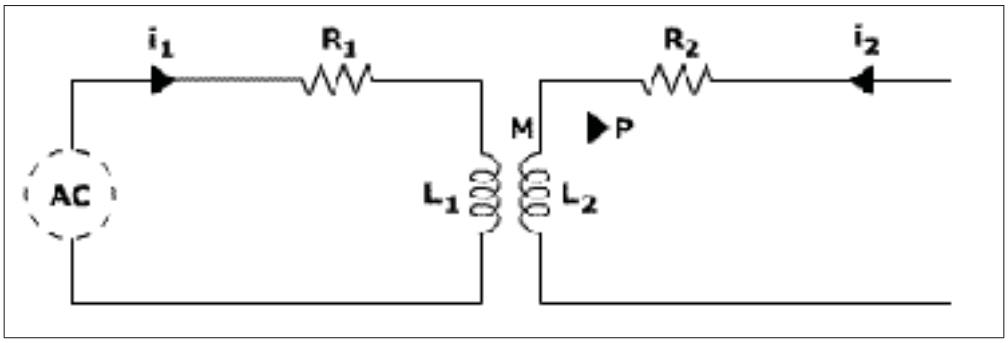

Figure 2.2 ET inspection equivalent system. The circuit on the left is the "circuit 1"; the circuit on the right, the "circuit 2".
Reproduced from NDT Resource Center (2010)

In ET, the inspection is a verification of mutual induction variations. The probe which performs the measurement is a coil whose wire receives an alternating current. The current must be measured with proper equipment. Regarding the figure 2.3, the probe would be electrically equivalent to the circuit 1 in figure 2.2 and any part of conductive material where the ET is executed represents the circuit 2 in figure 2.2 (NDT Resource Center (2010)).

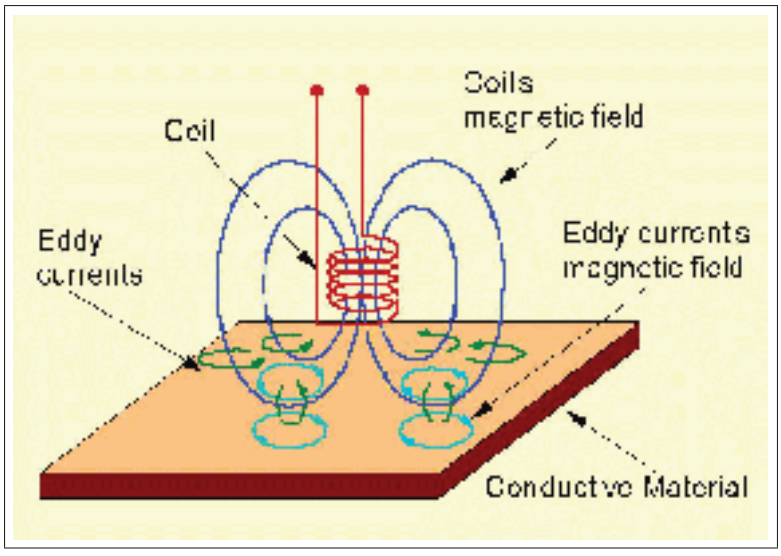

Figure 2.3 ET probe executing the inspection in a conductive material.
Reproduced from NDT Resource Center (2010)

The eddy current, as already mentioned, creates its own magnetic field that influences the primary magnetic field of the corresponding coil. Basically, variations in resistance and in coil reactance due to the approximation of the probe to a conductive test sample provide information

for its analysis. These data includes the quantity of material which modifies the coil's magnetic field, the electrical conductivity, the magnetic permeability, the presence of indications. The liftoff, which corresponds to the distance from the coil to the conductive material being tested has an important role in the net circuit mutual-inductance. It is the measured property that is employed for the estimation of thickness of nonconductive coatings (NDT Resource Center (2010)). The use of ET, can be a powerful tool for detecting discontinuities such as cracks and damages caused by excessive heating. It can be adapted for sorting the material in terms of conductivity, permeability and monitoring of heat treatments (American Society for Materials (2002b), Shull (2002), NDT Resource Center (2010)).

The ET, differently to PT, MT and UT is a non-contacting method. No surface preparation is required. It is a cost-effective, portable and sensitive NDT technique for inspection of diverse specimen geometries. Various material properties can be evaluated through eddy current. However, regarding cracks, its sensitivity decreases rapidly as the crack becomes parallel to the inspected surface. Once the probe is sensitive to diverse parameters, the interpretation of indications is complicated.

2.5 Ultrasound (UT)

The ultrasound is a *NDT* technique based on the emission of sound in a frequency from 0.2 to 25MHz that propagates through a workpiece. Any unexpected change in the acoustic impedance (behaviour that characterizes the presence of an indication) generates certain reflection of the emitted sound. This event is detected by a piezoelectric crystal that converts electrical energy into mechanical energy (ultrasound) and mechanical into electrical energy as well, being integrated to diverse signal acquisition systems for NDT inspection (American Society for Materials (2002b), Shull (2002), NDT Resource Center (2010)). Figure 2.4 depicts the inspection through UT of a workpiece.

The ultrasonic is employed for revealing internal indications in metals and alloys. The fabrication and maintenance of aircrafts, piping systems, pressure vessels, jet engines, vehicles, bridges, railroad, nuclear plant equipment which require safety demand ultrasound systems

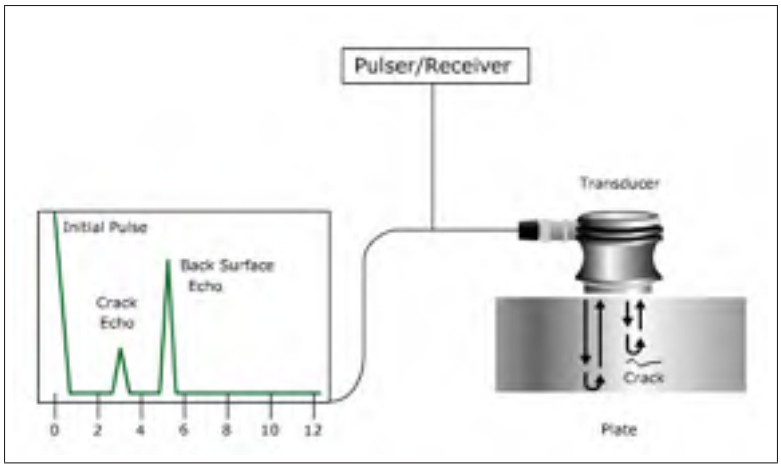

Figure 2.4 Workpiece inspected through ultrasound technique. Once the part contains a discontinuity, the corresponding echo is detected by the transducer.
Reproduced from NDT Resource Center (2010)

for inspection. Internal discontinuities such as cracks, voids, inclusions bursts, flakes, laminations, shrinkage, piping and bridging are detected through UT (American Society for Materials (2002b)).

Differently to RT, the ultrasound is not harmful to the environment or health. It can be used in inspection of all sort of materials and complex geometries. The UT allows the perfect detection of the size and location of indications while the radiography does not provide information related to the depth. Nonetheless, the method requires high experienced personnel. The information is not easily recorded as the radiography. In most cases, the transducer must be in contact with the object through a coupling layer. The cracks which are longitudinal to the ultrasound wave cannot be detected.

2.6 Radiography (RT)

The radiography is a nondestructive testing method through which variations of the specimen thickness, density and diverse material composition causes different absorption of penetrant radiation (American Society for Materials (2002b)). These indications are recorded in photographic films or image tubes or radiation electronic detectors (American Society for Materials (2002b)). The material density at certain part location can be compared to the surrounding

areas through RT (American Society for Materials (2002b)). It is widely used for inspecting castings, weldments, forged and rolled parts contained in high pressure equipment such as boilers, turbines for ensuring that they are free of internal discontinuities (American Society for Materials (2002b)). Figure 2.5 illustrates the technique.

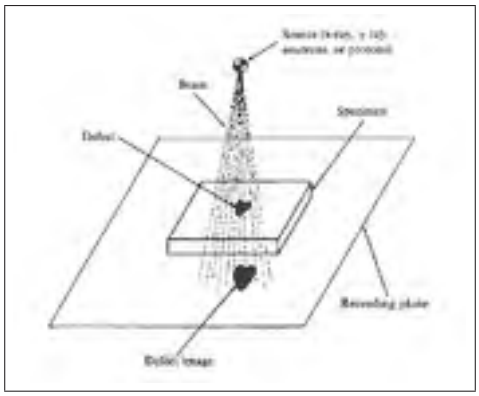

Figure 2.5 Radiography testing. Radiation reaches a surface containing a discontinuity. Variations in radiation absorption are registered on a radiographic film. Reproduced from Bray and Stanley (1997)

The method allows the record of an inspection for future comparison. It does not require prior calibration (American Society for Materials (2002b)). The geometry of the inspected part does not have impact on the analysis. Nonetheless, it is harmful for health, being required special facilities and equipment to ensure the safety (American Society for Materials (2002b)). It does not provide information about the depth of an indication (American Society for Materials (2002b)). The orientation of linear discontinuities plays important hole in detection. The access of both sides of the specimen is mandatory (American Society for Materials (2002b)).

2.7 Summary

The nondestructive testing aims at verifying the integrity of a part without any sort of deterioration. They are employed for ensuring in raw materials or finished components the absence of surface and internal discontinuities. Among the methods for detecting open to surface indications, the magnetic particle seems to be the easiest to conduct, because it does not require surface preparation like liquid penetrant and minimum training is mandatory for the test conduction. However, only workpieces made of ferromagnetic metals are feasible to be inspected

through this technique. Through the PT method, in spite of time-consuming surface preparation, almost all materials can be inspected (exception for porous structures). Considering the eddy current, even though none chemical application is required, the interpretation of the obtained signal is complex. This is consequence of the variety of properties that can be detected through ET.

Between the methods for revealing internal indications, the radiography requires special caution against the radiation hazard while the ultrasound is completely harmless. High level of experience and knowledge of the technique is required for the perfect UT interpretation. On the other hand, RT is simple to detect and interpret indications. Through the radiography, inspection data is easily recorded, while, in the ultrasonic, this is not so obvious. Tables 2.1 and 2.2 contain a brief description, advantages and disadvantages of the NDE methods explained in this chapter.

Table 2.1 Summary of PT, MT, ET, UT and RT technique descriptions

Method	**Technique Description**
PT	Penetrant is drawn into open to surface discontinuities. After dwell time, excess of penetrant is removed from the surface. Only the open to surface discontinuities remain with dye. The developer is applied for providing more background contrast. Visual examination of the specimen surface with or without black light is performed to detect indications.
MT	The inspected part is magnetized through diverse techniques. Ferromagnetic particles are suspended over the surface, being concentrated around surface where discontinuities are located due to field leakage.
ET	Using an inspection coil the conductance of the inspected material is verified based on changes of the mutual inductance. Surface and near surface indications are detected if variations in the expected mutual inductance are observed.
UT	High frequency sound is transmitted into the specimen. Any change in the acoustic impedance along the wave transmission must be detected as a signal corresponding to an internal indication.
RT	Penetrating radiation is emitted, passing through the specimen walls. The energy of the emission is absorbed according to the material density of the specimen. The net radiation energy is recorded on a radiographic film. In a film, the variations of the absorbed radiation correspond to indications.

Table 2.2 Advantages and disadvantages of PT, MT, ET, UT and RT techniques

Method	**Advantages**	**Disadvantages**
PT	All surface discontinuities can be detected in a single inspection, regardless of orientation. It is a cost-effective technique capable to detect fine and tight discontinuities. Can be employed in inspection of a wide range of materials.	The condition of the specimen in terms of cleanliness is important. Only surface openings are detected through the technique. Parts with porous structures cannot be assessed with PT.
MT	The most convenient method for the detection of shallow, fine surface cracks. It is a quick, simple and cost-effective NDT method. It is easy to conduct, not requiring much training.	Only workpieces made of ferromagnetic materials can be detected through MT. The orientation and intensity of the magnetic field is an important factor in inspection. The specimen must be frequently demagnetized after testing. Parts are often burnt. Electrical arcing may occur.
ET	It is a technique sensitive to discontinuities. It is highly repeatable. It is a noncontacting method, allowing high scanning speeds. It does not require prior surface preparation.	The teory related to the ET requires certain level of knowledge of mathematics and electrical principles. It is sensitive to a wide range of parameters, being complex the signal interpretation. Only workpieces made of conductive materials can be inspected.
UT	Excellent technique for detecting internal indications. It is not harmful for health or environment. It is possible to inspect all sort of materials and complex geometries.	The technique requires inspectors with high experience. The transducer must be in contact with the object through a coupling layer. All cracks whose length lies parallel to the direction of wave travel cannot be detected through UT.
RT	Provides information such as material density, thickness and the presence of indications. Permanent record is easily obtained per inspection. A wide range of materials can be inspected through the technique.	The radiation beam employed in the technique is dangerous, requiring special protection equipment and facilities. RT does not indicate the depth of discontinuities. It presents limited depth of penetration.

CHAPTER 3

THE STATE OF THE ART IN LIQUID PENETRANT INSPECTION

The liquid penetrant testing (PT) is a nondestructive evaluation method employed in the inspection of raw materials and component parts, revealing surface indications. For correct inspection, it is mandatory: (i) special cleaning of the specimen and (ii) either good eyesight (in case of a human inspector) or efficient detection system (in case of automated inspection) (Shull (2002), American Society for Materials (2002b), NDT Resource Center (2010)).

Through this technique, it is more likely to detect small round, deep, narrow and smooth surface discontinuities. These openings trap more penetrant than small linear and shallow. The penetrant spreads more easily over smooth surfaces, being more complicated to remove it in rough workpieces. Due to this reason, high roughness parts are proner to result in overwashing (NDT Resource Center (2010)).

In order to perform PT, the penetrant must wet the whole specimen surface, entering into surface discontinuities. According to Shull (2002), this process is composed by the following sequence of steps:

1. Detailed visual inspection of the specimen to be tested;
2. Pre-cleaning the specimen surface;
3. Penetrant application to specimen surface;
4. Dwell time;
5. Penetrant Excess Removal;
6. Developer Application;
7. Inspection.

In the detailed visual inspection of the specimen, it must be verified its condition in terms of cleanliness (Shull (2002)). Based on it, the part is cleaned according to inspection specifications. Contaminants such as oily films, dirt, grease, rust, paint scale, slag, welding flux and cleaning residues compromise the effectiveness of the penetrant testing and must be removed through a suitable method (Shull (2002)). Erroneous cleaning is one of the main causes of failure of the technique (Shull (2002)).

After, the cleaning, the penetrant may be applied. It flows on the specimen based on surface tension, contact angle, surface wetting, and capillarity. To visualize indications of a determined size, it takes some time for the dye to be drawn into surface discontinuities. This period is referred as *dwell time* (NDT Resource Center (2010), Shull (2002), American Society for Materials (2002b)).

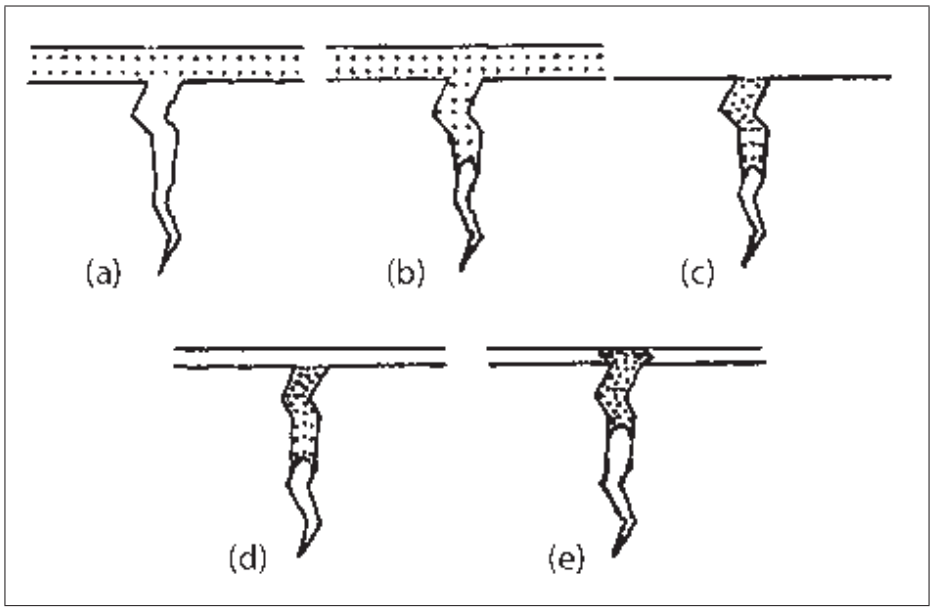

Figure 3.1 Liquid Penetrant Inspection Steps. In (a), the penetrant is applied in a clean surface; in (b), the penetrant is drawn into a discontinuity; in (c), the penetrant excess is removed from the surface; in (d), the developer application to the surface; in (e), the surface is ready for interpretation and detection of discontinuities.
Reproduced from Shull (2002)

Allowing suitable time for the dye entrapment, the excess of penetrant must be removed from the part surface. Only the discontinuities must be kept with penetrant. The materials used in

excess removal should be selected according to the nature of the penetrant (a proper emulsifier which must dilute the penetrant) (NDT Resource Center (2010), Shull (2002), American Society for Materials (2002b)).

Removing the excess of penetrant, an even thin layer of developer should be applied to the specimen surface. The developer acts as a blotter, in discontinuity locations, being the penetrant drawn from them, spreading over the surface. The developer is basically composed by a powder whose function is to increase the seeability of indications. The powder draws the penetrant from the discontinuity by merging absorption (where the penetrant is drawn into the powder particles) and adsorption (where the penetrant adheres to the surface of the particles) (NDT Resource Center (2010), Shull (2002), American Society for Materials (2002b)). Figure 3.1 depicts the process from the penetrant to developer application.

After the developer application, the specimen surface may be inspected. Either trained personnel or an effective vision system must identify the indications. In inspection, norms and procedures are specified. Any divergence from the norm may be demonstrated by some indicating medium (Betz (1963), Shull (2002)).

The remainder of this chapter is divided as follows: In section 3.1, the physical phenomena which are essential for the PT such as surface tension and capillarity are defined. In section 3.2, the importance of cleaning prior to chemicals application is described. The most used methods for removing contaminants are explained. In section 3.3, the penetrants are related according to classifications found in the literature. The most used techniques for applying this fluid are investigated. In section 3.4, two dwell modes, often employed in inspection, are analyzed. The methods which are used for the excess penetrant removal are mentioned in section 3.5. Developers, mechanism of fluorescence in penetrants, inspection, reference panels, performance metrics and FPI in aerospace are topics emphasized in sections 3.6, 3.7, 3.8, 3.9, 3.10 and 3.11 respectively. At the end, a summary recapitulates the most important aspects covered in this chapter.

3.1 Physical Phenomena related to PT

The liquid penetrant testing is a nondestructive method based on two main physical phenomena: the surface tension and the capillarity (also referred as capillary action or force) Shull (2002). The surface tension is a property which is responsible for contracting a liquid into a sphere due to cohesive forces among its surface molecules (Shull (2002), American Society for Materials (2002b)). It counterbalances the internal hydrostatic pressure of a liquid. The capillarity, in PT, is a force which transports a liquid into confined openings such as surface cracks, laps, porosities, cold shuts etc and exudes from these discontinuities, resulting in surface indications (Shull (2002), American Society for Materials (2002b)).

When a penetrant is applied to a solid surface of a part in PT testing, the surface tensions of the interfaces between solid and gas, gas and liquid and liquid and solid (identified respectively by γ_{sg}, γ_{gl} and γ_{ls}) compete with the adhesive force Ad among the molecules of the liquid and solid surfaces (Shull (2002), American Society for Materials (2002b)). The dye spreads over the specimen until the energy balance equilibrium is reached ($\sum F_{horizontal} = \gamma_{ls} - \gamma_{sg} - \gamma_{gl} cos(\theta) = 0$) where θ is an angle formed between the liquid and solid surfaces which is known as the contact angle or the wetting ability (Campbell and McMaster (1967), Glaskov (1989)). The magnitude of θ is dependent on (i) the penetrant compounds and (ii) the surface to which is applied. It indicates the degree to which the penetrant wets the inspected part (Shull (2002), American Society for Materials (2002b)). Figure 3.2 depicts the surface tensions of the interfaces, adhesive force and contact angle θ. According to Shull (2002), based on θ, the liquids present:

- *High Wetting Ability*, if $\theta < 90°$. Regarding that the penetrants must coat the specimen surface, low contact angle is a requirement (Shull (2002), American Society for Materials (2002b));
- *Low Wetting Ability*, if $\theta > 90°$ (Shull (2002), American Society for Materials (2002b)).

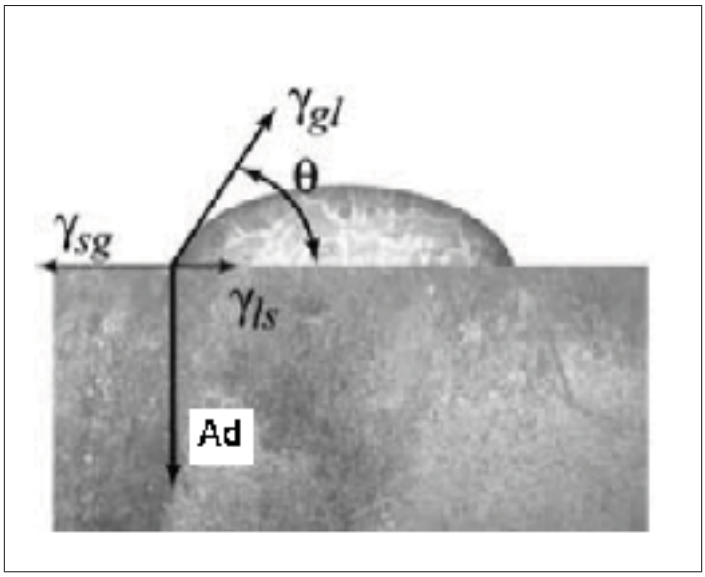

Figure 3.2 Interface among liquid, solid and gas. *Ad* is the attractive force from the fluid to the solid; θ is the contact angle; γ_{gl}, γ_{ls}, γ_{sg} are respectively the surface tension between gas and liquid, liquid and gas and solid and gas.
Reproduced from Shull (2002)

The wetting ability and density of the liquids has a direct impact on the capillary action in PT (Shull (2002), American Society for Materials (2002b)). Even though, the open to surface discontinuities are not capillary tubes, their interaction with penetrants resembles the meniscus rise and depression which characterizes the capillary action (Shull (2002), American Society for Materials (2002b)). In these tubes, the rise and depression of meniscus depends on the upward and downward forces (American Society for Materials (2002b)). The former is equivalent to $\gamma_{gl} * cos(\theta)$ times the perimeter of the meniscus which is given by $2\Pi r$ where r is the meniscus radius (American Society for Materials (2002b)). The latter corresponds to the weight of the liquid column given by $(\Pi r^2 h)\rho g$ where h, ρ and g are respectively the meniscus height, the density of liquid contained in the capillary tube and the acceleration of gravity (American Society for Materials (2002b)). If the upward force is greater, the capillary rise occurs. If they have the same magnitude, the meniscus is not formed. In the last case, if the downward force has the higher intensity, capillary depression happens. Figure 3.3 depicts the capillary rise and depression.

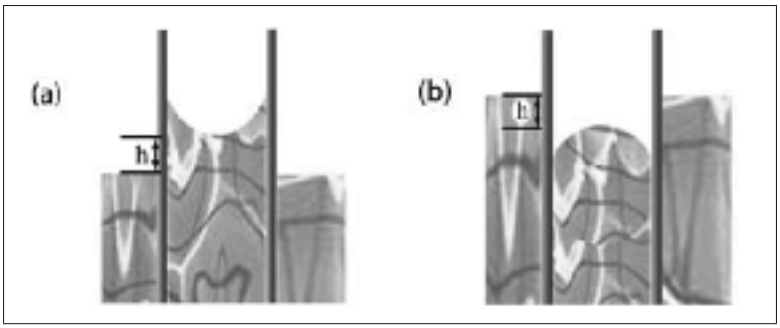

Figure 3.3 Capillary action of a fluid in a container. In (a) the fluid rises a distance *h* in the container forming a meniscus; in (b), it falls into the container a distance *h*. Reproduced from Shull (2002)

3.2 Pre-Cleaning and Effectiveness of the PT testing

The performance in penetrant testing is directly related to the effectiveness of the pre-cleaning methods. For instance, foreign liquids increase the surface tension and contact angle of penetrants and emulsifiers (Campbell and McMaster (1967)). Oxide coatings, if do not block the discontinuities, increase the drawing force for penetration into them. Monomolecular layer of oil increases the infiltration velocity (Campbell and McMaster (1967)). Regarding these concerns, a suitable technique must be conducted for eliminating all contaminants. It may not result in corrosion and dissolution. Based on the material properties and the present foreign particles, the workpiece may be cleaned through the following methods: detergent cleaning, solvent cleaning, vapour degreasing, descaling (Shull (2002)). These techniques are explained as follows:

- The *detergent cleaning* is basically washing the specimen with soap and water. The detergents may not cause the specimen deterioration during and after testing (Shull (2002));
- The *solvent cleaning* is conducted by applying alcohol or hydrocarbons for removing grease an oils. Care must be taken when applying these chemicals, because of its toxic fumes and flammability (Shull (2002));
- The *vapour degreasing* consists of suspending the specimen above a hot liquid. The vapour from the liquid enters the defects, condenses and returns to its source (Shull (2002));

- The *descaling* consists of cleaning the workpiece employing hydrochloric, nitric or hydrofluoric acids and even strong alkaline solutions. It is often used to remove dust and oxides from metallic surfaces (Shull (2002)).

These techniques previously described can be employed either isolated or combined. The ultrasound combined with those methods can provide good results. Nonabrasive materials such as rags and soft brushes may be used for the application of cleaning fluids without damaging the surface. In case these approaches are not able to clean properly the specimen, abrasive cleaning must be used (Shull (2002)).

The abrasive cleaning with techniques like peening, sanding, scrapping, grit blasting, lapping, honing, tumble de blurring cause the *material smearing*. It compromises the PT inspection, once the open to surface discontinuities can be obstructed by the removed metallic material (Larson (2002)). It is most likely from happening in soft materials such as plastics and aluminium alloys. However smearing is often present in high hardness materials. The machining operations may result in smearing particles as well (NDT Resource Center (2010)). In figure 3.4, there are three photographies which exemplify the smearing.

3.3 Penetrant types and application modes

The penetrant is a solution composed of dyestuff, light petroleum solvents or oils and an unctuous liquid (Sherwin (1974)). The dyestuff is a compound which allows the dye seeability (Sherwin (1974)). The unctuous liquid aims at dissolving the dyestuff in the mixture (Sherwin (1974)). The oils are added for reducing the viscosity of the final penetrant (Sherwin (1974)). In PT testing, the penetrant is the fluid which enters the discontinuities aiming at generating indications at the corresponding locations. It is the main chemical product utilized in this NDT method (Betz (1963)). In the literature, they are often divided into types and sensitivity levels. Regarding the first classification, there are two sorts of penetrants: i) fluorescent (type I) penetrant and ii) visible or color-contrast (type II) penetrant. The former requires blacklight in a dark environment for revealing indications. The latter demands visible light for detecting

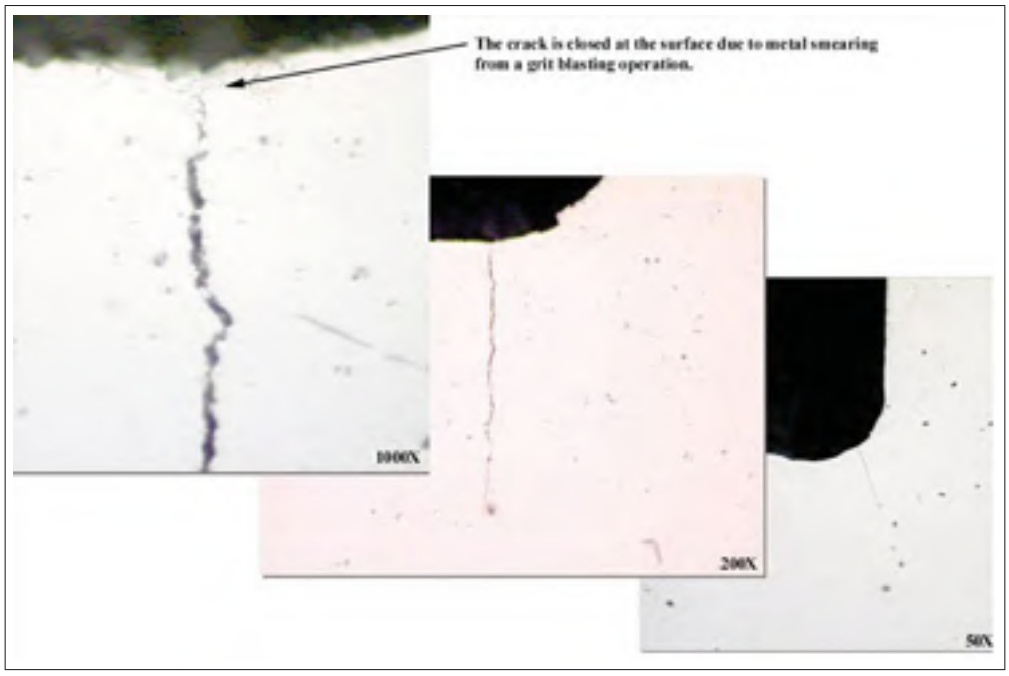

Figure 3.4 Three surface crack microscope photographies with diverse magnification. The crack opening is closed by the metallic residual particles. Reproduced from NDT Resource Center (2010)

them. When deciding the penetrant type, surface condition, features of discontinuities, size of workpiece, required sensitivity, time and place of inspection must be considered (American Society for Materials (2002b)). In general, when the discontinuities are small, fluorescent dyes are more capable to produce a detectable indication, once the human eye is more sensitive to fluorescent emissions especially on dark background. However, when discontinuities are large, high sensitivity may not be desired, because it can result in non-relevant indications. In this case and in the inspection of very high roughness surfaces, the visible dyes are the most recommended (NDT Resource Center (2010)). Figures 3.5 and 3.6 contain images of the inspection with type I and II penetrants respectively.

In addition, as previously mentioned, there is other classification of penetrants based on sensitivity levels related to the indication detection. They are inversely proportional to the penetrant viscosity which is the fluid resistance to flow on a surface. It influences the ability of the dyes to enter a discontinuity due to its effect on the penetration speed. As viscous as the fluid is, less

sensitive it is. The most sensitive penetrants are, in general, the most expensive. According to American Society for Materials (2002b), the five sensitivity levels are:

- Level 1/2 - Ultra Low Sensitivity,
- Level 1 - Low Sensitivity,
- Level 2 - Medium Sensitivity,
- Level 3 - High Sensitivity,
- Level 4 - Ultra High Sensitivity.

Figure 3.5 Inspection under UV light in a treated surface.
Reproduced from NDT Resource Center (2010)

The penetrant is mostly applied through two different manners (McMaster *et al.* (1982)): dipping and spraying. Through dipping, the parts are immersed in a dip tank which contains penetrant. They are placed inside baskets or hold by fixtures for the immersion (McMaster *et al.* (1982)). In case spraying is adopted, it is applied with a spray can or spraying systems (McMaster *et al.* (1982)). Figures 3.7 (a) and 3.8 respectively illustrate a basket containing parts during the application by dipping and a manual spraying system.

Figure 3.6 Indication formed using type II penetrant.
Reproduced from NDT Resource Center (2010)

3.4 Dwell Time and Modes

After applying the penetrant, the period during which it is drawn into surface discontinuities through capillary forces prior to excess removal is called *Dwell Time*. There are two dwell modes: the immersion dwell and the drain dwell (Sherwin (1974)). In the former mode, the workpiece is kept immersed into a dip tank prior to excess removal (Sherwin (1974)). In the latter mode, during the dwell time, the part is drained as illustrated in figure 3.9 and part of the excess of liquid penetrant is reused in other inspections. Albeit penetrant manufacturers may suggest specific dwell times for the detection of certain types of discontinuities, they must be defined based on experimentation. The most suitable period should be specified according to the peculiarities of the application for which the part serves. There is not enough effective literature for supporting it (Larson (2002)).

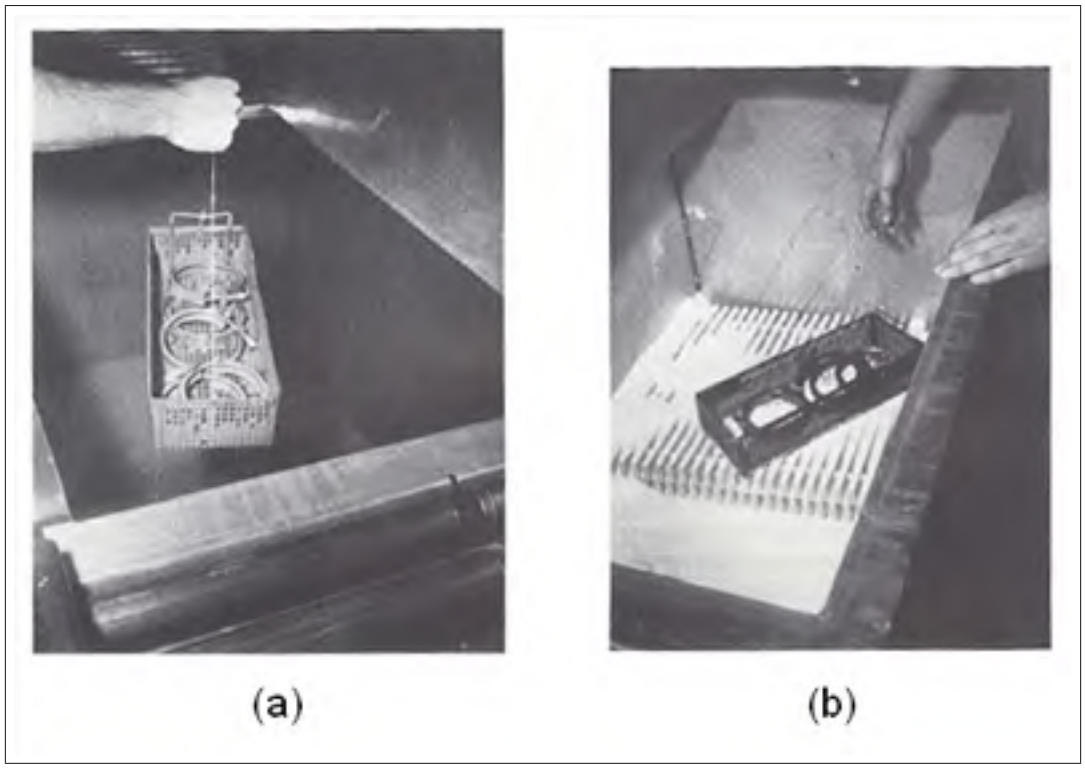

Figure 3.7 Example of liquid penetrant chemicals application. In (a), there is a picture of liquid penetrant application in a dip tank. The parts contained in the basket are immersed in it; in (b), the dry powder is applied to the workpieces.
Reproduced from McMaster *et al.* (1982)

3.5 Excess Penetrant Removal and Inspection Sensitivity

In PT, the sensitivity, according to Robinson and Schmidt in Robinson and Schmidt (1984), depends on the following factors: (i) The amount of penetrant entrapped into discontinuities and (ii) the resulting indication brightness. In fluorescent penetrant inspection, the ability of a dye to fluoresce only where indications are located is defined as sensitivity (Alburger (1966), Vaerman (1985)). This implies that the penetrant must be properly removed from the surface, enhancing the contrast among indications and background for achieving good sensitivity in inspection. The following methods for conducting this task are listed in the literature:

- The method A consists of using penetrants whose excess is removed through water spray jets. These dyes are often referred as water-washable dyes. It is recommended for quick

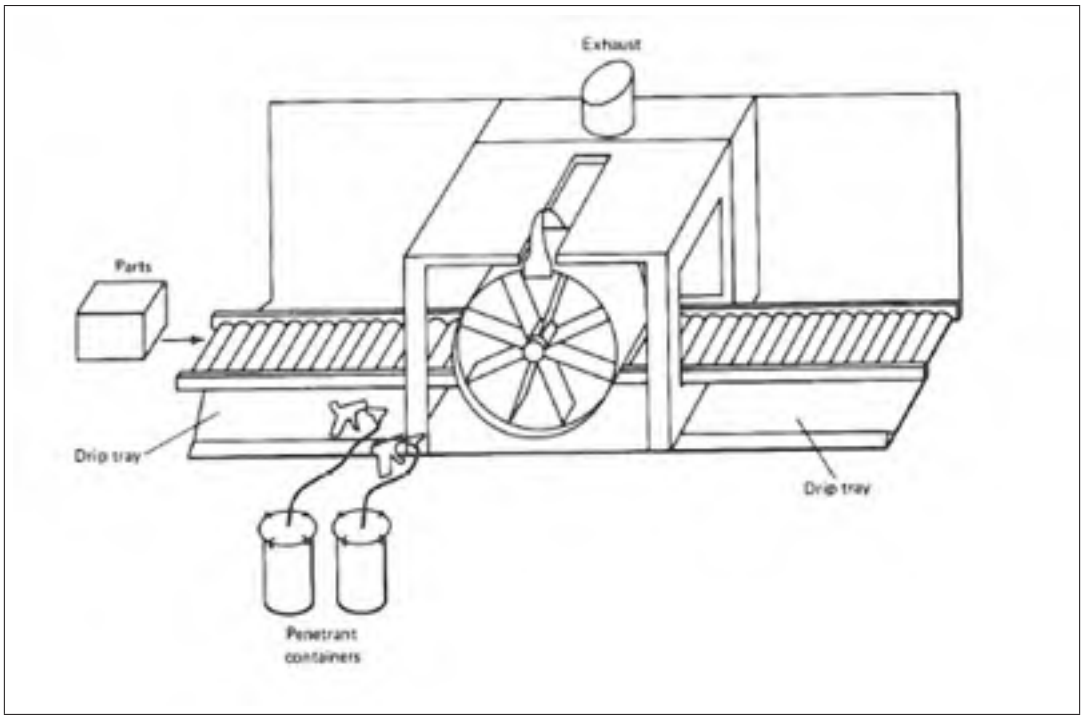

Figure 3.8 This schematics depicts a typical hand operated electrostatic spray gun station for the application penetrant. The parts are translated over the drip tray, an operator applies the penetrant with the electrostatic spray gun, and an exhauster removes penetrant particles from the air.
Reproduced from McMaster *et al.* (1982)

inspections. However, inadequate cleaning can result in overwashing (American Society for Materials (2002b)).

- Through the method C, the penetrant excess is removed with solvent. It is mostly employed for localized area inspections. Solvent-removable dyes are not convenient for high production rates. If properly conducted, it is regarded one of the most sensitive methods (American Society for Materials (2002b)).

- The methods B and D were developed for reducing the overwashing in the excess removal, which compromises the sensitivity. They consist of applying postemulsifiable penetrants which are not removed as easy as water washable penetrants. For their removal, it is required a emulsifier before rinsing. Two types of postemulsifiable penetrants are found in the market: Lipophilic and Hydrophilic. Inspections with the former characterizes the method B, requiring oil-based emulsifier for allowing the penetrant re-

Figure 3.9 Draining station picture. Part of penetrant excess is drawn back to the penetrant application dip tank. This guarantees less penetrant waste, once part of the excess removed is reused.
Reproduced from NDT Resource Center (2010)

moval; The use of the latter (which defines the method D), implies that the excess must be removed through and water-soluble emulsifier, lifting the penetrant excess from the surface with water rinse (American Society for Materials (2002b)).

3.6 Developers

The developer is an element of the PT which reveals indications for the inspectors gradually (Betz (1963)). It behaves as a blotting agent, improving the draw of penetrant from a open to surface discontinuity (Betz (1963)). It acts as a reflective layer increasing the amount of liquid penetrant exposed to the eyes entrapped in an indication (Betz (1963)). Composed by white

pigmentation, a high whiteness developer increases the contrast between the background and indication, improving the sensitivity of the inspection (Glaskov and Bruevich (1985)).

There are four types of developer: The *water-soluble*, the *water-suspendable*, the *solvent-suspendable* and the *dry powder* developers.

- The *water-soluble* developer consists of chemical components dissolved in water. Evaporating the water, the remaining elements results in a developer layer (Shull (2002), NDT Resource Center (2010)).
- The *water-suspendable* developer consists of insoluble developer particles suspended in water. The suspension must be agitated for keeping the concentration. Evaporating the water, after the application, only a developer layer remains on the surface (Shull (2002), NDT Resource Center (2010)).
- The *solvent-suspendable* developer comprises insoluble developer particles suspended in a volatile solvent. In order to keep the suspension concentration, it must be constantly agitated. After, applying the suspension, the solvent evaporates resulting in a developer layer (Shull (2002), NDT Resource Center (2010)).
- The *dry powder* is the pure developer which is applied directly to the surface (Shull (2002), NDT Resource Center (2010)). Figure 3.7 (b) illustrates the dry powder application using a basket containing parts.

3.7 Mechanism of Fluorescence in Penetrants

In PT testing, when type I penetrants are being used in surface preparation, it is required black-light illumination in a dark environment for revealing indications (Betz (1963)). Lamps whose light energy is just below the visible spectrum of violet (mostly around 365nm) provide this necessary radiation (Betz (1963)). The absorption of this exciting emission by penetrant entrapped in discontinuities generates their fluorescence which characterizes a variation of penetrant testing that is identified as *Fluorescent Penetrant Inspection (FPI)*.

The FPI is mostly employed when it is mandatory high sensitivity in detection. The characteristic fluorescence is explained by the photon absorption of the incident energy at certain wavelength by a fluorescent material surface which consequently re-emits light with the same energy at either identical or longer wavelength (Larson (2002)). This happens, because the absorbed radiation causes changes in the electronic distribution which forces changes in the molecular structure and consequently fluorescent light is emitted (Graham (1967)).

3.8 Inspection and Evaluation

The liquid penetrant testing allows the inspector or machine vision system to detect surface discontinuities. This includes all cracks, porosities, inclusions, segregations, laps, etc which can be found directly on the surface. Whenever an indication is revealed, the inspector must investigate its pattern in order to define which discontinuity it may represent, its actual dimensions and what consequences will happen if the corresponding part is placed in service (Tracy and Moore (2001)).

The evaluation of indications is usually based on quantitative data extracted from them. In case of PT, this information is represented by their dimensions which are generally larger than the actual discontinuity (Tracy and Moore (2001)). Based on the inspector's experience, he/she may identify the corresponding type and the approximate height/width. Analyzing this data, the effect of them may be evaluated (Tracy and Moore (2001)).

Examples of patterns usually observed in PT are illustrated in figure 3.10. Laps can be represented by long, continuous indications as exemplified in (a) and (b) (Tracy and Moore (2001)). If this discontinuity is submitted to successive forging, a welded lap can be formed, resulting into indications as depicted in (c) (Tracy and Moore (2001)). Furthermore, the patterns in (a) and (b) can be interpreted as cracks (Tracy and Moore (2001)). The sketched shape in (b) can be classified as a cold shut as well (Tracy and Moore (2001)). Subsurface cracks with intermittent openings to surface and seams without adequate amount of entrapped penetrant may result in the same indication drawn in (c) (Tracy and Moore (2001)). The porous surface appearance illustrated in (d), may be interpreted as porosities caused by entrapped gases in casting or

welding if applicable or surface shrinkage cavities formed during the solidification in casting operations (Tracy and Moore (2001)).

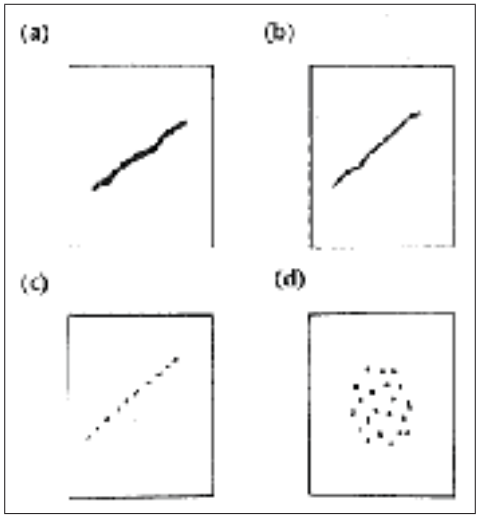

Figure 3.10 Schematics representing often detected indication patterns. In (a), an opening which may be a surface crack; in (b), a thin indication which may represent a tight open to surface crack or a surface cold shut; in (c), there is a partially welded lap; in (d), the indications rounded in the shape of bubble may be porosities or pits. Reproduced from Tracy and Moore (2001)

3.9 Comparators and Reference Panels

For the analysis of inspection system and materials performance, the development of programs for the quality control are highly recommended (Tracy and Moore (2001)). In the market, reference panels with a wide range of crack sizes are available, being suitable to utilize them as parameter for comparisons. Applying liquid penetrant, developer, emulsifier(if applicable) onto these standard references, recipe dependent amounts of these chemicals can be defined for obtaining a desired seeability/brightness ratio, according to crack dimensions (Tracy and Moore (2001)).

Using the twin NiCr tapered test panel, as depicted in the figure 3.11, it is feasible to develop a side-by-side comparison between two diverse sets of PT chemicals (2 sets of liquid penetrants, developers, emulsifiers)(Tracy and Moore (2001)). This panel is divided into two identical sections of cracks separated by a parallel line placed in the intersection of the two sections

(Tracy and Moore (2001)). The emulsification, dwell and development times can be adjusted using this panel comparing the sections with different settings (Tracy and Moore (2001)).

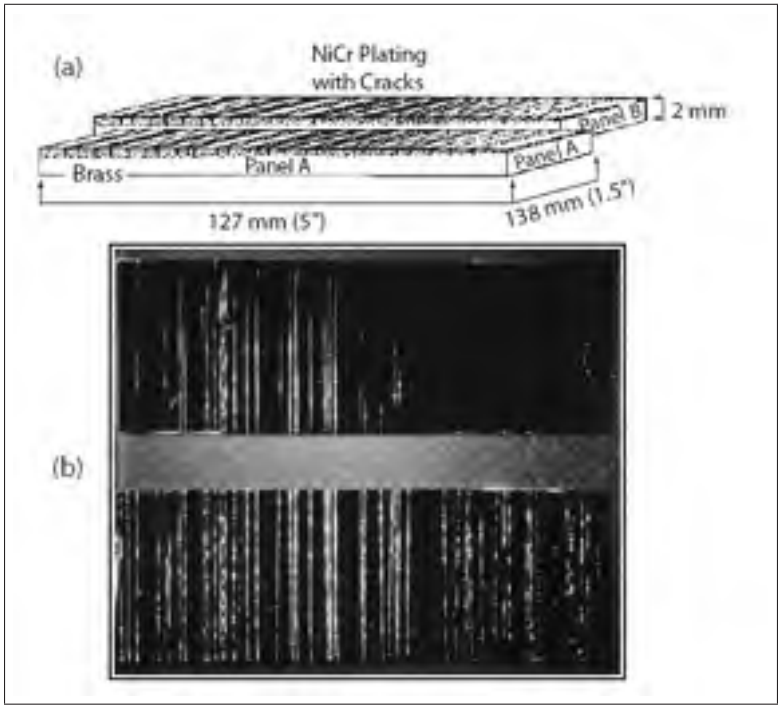

Figure 3.11 In (a), there is a schematics of twin NiCr tapered test panel; in (b), the effect of two different penetrant is evaluated with the twin panels.
Reproduced from Shull (2002)

Other option for comparing penetrant testing settings is the use of the twin penetrant system monitor (PSM) panel. This panel was designed by Pratt Whitney Aircraft Corporation. It is widely used in the observation of anomalies in systems. It is made of stainless steel with 100, 150 and 2.3 millimeters of width, height and thickness respectively (Tracy and Moore (2001)). In each side of this panel, five star-shaped cracks are generated through an indentation similar to the applied in hardness testing. They are formed and organized vertically according to the length as illustrated in figure 3.12. The cracks 1, 2, 3, 4 and 5 measure respectively 0.38x0.79mm, 1.17x1.57mm, 1.91x2.36mm, 3.18x4.34mm and 4.57x6.35mm (Vasquez (1997), Vasquez (2002)). This panel, likewise the NiCr tapered panel in figure 3.11, may alert inspectors/machine vision systems for contaminants in chemicals like penetrant, developer,

emulsifier. It may provide useful information concerning the change of these components, considering that they influence directly the seeability of indications (Tracy and Moore (2001)).

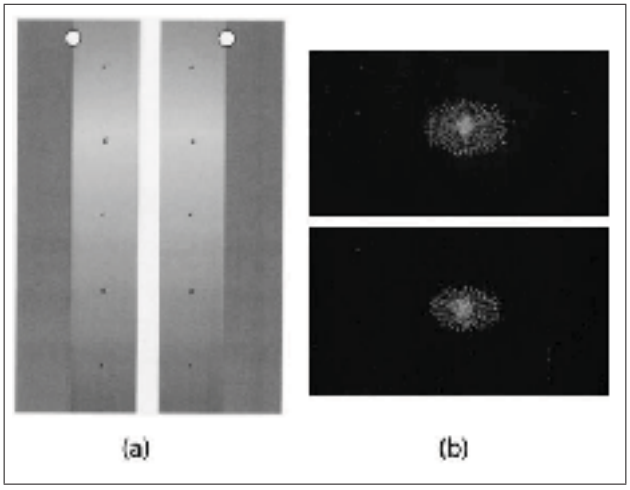

Figure 3.12 In (a), twin known defect test panels with 5 star-shaped cracks each; in (b), there are two pictures of the PT patterns of two cracks contained in the panels of (a). Reproduced from Shull (2002)

3.10 The Capability and Reliability in PT inspection

The liquid penetrant inspection can be evaluated based on the smallest detectable surface discontinuity length (or width or depth) (Tracy and Moore (2001)). This factor, named as *detection threshold*, is dependent on various parameters related to the specimen, chemicals involved, application technique, contamination, dwell time, etc (Tracy and Moore (2001)). The most common metric for quantifying the capability of a liquid penetrant procedure is the probability of detection *(POD)* curve (American Society for Materials (2002b), Rummel (1998), Grills (2001)). It can be traced, if diverse probabilities of detections according to length (or width or depth) of surface discontinuities are obtained (Tracy and Moore (2001)).

In figure 3.13, there is a example of curve POD(%) X crack length (mm) extracted from Tracy and Moore (2001). In Tracy and Moore (2001), it is recommended that the detection threshold should be the point where the curve crosses 90% of POD. In this case, it was set to 3.5 millimeters of length. This value represents the *capability* of the procedure or inspection system with a reliability of 90% (the respective probability of detection) which is regarded as metric

of repeatability and reproducibility in detection of cracks. The *confidence level* for the 3.5 millimeter crack is obtained according to the crack distribution used in the referred experiment (Tracy and Moore (2001)).

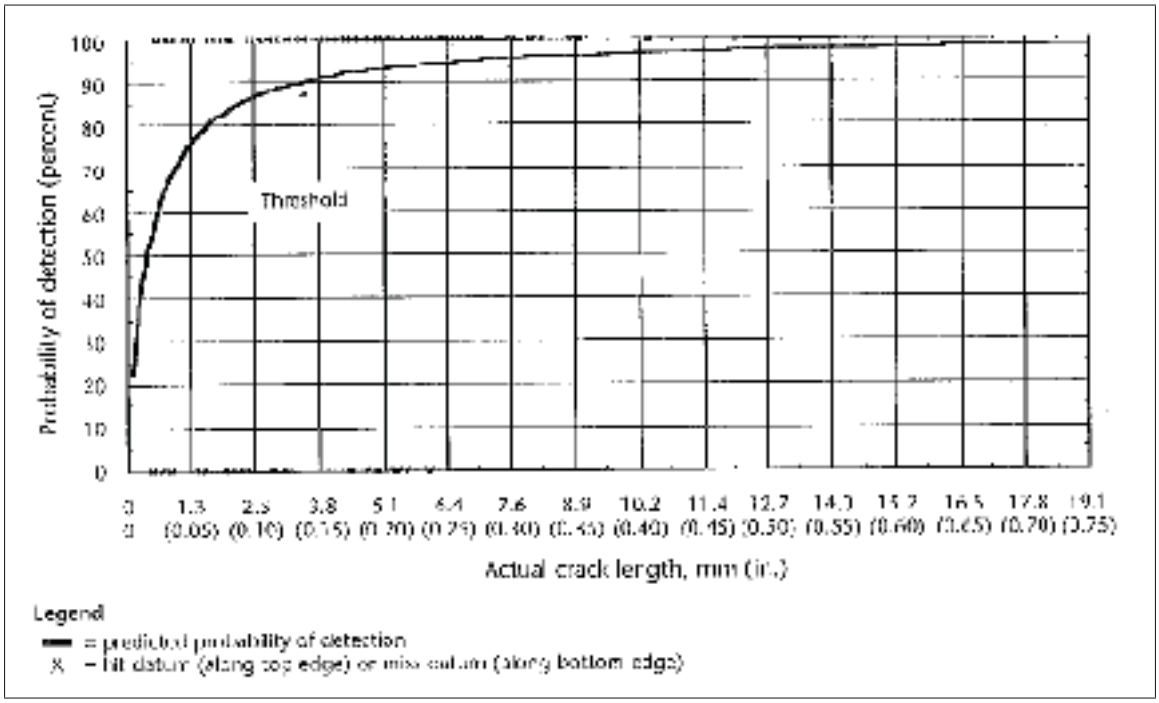

Figure 3.13 Example of Probability of Detection (%) X Actual crack length (mm(in.)) curve whose detection threshold was set 3.5 millimeters (0.14 inches) of crack length. Reproduced from Tracy and Moore (2001)

3.11 Fluorescent Penetrant Inspection in Aerospace

In nonmagnetic aircraft workpieces, the fluorescent penetrant inspection is largely employed in the detection of open to surface indications. Parts which comprise the wings, the fuselage, the turbines, compressors, the engines of planes are inspected through PT. Aircraft structures made of honeycomb core (such as illustrated in figure 3.14) are verified through FPI for preventing the water entry (Tracy and Moore (2001)). Among the aircraft fleet most often detected indications, in Tracy and Moore (2001), two categories are specified for their classification:

1. *Linear Indications* comprises all indications whose length is either equal or greater than three times the width;

2. *Rounded Indications* comprises the remainder detected indications.

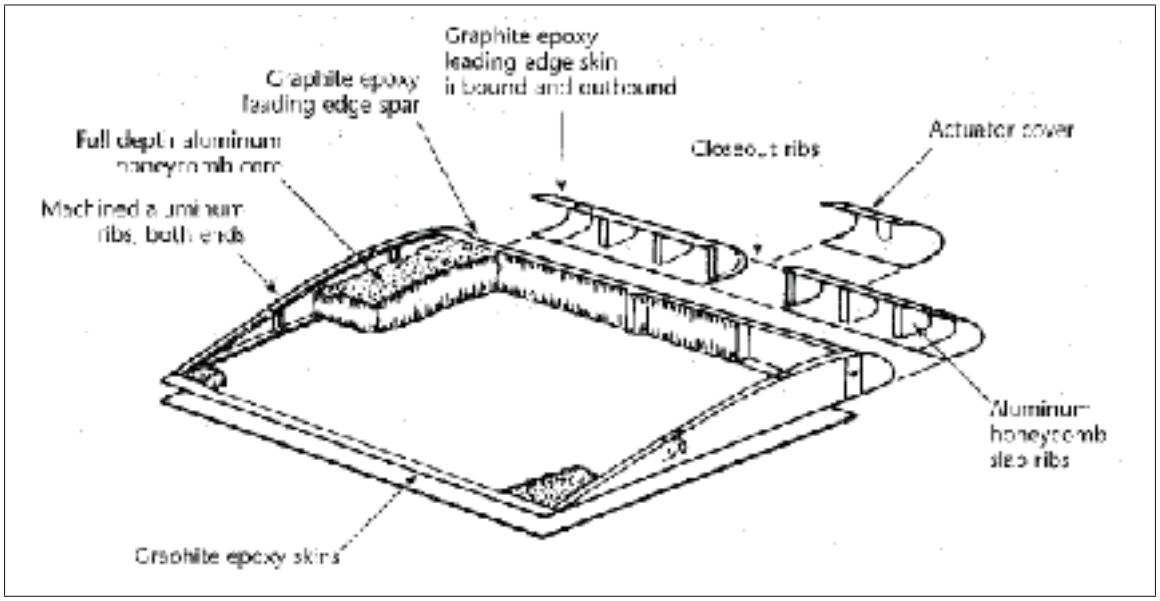

Figure 3.14 This schematics represents a typical aircraft wing structure made of aluminium honeycomb core and graphite epoxy skin.
Reproduced from Tracy and Moore (2001)

For the improvement of the technique in the inspection of certain materials and workpieces, variations in the standard fluorescent penetrant inspection are often employed in aerospace. Two examples are reported below:

- *Chelating Agent*: Adding a chelating agent to penetrant, can be an efficient approach to detect specific metals. It binds to specific metallic ions, resulting into the fluorescence under visible spectrum, if illuminated by ultraviolet radiation. According to Tracy and Moore (2001), this compound is used for detecting aluminium, bismuth, cadmium, copper, iron, magnesium, nickel, zinc in aerospace workpieces. It is employed as well to verify the presence of corrosion initiation sites in parts (Tracy and Moore (2001)).
- *Ultrasonic Pumping*: Certain aerospace workpieces which are previously tested through PT and destroyed demonstrate that the penetrant was drawn into minute cracks. However, it did not exude at a rate above the dimensional threshold of fluorescence. Therefore, no indication was detected (Tracy and Moore (2001)). It is usually observed in parts on

service which often contain acids, chromates and combustion byproducts in very tiny discontinuities, compromising the seeability (Tracy and Moore (2001)). The ultrasonic pumping is an alternative for enhancing the indication seeability. According to Tracy and Moore (2001), the investment cast bearing housing found in aircraft components welded to high temperature strength sheet material (nickel-chromium-iron-molybdenum alloy resistant to oxidation and stress corrosion cracking) obtains better inspection results with ultrasound pumping.

3.12 Safety Concerns

The penetrant testing requires special attention to involved materials. Injuries to inspectors may occur, if proper equipment which ensures the safety in inspection is not provided. This concern is related to the ultraviolet light employed in FPI and chemicals related to the overall PT testing (NDT Resource Center (2010)).

Ultraviolet radiation also referred as black light comprises invisible light whose wavelength varies from 180 to 400 nanometers. Excessive exposure of UV light around 320 nanometers and shorter wavelengths may cause skin and eye damages. It may accelerate wrinkling, increasing the risk of skin cancer. Nonetheless, the standard UV lamps utilized in FPI are designed to provide light around 365 nanometers (wavelength where, in general, the penetrants are developed to fluoresce). Therefore, the lamps employed in inspection may not provoke injuries (NDT Resource Center (2010)).

Among the chemicals involved in the processing of a specimen prior to inspection, the penetrant and developer remove oils from the skin. In some cases, it can become so dry, causing dermatosis, being vulnerable to infection. Thus, gloves are highly recommended in order to prevent this inconvenience. Furthermore, if products containing solvents (i. e. non-aqueous developers and solvent removable penetrants and other products for pre/post cleaning), hydrocarbon, ketones and alcohols are being employed in the PT, suitable ventilation is mandatory, once these chemicals are flammable and toxic (Canadian Institute for NDE (2010)).

3.13 Summary

The *liquid penetrant testing (PT)* is a simple, cost-effective, and sensitive nondestructive evaluation technique largely employed in aerospace, automotive, marine, petrochemical, electrical power, electronics, metal production, metal fabrication and composites industries (Shull (2002)). It is a powerful method for detecting open to surface indications in nonporous materials and workpieces (Betz (1963), Shull (2002)). It is conducted through the following sequence of ordered steps (Betz (1963), Shull (2002)):

- *Pre-cleaning)* If the specimen contains contaminants, the part must be cleaned through a suitable method (Shull (2002));
- *Penetrant Application)* The liquid penetrant is applied to the part surface. Through capillary forces, it is transported into open to surface discontinuities (Shull (2002));
- *Excess Removal)* After suitable *Dwell Time*, the penetrant is removed from the specimen surface. Only the discontinuities must remain with entrapped penetrant(Shull (2002));
- *Developer Application)* An even thin coating is applied to the specimen surface, enhancing the contrast among the indications and background (Shull (2002));
- *Inspection)* The specimen is inspected and indications are detected. If type I penetrant is being used, it must be conducted under blacklight illumination in a dark environment. In case type II penetrant is being utilized, minimum visible illumination is required for inspection (Shull (2002)).

Comparing with other *NDT* techniques, the *PT* is economical and easy to learn (Shull (2002)). Portable testing kit are available in the market, being easily transported by one single inspector to remote sites (Tracy and Moore (2001), Betz (1963), Shull (2002)). Reliable analysis is obtained with few false indications if personnel with experience conducts the inspection (Shull (2002)). The penetrant testing is feasible to be automated, increasing the inspection repeatability (Shull (2002)).

Furthermore, this method presents several disadvantages. For instance, extreme tight discontinuities are usually not detected, once penetrant is barely entrapped into them (Betz (1963)). The cleanliness of the part prior to penetrant application is mandatory, because contaminants compromise the inspection (Betz (1963)). The temperature and humidity have a direct impact in the sensitivity of the method (Shull (2002)). The technique requires suitable ventilation for the safety of inspectors (Shull (2002)).

CHAPTER 4

FLUORESCENT PENETRANT INSPECTION - INSPECTION SYSTEM CONFIGURATIONS - AUTOMATION FEASIBILITY

The fluorescent penetrant equipment must be chosen considering aspects related to the part being inspected and the overall production. The material which the part is made is essential for defining the cleaning method and liquid penetrant used. The part may not be damaged due to chemical attack resulted from reaction between either part surface and the liquid penetrant or the part surface and the solution applied in cleaning (pre-cleaning and postcleaning) or penetrant excess removal(emulsifier). The size and weight of the part define the method for applying the penetrant. When parts are large, heavy and difficult to manipulate, the application of penetrant with spray is mostly recommended. On the other hand, if parts are light and small-sized, the immersion into dip tanks is suggested, once it spreads the penetrant more uniformly (Tracy and Moore (2001)).

Considering the overall production, it must be defined how the parts arrive for testing. According to the production rate, it must be evaluated the equipment level, the required number and skill of operators and inspectors. Whether a testing line reach a point where manual testing operations cannot follow the required production rates, the automation is recommended. The automation allows a better control of the process, minimizing the possibility of overprocessing or underprocessing (Tracy and Moore (2001)). It provides the advantage of obtaining reliable and reproducible results. It increases the inspection speed to a level that cannot be achieved by human inspectors (Tracy and Moore (2001)).

The fluorescent penetrant testing equipment can be separated into three categories (Tracy and Moore (2001)):

a. Category I) Simple, hand operated, portable equipment that can be moved about easily as needed. Figure 4.1 exposes one example of equipment of this category (McMaster *et al.* (1982));

b. Category II) Larger and complete stationary equipment that can either be universal in the variety of parts it can accommodate or be specialized to inspect specific types of parts and generally designed to function as an integral part of production line. In figure 4.2, there is an example of stationary non-automated FPI stations;

c. Category III) It is composed of stationary equipment, being either universal or specific in terms of variety of parts being inspected with either fully or semi-automated equipment. In Armstrong (1986), a fully automated FPI system was developed for the inspection of aircraft compressor blades, increasing the inspection resolution in 300%. The penetrant and developer were applied through electrostatic spray guns, blades were handled by robots and transported in a motorized conveyor. During the inspection, the part was illuminated with an UV lamp and images were acquired with a video camera.

The liquid penetrant testing kits are included in category I, being suitable for conducting portable crack analysis. These kits are small sized, low weight and contain fluorescent penetrant materials such as application brush, swabs, cleaning rags, penetrant liquid, developer, emulsifier and a portable ultraviolet lamp (Tracy and Moore (2001)). The inspectors must be trained beforehand. It is highly recommended previous experience in FPI.

If the production testing rate is higher, but it still can be managed with human inspectors, category II equipment is more suitable. In this case, it is also mandatory human inspectors with experience and training in FPI (Tracy and Moore (2001)).

In case either the production rate reaches a point that human inspectors cannot respond or the required inspection accuracy is so high, the category III equipment is recommended. Through this configuration, it will be achieved more easily the desired sensitivity, reliability and repeatability (Tracy and Moore (2001)).

Figure 4.1 Magnaflux portable kit for the fluorescent penetrant inspection. The kit contains all required chemicals for the FPI, UV lamp and an instructions manual. Reproduced from McMaster *et al.* (1982)

4.1 Automated Fluorescent Penetrant Inspection System

In this section, it is described a general example of automated fluorescent penetrant inspection system. It is composed by the following stations:

a. Part Loading Station) In this station, a human operator places parts on carriers which are loaded onto the inspection line conveyor. A computer may be integrated to the station for enrolling the part into the inspection process and tracking the carrier of the part being inspected (Adair et al. (1998), Tracy and Moore (2001)).

b. Pre-cleaning Station) After passing by the loading station, the carrier is moved by the conveyor into the pre-cleaning station. In this module, the parts are cleaned using fluids (which can be detergent, alkaline or acid solution) and vapour (in this case, a hot liquid is dispensed). Before and after each fluid application, an air knife must be placed for preventing contamination the next cleaning solution. Per cleaning fluid employed to the specimen, a piping system has to be installed. Each is composed by an electric

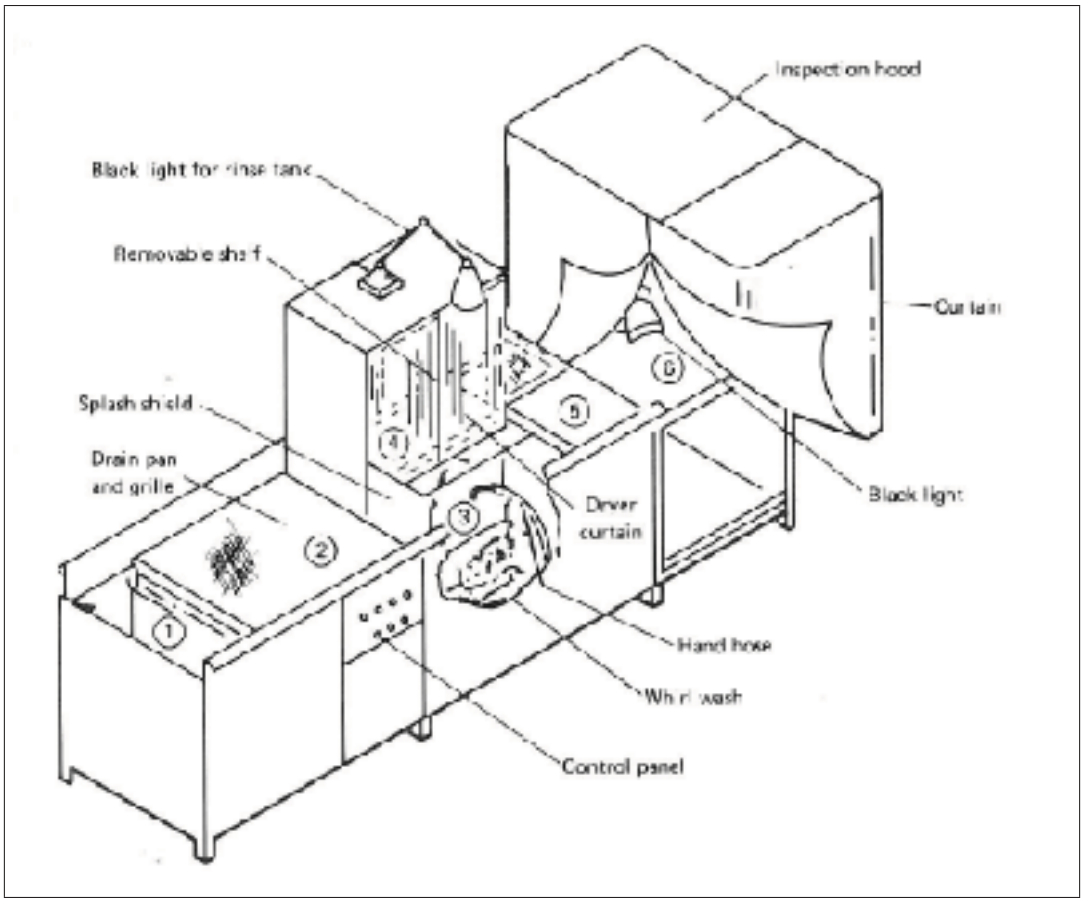

Figure 4.2 Stationary non automated fluorescent penetrant inspection system configuration widely used in non mechanized industry. In 1, there is a representation of a dip tank for the penetrant application; in 2, a drain pan is used for draining the excess of liquid penetrant allowing the desired dwell time (drain dwell mode); in 3, there is a rinse tank for excess penetrant removal; in 4, there is a drier; in 5, there is a small station for the developer application and in 6, there is an inspection booth with black light lamp. Reproduced from McMaster *et al.* (1982)

motor driven pump, a steam jet heater and a valve. The piping system aims at providing cleaning fluid according to pressure and temperature cleaning recipes to a manifold which sprays the fluid onto the parts. The mechanical force provided by the fluid valves helps removing surface contaminants. The electrical, hydraulic and pneumatic interfaces among the facility and the pre-cleaning station is controlled by the station main control panel. It also allows communication between the remaining station controlling computers. Each fluid spray pressure and temperature is recipe dependent. These parameters may be configured differently for diverse parts. An electric motor driven exhaust fan

must be installed for removing humid air from inside the station (Adair et al. (1998), Tracy and Moore (2001)). Furthermore, an automatic washing machine such as the example illustrated in figure 4.3 can be adapted for the mechanization and standardization of this station (McMaster *et al.* (1982)).

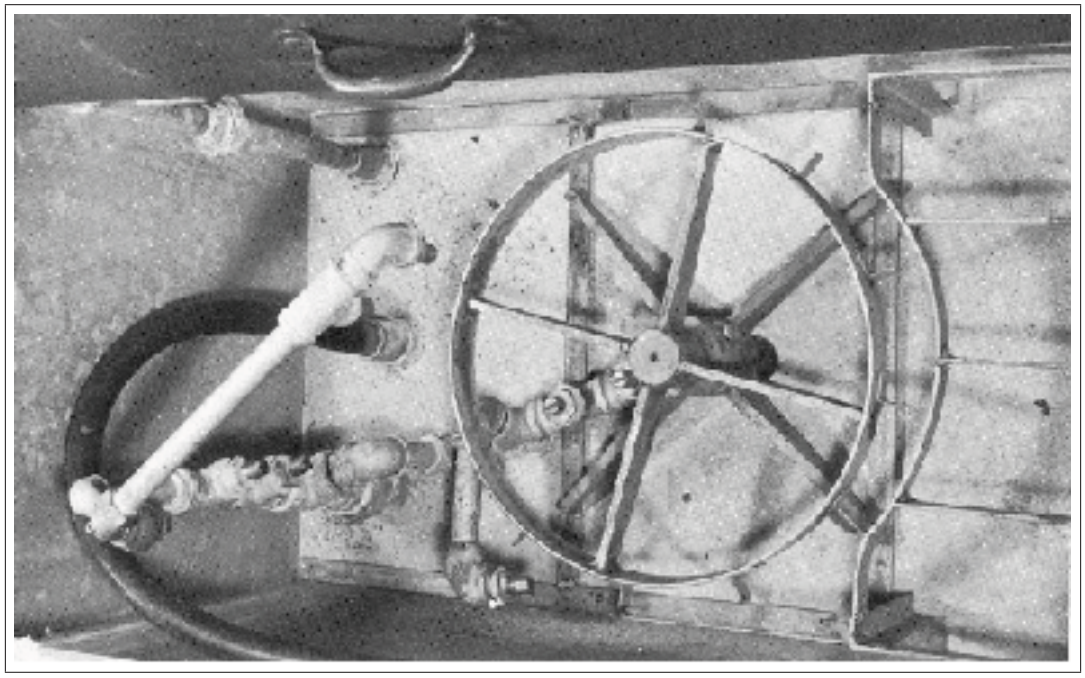

Figure 4.3 Automatic washing machine that can be used for pre-cleaning and post-cleaning processes.
Reproduced from McMaster *et al.* (1982)

c. Drier Station) After passing by the pre-cleaning station, the part goes to a drier station through a conveyor. It is a cabinet whose walls are insulated and the interior is electrically heated with the temperature being controlled by an adjustable thermostat. It is equipped with fans built into unit which expels the wet air replacing the cabinet with dry air. Only water is evaporated in the drier (Adair et al. (1998), Tracy and Moore (2001)).

d. Penetrant Application Station) After conducting the part cleaning recipe, the carrier is moved by the conveyor into the penetrant application station. It can be organized into, at least, two configurations: (i) the penetrant is applied through electrostatic sprays and (ii) the penetrant is applied through a dip tank. In case configuration (i) is adopted, elec-

trostatic spray guns fed with liquid penetrant wet the part surface with liquid penetrant (as illustrated in figure 4.4). They are controlled by the station main computer. If configuration (ii) is chosen, a robot controlled by the station main control computer removes the part from the carrier and immerses it into a dip tank. After a few seconds, the part is replaced by the robot into the carrier. In both configurations, air knives and mist collectors may be installed for preventing the drifting of liquid penetrant out of the application module (Adair et al. (1998), Tracy and Moore (2001)).

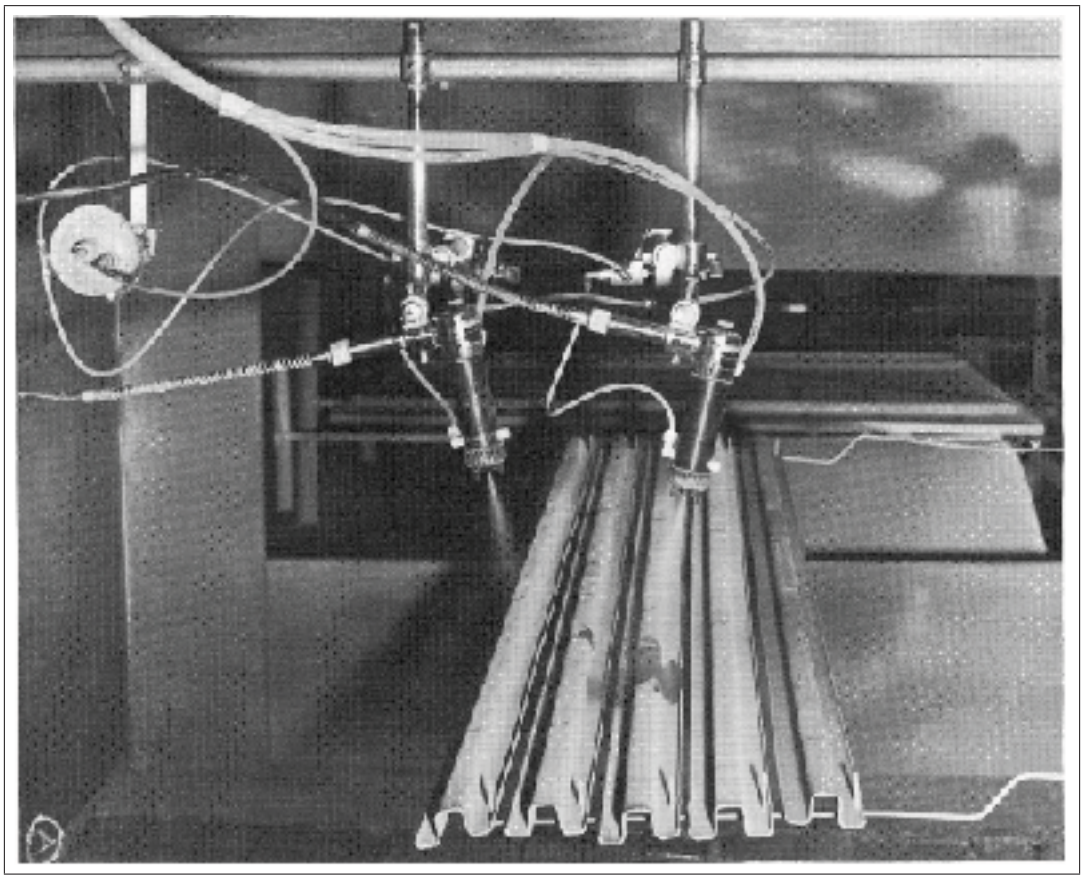

Figure 4.4 Picture of an automatic electrostatic spray gun system controlled by a computer processor. This automated system guarantees the repeatability required for the inspection of high safety workpieces.
Reproduced from McMaster *et al.* (1982)

e. Dwell Station) After applying the penetrant, the carrier is moved to the dwell station. The entry of a carrier generates a signal to a timer in a controlling computer. The exit carrier stop remains activated until the dwell time expiration. At the end, the carrier

stop is released and it is moved to the next station (Adair et al. (1998), Tracy and Moore (2001)).

f. Penetrant Excess Removal Station) After the dwell time, penetrant excess must be removed in a subsequent station. The carrier is moved to the penetrant excess removal station. It is a closed cabinet with rolling curtains to prevent the washing liquid from drifting outside the enclosure. This process depends on the penetrant type being used. In case it is water-soluble, the washing is executed by streams of water from moving spray nozzles. In case the penetrant is postemulsifiable (either lipophilic or hydrophilic), the emulsifier is employed through solution streams from spray nozzles. A piping system composed by an electric motor driven pump, a steam jet heater and a valve must be installed in order to provide water and postemulsifiable solution at proper temperature and pressure (Adair et al. (1998), Tracy and Moore (2001)).

g. Developer Application Station) In this station, the developer must be applied using automatic electrostatic spray guns. Air knives and mist collectors are installed to eliminate its drifting out of the spray application module (Adair et al. (1998), Tracy and Moore (2001)). The developer layer thickness is an important factor in inspection. If it is too thick, it is complicated for a liquid penetrant to flow from a discontinuity to part surface. On the other hand, if it is too thin, it may result in lack of contrast between indications and part surface. Non-uniform developer application leads to non-representative detection (Brasche et al. (2009), Sekerin and Kornev (1997), Migoun et al. (2002)). Thus, the quantity and uniformity of the layer (which is controlled by either by the spray translation and rotation or part rotation and translation) are recipe dependent parameters.

h. Fluorescent Penetrant Inspection Station) After treating the surface with chemicals, the part is prepared for inspection. It must be conducted through an automated system. This stage is detailed in section 4.2.

4.2 Ultraviolet Inspection Systems

In the literature, there are several examples of automated systems for the FPI inspection. They consist of ultraviolet scanners and camera-based systems. The UV scanners are composed of four basic elements: (i) an UV light source; (ii) a photodetector sensitive to visible light and not to ultraviolet radiation; (iii) signal conditioning and (iv) pattern recognition hardware and software required to decode the produced signal. In addition, materials handling accessories are necessary for moving parts to and from the scanner to loading/unloading equipment. Rejected and approved parts must be marked or separated after inspection (Tracy and Moore (2001)).

In the ultraviolet laser-scanning system proposed in Tracy and Moore (2001), a focused UV laser spot illuminates only a D millimeters diameter area of a part treated with chemicals in one cycle and a photodetector verifies the presence of any fluorescent spot in the place where the UV light is being projected. If the level of fluorescence in the area covered by the beam is low, no indication is detected by the photodetector. Otherwise, if a larger amount of fluorescent radiation is acquired, it demonstrates that the laser spot strikes an indication (Tracy and Moore (2001)). In order to scan the whole surface, the direction of the laser spot is changed continuously through the mirrors (as depicted in figure 4.5), being the spot translated in x and y axes in steps of D millimeters. The photodetector must follow the illumination trajectory provided by the mirrors. Similarly in Burkel (1990), the fluorescent patterns are captured by a fibber-optic bundle and detected by a photomultiplier detector (depicted in figure 4.6). As the example illustrated in figure 4.5, the laser spot is displaced over the part surface by mirror rotations. The spot diameter is the resolution in both systems.

Furthermore, in Armstrong (1986), a camera-based system for the inspection in FPI was developed. It composed of (i) a mercury vapour ultraviolet light source which illuminates the part being inspected, (ii) a camera that acquires images of the treated specimen in a single snapshot, (iii) a robot arm for handling and positioning the inspected workpiece in front of the camera and (iv) a digital image processing system for identifying the relevant features of the acquired images. This fully automated system improved the inspection results, eliminating errors inher-

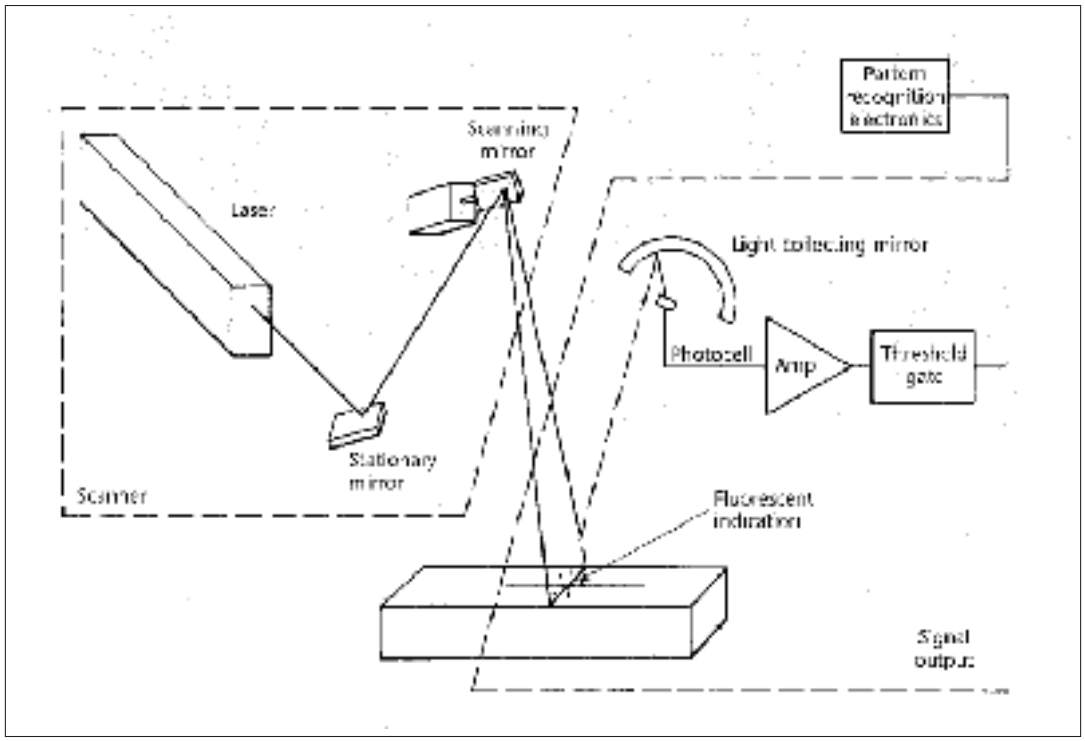

Figure 4.5 Laser-scanning system. The laser spot is translated over the surface aided by a scanning mirror. A light-collecting mirror transmits fluorescent indications to a photocell. The signal captured by the photocell is conditioned by an amplifier and threshold gate.
Reproduced from Tracy and Moore (2001)

ent to human inspectors. The resolution of the inspection system is given by the number of pixels of the camera sensor.

4.3 Summary

In this chapter, the fluorescent penetrant inspection has been discussed. Portable, stationary and automated equipments for conducting this technique have been exemplified. A hypothetic fully automated FPI line has been explained.

Ultraviolet image acquisition and processing systems are capable to automate the inspection in FPI. The analysis of workpieces by a machine vision system must be performed in a light blocking booth under only blacklight illumination. Automatic electrostatic spray guns, wash-

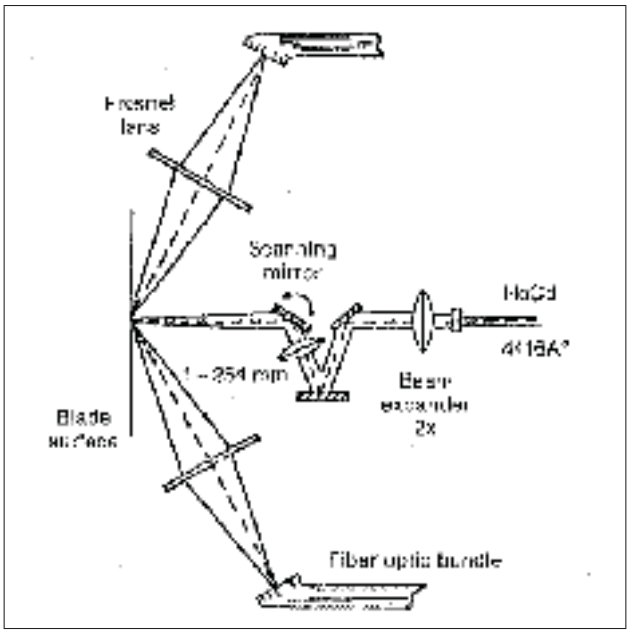

Figure 4.6 Laser-scanning system developed by General Electric. The rotation of the scanning mirror translates the focused spot over the treated surface. Reproduced from Burkel (1990)

ing machines, robots, conveyors, etc comprise equipment for allowing the automation of the part pre/post cleaning, application of PT chemicals and specimen handling.

Even though the automation is capable to reduce drastically the variability in inspection, nowadays several challenges are still present mechanized FPI. For instance, automatic washing machines are set for cleaning parts according to recipes defined experimentally. Unexpected contaminants or excessive amounts of impurities may require the modification of the cleaning parameters/method. Moreover, the automated processes are developed for the analysis of determined parts and discontinuities. If specifications related to the part and detected indications are changed, these systems may become obsolete, if they are not flexible enough to be adapted to future needs in inspection.

CHAPTER 5

DIGITAL IMAGE ACQUISITION AND PROCESSING

In the chapters 1, 2, 3, the manufacturing processes, service degradation, nondestructive evaluation and the state of the art in penetrant testing were discussed respectively. In chapter 4, some approaches for the automation of the fluorescent penetrant inspection were described. Nonetheless, the image acquisition and image processing which are mandatory for a machine vision system were not discussed previously in details. Therefore, it is necessary to analyze these subjects in an attempt to define a procedure for extracting features.

The extraction of data suitable for a classifier from an image requires the following steps: image acquisition, image filtering, image segmentation and feature extraction. The image acquisition comprises all techniques which generate an image from an imaging sensor. The image filtering is responsible for accepting or discarding image elements of certain frequencies, smoothing and/or sharpening images for enhancing the elements which are verified in image segmentation, removing noise. The image segmentation comprises image processing operations that separate objects or regions which are capable to provide important information for the application. It can be a point, a line, an edge or pixels detected by thresholding in a region of interest (ROI) or in the whole image. The feature extraction, as the name says, consists of extracting features from the segmented objects getting suitable data for a classifier.

The image processing operations are mostly performed either in the frequency domain or in the spatial domain. The spatial domain refers to image processing using information from the pixel directly. The frequency domain requires primarily the conversion of an image into the frequency domain. Then, the image processing operations are conducted and an inverse transformation is performed for converting it back to the spatial domain. The spatial domain, regarding that all operations are direct, is less memory-consuming that frequency domain operations (Gonzalez and Woods (2008)).

In this chapter, in the first section, techniques employed for acquiring images are described. In section 5.2, image filtering techniques are explained for obtaining images free of noise, enhancing objects of interest in image. The sections 5.3 and 5.4, two image segmentation techniques are described. In section 5.5, a feature extraction algorithm is analyzed as an attempt for providing features to an image classifier. At the end, there is a summary which covers the main topics exposed in this chapter.

5.1 Image Acquisition

For the detection of indications, through optical means, images must be acquired using a camera or a single photodetector or a line of photodetectors Gonzalez and Woods (2008). With a camera, a single snapshot provides a matrix of pixel intensities. Using a photodetector, it must be translated in x and y axes and the intensities acquired after each displacement form as well a matrix of pixel intensities, resulting into an image. If the image acquisition is carried with a sensor which is a line of photodetectors, in each acquisition shot, an $1XN$ array is obtained where N is the number of photodetectors that composes the sensor disposed in a line. Therefore, translating this array of photodetectors in the direction perpendicular to the sensor extension and acquiring the signal at each sensor displacement, an image is generated also (Gonzalez and Woods (2008)).

In an image, the pixel intensity is the information provided by the acquisition system. In FPI inspection, if a specimen has been properly processed, defect free areas remain dark under UV illumination. However, if a discontinuity traps fluorescent chemicals and it is illuminated by ultraviolet radiation, this zone becomes bright in an image. Based on these facts, the pixel intensity can be extracted as preliminary information for the indication size measurement. Figure 5.1 depicts image digitization of a part submitted to fluorescent penetrant inspection.

5.2 Image Filtering

In Gonzalez and Woods (2008), the filters in frequency and spatial domains are divided into smoothing and sharpening filters which are respectively known also as lowpass and highpass

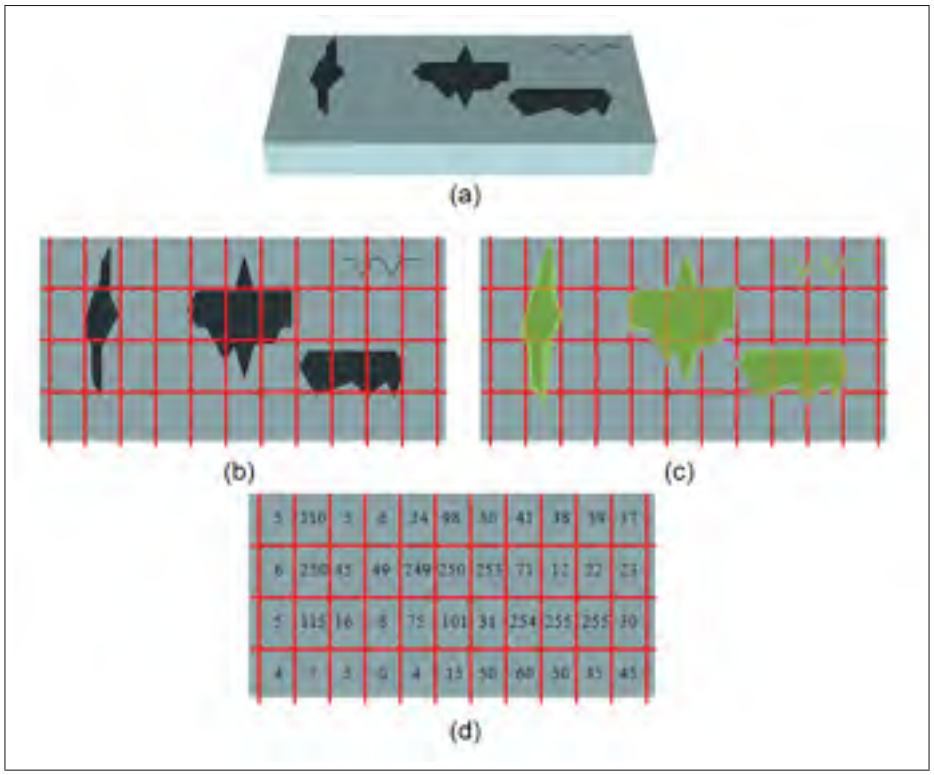

Figure 5.1 This schematics depicts the effect of the digitization. In (a), there is an example of workpiece with defects indicated in black. In (b), the pixels in the image are indicated by the red lines. In (c), the fluorescent green regions illustrate where defects are illuminated and trapped by liquid penetrant and developer. In (d), the digitized intensity per pixel obtained during image acquisition

filters. The smoothing filters are mostly used for reducing the noise, attenuating isolated image anomalies. The sharpening filters, on the other hand, enhances abrupt changes in the image, highlighting details (Gonzalez and Woods (2008)).

In the frequency domain, the smoothing operations are represented by all sort of *frequency lowpass filters* which includes Butterworth lowpass and Gaussian lowpass filters (Gonzalez and Woods (2008)). A simple multiplication between the transformed image and these filters, removes noise from the edges (Gonzalez and Woods (2008)). In the spatial domain, the convolution of the image with *averaging lowpass masks* obtains the same results (Gonzalez and Woods (2008)). In figure 5.2, there is an example of *non-weighted* and *weighted averaging masks* (Gonzalez and Woods (2008)).

The sharpening of an image in the spatial domain, according to Gonzalez and Woods (2008) is accomplished by the extraction of image gradients which measure the magnitude and direction of the greatest change in intensity in a small neighbourhood of a pixel. The gradients can be computed by convolving Sobel, Prewitt, Roberts, etc operator masks. The horizontal components of the Sobel and Prewitt operator masks, given by TX are represented in figure 5.3. The vertical, given by TY are illustrated in figure 5.4. The convolution of an image with TX results into S_H; the convolution of the same image with TY, into S_V. The gradient magnitude r(x,y) is calculated as demonstrated in equation 5.1. The orientation of the corresponding point given by $\theta(x,y)$ is obtained through equation 5.2.

$$r(x,y) = \sqrt{S_H(x,y)^2 + S_V(x,y)^2} \tag{5.1}$$

$$\theta(x,y) = atan(S_V/S_H) \tag{5.2}$$

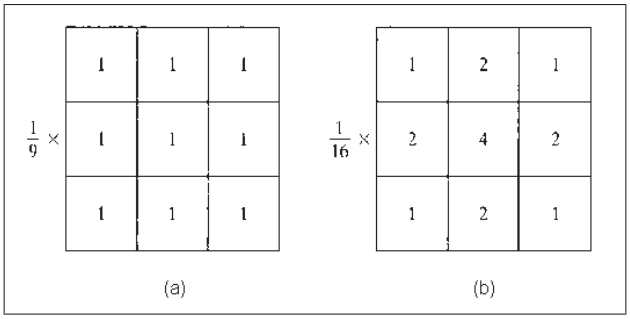

Figure 5.2 Examples of smoothing masks. In (a), there is a nonweighted averaging mask; in (b), there is a weighted averaging mask.
Reproduced from Gonzalez and Woods (2008)

In the frequency domain, similar sharpening results can be obtained by applying frequency highpass filters. The most employed are the Butterworth highpass and Gaussian highpass filters.

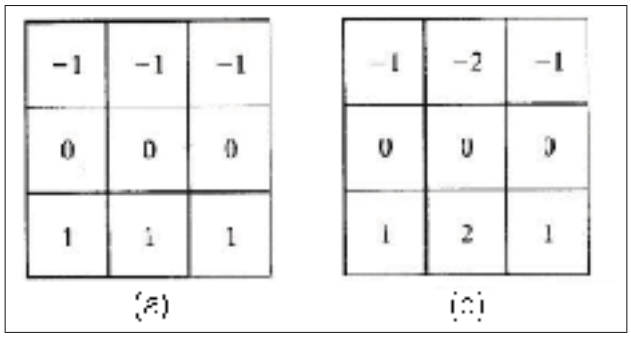

Figure 5.3 Masks which are convolved with images for obtaining horizontal gradients. In (a), Prewitt operator mask; and in (b), Sobel operator mask. Reproduced from Gonzalez and Woods (2008)

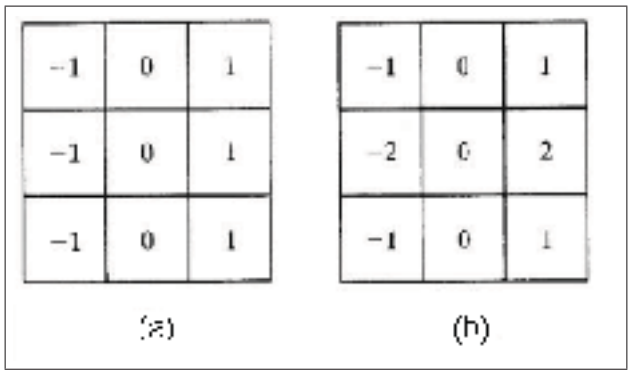

Figure 5.4 Masks which are convolved with images for obtaining vertical gradients. In (a), Prewitt operator mask; and in (b), Sobel operator mask. Reproduced from Gonzalez and Woods (2008)

5.3 Image Segmentation Based on Edge Detection

In order to measure the maximum euclidean distance and area of an indication, it is necessary to provide to the software beforehand information related to its extension. The detection of the boundaries based on transitions (the edges) can be a good approach. In Gonzalez and Woods (2008), the authors recommend three fundamental steps for the detection of edges:

a. *Image smoothing for noise reduction* - The smoothing operations improve the results in the detection of edges (Gonzalez and Woods (2008));

b. *Detection of Edge Points* - Operation which extracts all points that can be classified as edges (Gonzalez and Woods (2008));

c. *Edge Localization* - this step aims at selecting, among candidate points, only the members which truly represent the edge (Gonzalez and Woods (2008)).

The edges can be classified into three by intensity profiles: the *step edge*, the *ramp edge* and the *roof edge* (Gonzalez and Woods (2008)). A *step edge* (illustrated in figure 5.5(a)) is a transition between two pixel intensity levels whose distance which separates them is only one pixel. This type is the most suitable for pattern recognition, because it provides clear distinction from the image background and does not require any filtering operation (Gonzalez and Woods (2008)). However, in most real life situations, they are more likely detected either as a *ramp edge* or *roof edge* profiles (Gonzalez and Woods (2008)). In the former case (depicted in 5.5 (b)), the slope of the ramp depicts how blurred it is (Gonzalez and Woods (2008)). It cannot be represented by only one pair of adjacent pixels, being a set of transition points. The latter case, represented by figure 5.5 (c) is mostly obtained when objects like pipes are being imaged (Gonzalez and Woods (2008)). In the case of liquid penetrant indications, the edges, in general, are represented by the *ramp edge* profile.

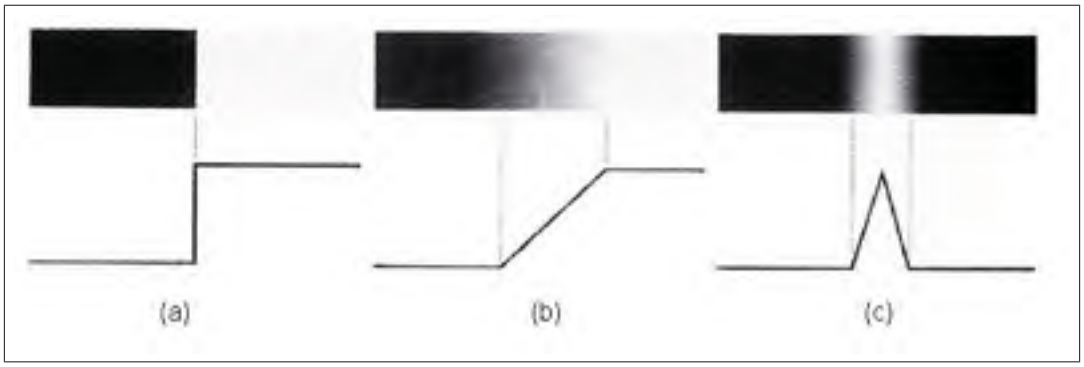

Figure 5.5 Edge profiles representation. In (a), there is a representation of a step edge; in (b), of a ramp edge; and in (c), of roof edge.
Reproduced from Gonzalez and Woods (2008)

The edges are extracted detecting changes in intensity. According to Gonzalez and Woods (2008), the extraction of gradients in spatial domain, as explained in section 5.2, is a good approach for accomplishing this task. However, in most real digital image processing cases, the resulted pixels do not completely represents the edges due to noise in the image, being required an edge linking algorithm for generating the whole indication boundary.

5.4 Image Segmentation Based on Thresholding

The processing required for linking edges to form a boundary can be avoided if all pixels which constitute a single indication are segmented. This can be obtained by employing segmentation based on thresholding. In this case, the indications are regions of pixels which contain intensities above the background.

The figure 5.6 contains a histogram reproduced from Gonzalez and Woods (2008) which represents the quantity of pixels found in the image according to specific intensities. This histogram demonstrates two dominant groups of pixels which depicts the intensity of the background and the intensity of the objects of interest. In this case, the thresholding can be employed for selecting objects whose intensity is above certain segmentation threshold. These objects would be part of the class 1 while the background would be part of class 0 as represented by the equation 5.3. The effect of the segmentation threshold setup is depicted in figure 5.7.

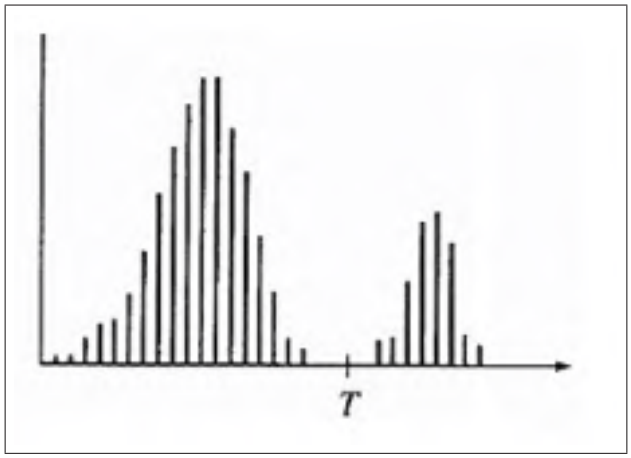

Figure 5.6 Ideal histogram representation whose intensity distribution of the background (the left distribution) is well separated from the indication distribution (the right distribution). In this case, the segmentation threshold must be set to the intensity T. Reproduced from Gonzalez and Woods (2008)

$$g(x,y) = \left\{ \begin{array}{cc} 1 & if\ f(x,y) > T \\ 0 & otherwise \end{array} \right\} \tag{5.3}$$

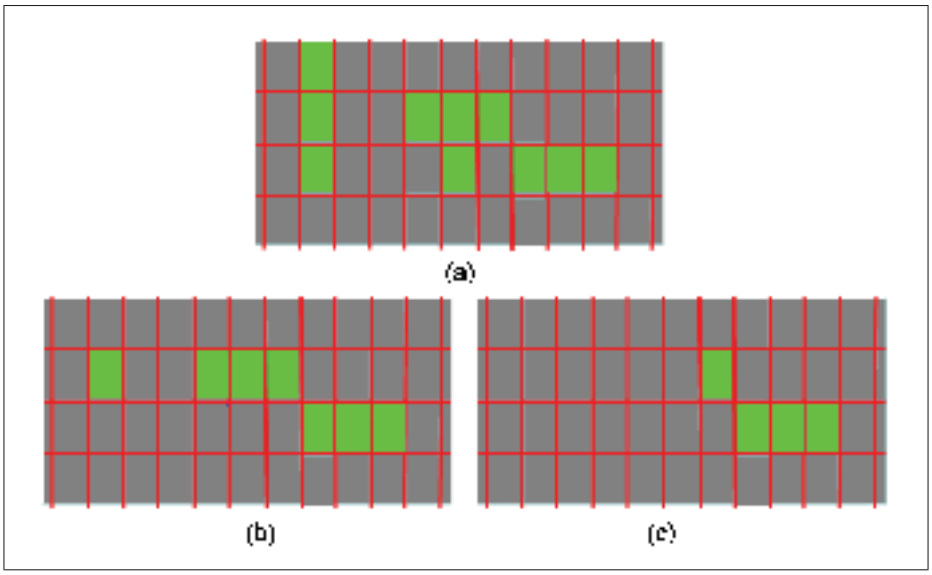

Figure 5.7 This figure depicts the effect of the segmentation threshold setup. The same sample sketched in figure 5.1 was considered for this analysis. The squares in fluorescent green illustrate the segmented pixels according to the set segmentation threshold. In (a), (b) and (c), it was respectively adjusted to 100, 200 and 253.

5.5 Feature Extraction

In the previous sections, image acquisition approaches, filtering techniques and two methods for segmenting objects that represent indications were described. Regarding that, in inspection, a data analysis procedure must evaluate each detected indication based on its characteristics, a feature extraction method must be defined for providing quantitative information to a classifier. Using the segmentation described in section 5.3, the obtained boundaries are used for this task. However, the thresholding must be applied to the boundaries beforehand. In case segmentation of section 5.4 is adopted, all detected pixels are information for the feature extraction. For assigning a boundary of a group of pixels as an indication, the following procedure extracted from Gonzalez and Woods (2008) is proposed:

- Step 1: As demonstrated in figure 5.8, in a thresholded image with an indication, as depicted in (a), the uppermost, leftmost point is defined as the starting point b_0 as illustrated in (b). The point c_0 will be always a background point (class 0) placed on the west of b_0. From the point c_0, in clockwise direction, the 8 neighbours of b_0 are verified if the

corresponding class is 1. The first class 1 pixel found is assigned to the variable b_1. The background pixel just before b_1 is assigned to the variable c_1. The variables b_1 and b_0 are kept in the memory for the step 4 (Gonzalez and Woods (2008)).

- Step 2: The variables b_1 and c_1 are assigned respectively to the variables b and c (Gonzalez and Woods (2008)).
- Step 3: All pixels neighbours of b, starting at c are examined in clockwise direction. These pixels from c are assigned to the variables n_1, n_2,...,n_8. If a k^{th} pixel is a member of class 1, n_k and n_{k-1} are respectively assigned to b and c (see figure (c)) (Gonzalez and Woods (2008)).
- Step 4: The step 3 is repeated until $b = b_0$ and the subsequent boundary point is equal to b_1 (Gonzalez and Woods (2008)).

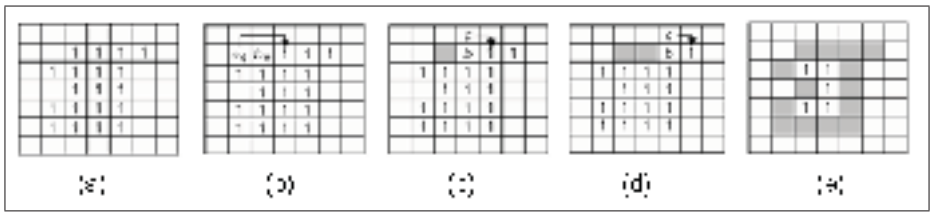

Figure 5.8 Boundary extraction algorithm example. In (a), there is an example of an image which indicates the classes of the pixels. The pixels in blank belong to class 0; the others, to class 1. In (b), with the starting point b_0, from c_0, in clockwise direction, the first $b0$'s neighbour which belong to class 1 is searched; in (c), after assigning $c = c_1$ and $b = b_1$, from c, in clockwise direction, the first b's neighbour which belongs to class 1 is searched; in (d), the subsequent search for b's neighbours; and in (e), the detected boundary is colored in gray.
Reproduced from Gonzalez and Woods (2008)

All pixel locations that were assigned to the variables b_0 and b_1 and all bs detected in the step 3 form the a^{th} indication boundary that comprises the set $B_a = \{(x_i, y_i)\}_{i=0}^{i=N-1}$ whose cardinality is given by N. With the i^{th} and j^{th} points contained in the set B_a, the euclidean distance in pixels is calculated through the equation 5.4. Having the euclidean distance for all possible combinations of pairs of B_a points, using the highest value that has been obtained, the maximum euclidean distance in millimetres for the a^{th} indication is given by equation 5.5. Using the pair of elements of B_a that resulted in the maximum euclidean distance, a line $y = ax + b$ is

fit. This line starts in one extremity of the boundary and ends in the other. In the line midpoint, a normal line is traced. The two points where the normal line crosses the boundary are used for calculating the width of the indication in pixels according to equation 5.6. If the maximum euclidean distance is at least three times greater than the width, the shape of the indication is labelled as linear. Otherwise, it is classified as rounded. The indication area is given by equation 5.7 where *PB* and *PI* are the number of pixels which form the indication boundary and the number of pixels inscribed in the boundary. $(x_{normal_i}, y_{normal_i})$ and $(x_{normal_j}, y_{normal_j})$ are the coordinates of the two points where the normal line that crossed the indication boundary. R is the width of the field of view in millimeters divided by the number of columns that form a raw image in the application.

$$euclidean\ distance_{ij}\ in\ pixels = \sqrt{(x_i - x_j)^2 + (y_i - y_j)^2} \tag{5.4}$$

$$maximum\ euclidean\ distance\ in\ mm = maximum\ euclidean\ distance\ in\ pixels * (R) \tag{5.5}$$

$$width_{ij}\ in\ pixels = \sqrt{(x_{normal_i} - x_{normal_j})^2 + (y_{normal_i} - y_{normal_j})^2} \tag{5.6}$$

$$area\ of\ indication\ in\ pixels = (PB + PI) * (R)^2 \tag{5.7}$$

5.6 Summary

In this chapter, we were concentrated on image acquisition and processing techniques for automating the inspection in FPI. The feature extraction procedure in section 5.5 is an approach for obtaining characteristics such as maximum euclidean distance, area and shape of an indication. It is based on the location of pixels which represents its boundary.

Even though the boundary extraction is essential for the feature extraction technique which was explained, prior to this stage, the image should be filtered followed by segmentation. According to Gonzalez and Woods (2008), the image filtering removes noise and spurious pixels of the image. The segmentation selects the objects in an image which are feasible to provide characteristics in feature extraction. In this chapter, two strategies for image segmentation have been described applied to the detection of indications: I) segmentation based on edge detection; and II) segmentation based on thresholding. The former method requires an edge linking algorithm prior to feature extraction. The latter method is simpler, obtaining separated clusters of pixels which represent unique indications.

Therefore, in our evaluation, based on our limited review of literature, the most suitable image acquisition and processing includes the following ordered steps for the detection, measurement and classification of FPI indications:

- Step 1 - Image acquisition using a camera or a photodetector or an array of photodetector;
- Step 2 - Image filtering by averaging mask convolution;
- Step 3 - Image segmentation based on thresholding;
- Step 4 - Feature extraction based on boundary determination.

CHAPTER 6

EXPERIMENTAL PROTOCOL

In the previous chapters, background about materials science, manufacturing processes, service degradation, nondestructive testing, penetrant testing, automation of fluorescent penetrant inspection and digital image acquisition and processing have been discussed. These subjects comprise introductory information for conducting experiments related to the development of system for this work. In this chapter, the experimental protocol is described in details. It is composed of the description of the proposed systems, samples and experiments.

The proposed system whose given name is *Indication Detection System (IDS)* comprises of an optical sensor which detects open to surface indications, measuring the corresponding area in mm^2, maximum euclidean distance in *mm* and classifies its shape as either linear or rounded. Using this system, three experiments have been conducted as follows:

- Experiment I, for setting parameters such as α and C. These variables have been described in section 6.1;
- Experiment II, for tracing probability of detection curves according to the selected segmentation threshold evaluating the capability and reliability of the system;
- Experiment III, for evaluating the performance of the system related to the measurement of the maximum euclidean distance, area and shape classification of indications.

This chapter has been divided as follows: In section 6.1, the system *IDS* has been described. The optical hardware and software which analyzes indications have been related. In sections 6.2 and 6.3, the samples that have been verified through experiments have been reported. In section 6.4, the steps for preparing them have been defined. In sections 6.5, 6.6 and 6.7, the methodologies for conducting respectively the experiments I, II and III have been explained. At the end, in section 6.8, a summary has been written recapitulating briefly the experimental protocol.

6.1 Indication Detection System (IDS)

The system IDS that has been utilized in the experiments is composed of three different modules as follows:

- First Module) - The *image acquisition hardware* which is comprised of an analog CCD 640X480 black/white camera, a framegrabber board that converts the analog image provided by the camera into a digital image, a 2/3 inch objective with 12mm of focal length for focusing the camera CCD on the light emitted from a surface area of 100mmX74mm and a filter which transmits only light within 510-560 nanometers. These components are positioned perpendicular to the inspected surface. They are placed 179 millimeters away from the inspected object;
- Second Module) - The *illumination hardware* which consists of a 24W UV, 365 nanometers lamp separated C millimeters to the specimen inclined in an angle α with respect to the specimen surface. Figure 6.1 contains a schematics which illustrates how the hardware of the first and second modules have been positioned;
- Third Module) - An image acquisition, processing and indication analysis software. It grabs analog images, converting them into 255 graylevel images; it filters the digitized image removing noise; it detects indications, calculating their maximum euclidean distance, area and classifying their shape (either as linear or rounded according to the criteria in section 5.5). In subsection 6.1.1, this software has been better described.

6.1.1 Software of Image Acquisition, Image Filtering and Detection of Indications

The software which has been developed for conducting experiments has been divided into three different procedures: one for image acquisition; a second for filtering the digitized image, removing noise; and a third for detecting indications, measuring the area, maximum euclidean distance and classifying the shape of them.

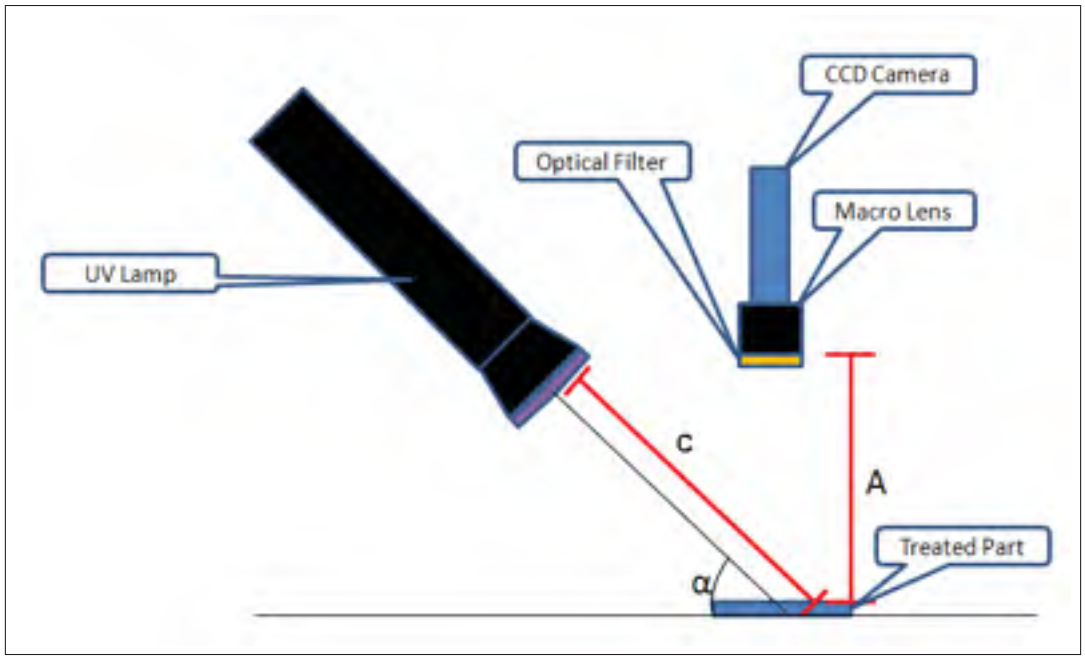

Figure 6.1 This figure illustrates the proposed system for conducting experiments for this work. The distance C and the angle α are the parameters which have been selected through the experiments described in section 6.5. The distance *A* has been set to 179*mm*

The image acquisition procedure (which has been named as *Procedure I*) captures images from a 640X480 analog CCD camera. The framegrabber board which is connected to the camera converts the acquired image into an 8-bit (255 graylevel) image. The *Procedure I* returns the digitized image which is the input signal for the subsequent procedure.

The image filtering procedure that has been identified as *Procedure II* filters the input digital image by convolving the weighted averaging filter described in section 5.2. It removes spurious pixels, enhancing the contrast between indications and the background of the image.

The *Procedure III*, which aims at detecting indications, measuring the area and maximum euclidean distance and classifying the shape of them, firstly segments the filtered image based on thresholding (as explained in section 5.4). The background and indications after segmentation are represented respectively by the classes 0 and 1. The resulting clusters of pixels which have been segmented as object of class 1 correspond to unique indications. Running the feature extraction procedure described in section 5.5 as function of an indication starting point *(ISP)* and the segmented image, the maximum euclidean distance, area and shape of

indications are returned. In this work, it has been extracted through the starting points extraction *(SPE)* algorithm. It aims at defining them for the boundary extraction in the image $I = \{im(x,y)\}_{x=0,y=0}^{x=W-1,y=H-1}$ where $im(x,y)$, W and H are respectively the (x,y) pixel class, width and height of I. The starting points are defined through the following steps:

- Step I - In a row y, the algorithm searches in I for the leftmost pixel whose class is 1. If it is detected, the corresponding location (x,y) is enrolled to the set $SP = \{(x_i,y_i)\}_{i=0}^{i=N-1}$ and step II is conducted. In case all pixels of this row belong to class 0, the step VI is executed. N is the SP's cardinality.
- Step II - In the same row y, analyzing I from the column where the leftmost pixel of class 1 has been found to the right of the row, the first pixel whose class is 0 is searched. If it is detected and if its column is smaller than $W-1$, the step III is conducted. Otherwise, the step IV is executed.
- Step III - In the same row y, analyzing I from the column of the pixel which has been detected in the previous step to the right of the row, the leftmost pixel whose class is 1 is searched. If it is detected, its location (x,y) is enrolled to the set $SP = \{(x_i,y_i)\}_{i=0}^{i=N-1}$. If either $x = W-1$ or none pixel of class 1 has been found, the step VI is run. Otherwise, the step IV is executed.
- Step IV - In the same row y, analyzing I from the column of the pixel detected in the previous step to the right of the row, the first pixel whose class is 0 is searched. If it is detected and if its column is smaller than $W-1$, the step V is conducted. Otherwise, the step VI is run.
- Step V - The steps III and IV are run in a loop until the condition for executing the step VI is satisfied.
- Step VI - If y is smaller than $H-1$, $y = y+1$ and the procedure is executed again from the step I. Otherwise the detection of ISPs has been concluded. This procedure must run, verifying all rows of the thresholded image.

The set *SP* comprises the starting points used to begin the feature extraction. If a point in *SP* has been previously detected as part of other indication boundary, it is ignored and the procedure described in section 5.5 is not run for the corresponding coordinate.

These procedures have been run together or separated depending on the experiment. In the parameter setting which has been described in section 6.5 only the *Procedure I* has been executed. In the *Experiment II*, a preliminary evaluation based on histograms has been conducted only with the *Procedure II*. The POD curves have been traced running the *Procedure II* followed by *Procedure III*. In the *Experiment III*, the three procedures have been performed.

6.2 Sample Description for setting the parameters α and C and plotting POD curves

For setting the parameters α and C and plotting POD curves, three sensitivity test panels made of brass, manufactured by Eishin Kagaku Inc. have been evaluated. They have been described as follows:

- The first test panel which has been called as *Coarse Test Panel* (see figure 6.2) contains 30 cracks around 70 millimeters of length, 2 microns of width and 50.2 microns of depth;
- The second test panel whose given name is *Medium Test Panel* (see figure 6.3) presents 33 cracks measuring around 70 millimeters of length, 1 micron of width and 21.6 microns of depth;
- The third test panel that has been named as *Fine Test Panel* (see figure 6.4) has 85 cracks around 70 millimeters of length, 1 micron of width and 10.8 microns of depth.

6.3 Sample Description for the Measurement of Area, Maximum Euclidean Distance and Shape Classification of Indications

For the evaluation of the system performance related to the shape classification and measurement of the area and maximum euclidean distance of indications, three weld joint references made of steel, containing open to surface discontinuities have been analyzed. All of them have been manufactured by the company Flawtech. They have been described below:

Figure 6.2 Radiography of Coarse Test Panel containing open to surface cracks used to trace a POD curve.

- The first reference has three rounded discontinuities which are porosities formed during the welding. The uppermost, the one located in the middle and the last have been identified respectively as *Discontinuity I*, *Discontinuity II* and *Discontinuity III*. The manufacturer has not informed the length and width of each separately. It has been only mentioned that the total flaw length is 10*mm*;
- The second contains a lack of fusion and a centerline crack. As a convention, these discontinuities have been related as *Discontinuity IV* and *Discontinuity V*. The length of the former and the latter are 18*mm* and 8*mm* respectively;
- The third weld joint reference contains a toe crack whose length is 20*mm* that has been reported as *Discontinuity VI* in the experiments.

6.4 Sample Preparation

The inspection in FPI requires prior and post surface preparation. Even though the laboratory where the chemicals have been applied have allowed the control of temperature and pressure of

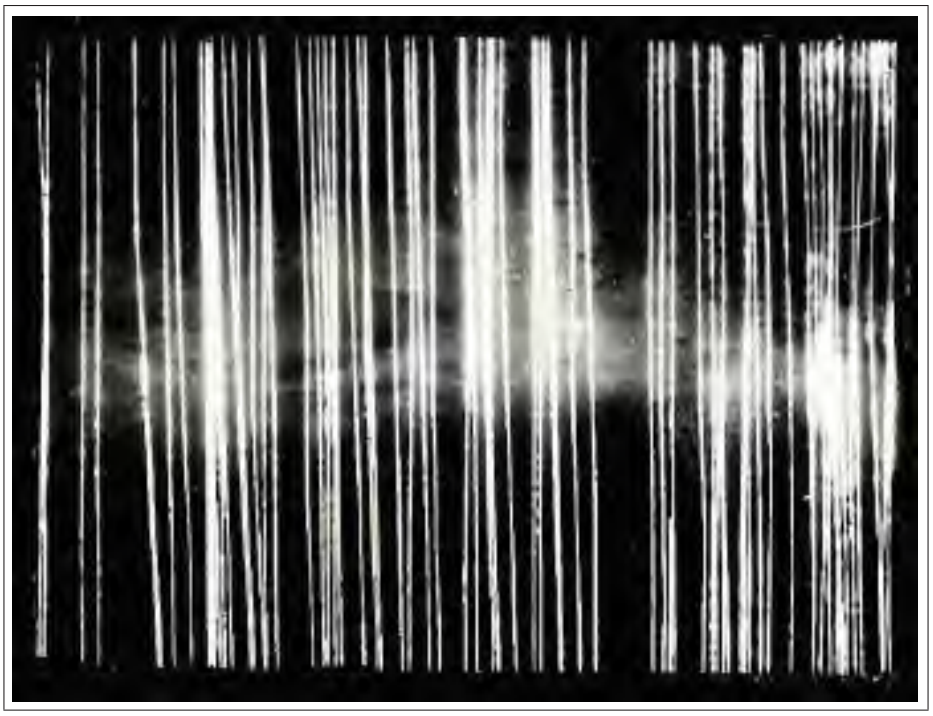

Figure 6.3 Radiography of the Medium Test Panel containing open to surface cracks used to trace a POD curve.

the water and drying oven, the overall part preparation has been conducted manually. The full automation of the chemical's application would have provided higher repeatability. Nonetheless, in order to ensure certain level of control, the application of penetrant, emulsifier and developer has been executed as the following recipe:

a. Prior to penetrant application, the samples are cleaned. The parts are immersed during 1 hour in acetone, followed by 1 hour of ultrasound cleaning;

b. Each part is immersed in a dip tank containing type I method D penetrant. Dwell time is set to 1 hour;

c. The samples are pre-rinsed with a coarse water spray under pressure of 35PSI and temperature of 27$^{\circ}C$. The water spray is placed 30cm away from the part inclined in a angle of 45°. This step must be conducted under blacklight illumination;

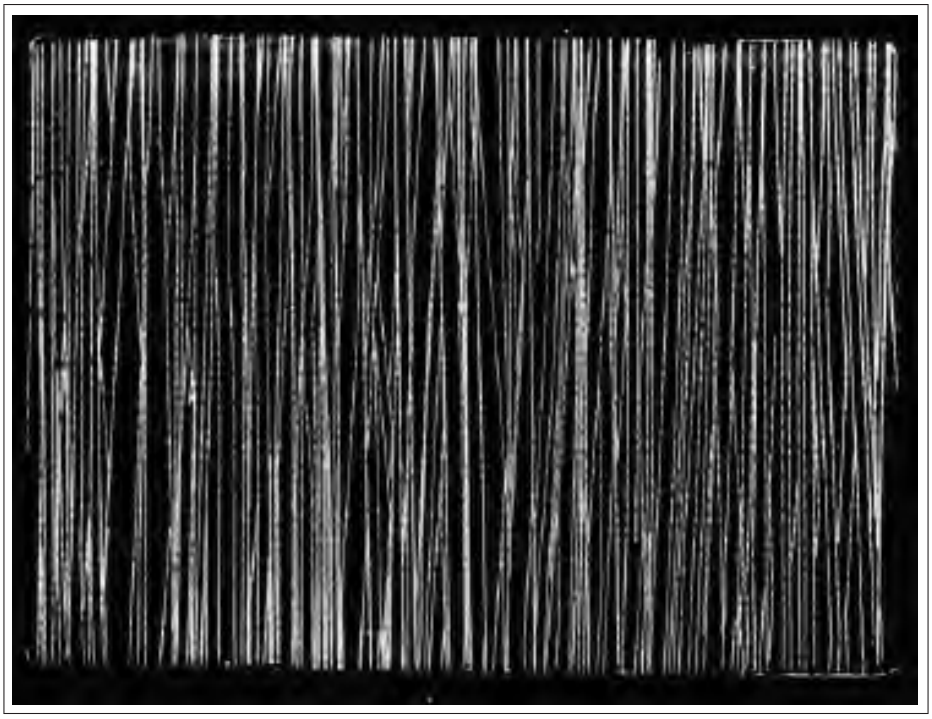

Figure 6.4 Radiography of Fine Test Panel containing open to surface cracks used to trace a POD curve.

d. The parts are immersed in a dip tank containing emulsifier. An emulsification time of 90 seconds is allowed;

e. The excess of penetrant is removed with a coarse water spray under pressure of 40*PSI* and temperature of 21°*C*. The water spray is placed 30*cm* away from the part inclined in a angle of 45°. Periodically, it must be verified under blacklight illumination if all excess has been removed from the surface;

f. The part is dried in an oven set at a temperature of 71°*C*. The part must be verified each 30 seconds, if there is remaining water from excess removal. The part is removed when dry;

g. Nonaquous developer is applied by spraying. The spray can be placed 50*cm* away from the part. Ten minutes is allowed for the development time and the specimen is ready for analysis.

6.5 Experiment I - Selection of the most suitable angle α and distance C in image acquisition

Setting the illumination parameters α and C has a direct impact in the light power in image acquisition. They should be adjusted in order to optimize the incident UV intensity for the detection of indications. Shallow and thin discontinuities, for example, entrap less liquid penetrant than deep and wide ones, being necessary higher ultraviolet power for the seeability of indications. On the other hand, into the latter discontinuity type more liquid penetrant is drawn, being susceptible to result in indications with extreme glare if it contains excessive incident light power. Therefore, the decision of the most suitable α and C must avoid the following possible inconveniences:

- The excessive glare mostly seen in deep and wide indications, if extreme UV power is being provided;
- The lack of UV power in shallow and thin indications, compromising the seeability.

These two inconveniences have been regarded in the experiment for the choice of the most suitable α and C. This experiment has been divided into two parts:

- The *Part I* consists of verifying the impact of setting the angle α with C adjusted to 30 centimeters. With α set to 10°, 25°, 45°, 65°and 75°, the three sensitivity test panels have been prepared four times as specified in section 6.4. After each preparation, an image per sensitivity test panel has been captured running the *Procedure I*. The setting of α whose images have obtained the best quality has been adopted for the analysis which has been described in Part II.
- The *Part II* aims at evaluating the influence of the C adjustment. Using the chosen α, with C set to 10, 20, 40 and 50 centimeters, the sensitivity test panels have been prepared four times through the same recipe, acquiring an image per panel after each single preparation executing the *Procedure I*. After comparing these images with the

ones acquired with the selected α and C=30 centimeters, the most suitable setting of C has been adopted. The distance C has been chosen aiming at achieving the best image for the detection of indications. Through this experiment, the images have been evaluated qualitatively. In other words, no quantitative metric has been analyzed for choosing α and C. It has been based only on subjective judgment.

6.6 Experiment II - Probability of Detection Curves Plot

The probability of detection curves allow an evaluation of the capability and reliability of the nondestructive evaluation equipment and personnel which conducts the *NDE*. This performance metric applied to the system of this project depends on the manner that the image has been acquired, filtered and segmented. Regarding that the segmentation in *Procedure III* extracts the relevant objects from a filtered image, it is important to know beforehand the distribution of its graylevel intensities. All images of the sensitivity test panels which have been acquired with the chosen α and C in the previous experiment using the *Procedure I* have been filtered with the *Procedure II* for this experiment. Histograms of these filtered images have been traced for providing information about the intensity range that separates the indications from background. Three segmentation threshold values within this interval have been adopted for the POD curve plot.

Executing the *Procedure III* with the filtered images using the three segmentation thresholds separately have allowed the plot of three POD curves. The value whose POD curve has achieved the best capability and reliability has been selected for the measurement of area, maximum euclidean distance and shape classification of indications. The POD curve for a segmentation threshold T has been plotted according to the steps below:

- Step 1. - One filtered image of the coarse test panel is inspected with *Procedure III* using T. Regarding that this panel contains 30 cracks, the number of detected cracks is recorded. This number is divided by 30, obtaining the probability of detection in % of the corresponding image.

- Step 2. - The final probability of detection in % for the coarse panel is calculated for the remaining three filtered images of the coarse sensitivity panel. The average of the POD of the four images is the final POD of the coarse sensitivity test panel in %.
- Step 3. - For the images of the medium and fine sensitivity test panels, the probabilities of detection are calculated as specified in Steps 1 and 2. Nonetheless, the medium and fine test panels contain 33 and 85 cracks respectively. The POD in % must take into account these values instead of 30 cracks.

6.7 Experiment III - Measurement of Area, Maximum Euclidean Distance and Shape Classification Experiments

Regarding that the developed system aims at measuring the maximum euclidean distance, the area and classifying the shape of indications, it is relevant to conduct experiments to evaluate its performance based on these measurements and classifications. The samples which have been described in section 6.3 have been utilized for this analysis. Each has been prepared five times as specified in section 6.4. After each preparation, an image per sample has been acquired through *Procedure I*, followed by image filtering through *Procedure II*, succeeded by the measurement of maximum euclidean distance, area and shape classification of indications through *Procedure III*. The measurements of area and maximum euclidean distance and shape classification have been recorded. The precision uncertainties, using the student method, have been calculated with 90% of confidence level.

6.8 Summary

In this chapter, important aspects related to the experiments for concluding this dissertation have been described. Primarily, the tests which have been conducted for positioning the ultra-violet lamp for optimizing the inspection have been explained. The methodology for plotting the probability of detection curves that provide means to evaluate the capability and reliability of the detection system has been proposed. The measurements of area and maximum euclidean distance of indications followed by the respective precision uncertainty calculation have been

analyzed accordingly to the description that has been written in this chapter. Table 6.1 contains a summary of the experiments which have been proposed.

The system *IDS* acquires images in an area of $100mmX74mm$. It digitizes it resulting in digital images with $640X480$ pixels. Each pixel in the image corresponds to and area of $0.15mmX0.15mm$ of the surface being inspected. R is equivalent to $0.15mm$.

Table 6.1 Summary of the proposed experiments

Experiment	**Brief Description of the Experiment**
I, Part I	For an angle α, the coarse, medium and fine sensitivity test panels have been prepared four times with the required chemicals. After each preparation, images of the treated panels have been acquired. Angles such as 10°, 25°, 45°, 65°and 75°have been analyzed.
I, Part II	With the selected angle in the previous experiment, for a distance C, the coarse, medium and fine sensitivity test panels have been prepared four times with the required chemicals. After each preparation, images of the treated panels have been acquired. Distances C such as $10cm$, $20cm$, $40cm$ and $50cm$ have been analyzed. The system configuration which have obtained the best image quality has been adopted for the remaining experiments that have been mentioned in this chapter.
II	After deciding the most suitable α and C configuration, using the images of the adopted system which have been acquired in the previous experiments, three POD curves have been traced. The segmentation threshold whose POD curve provides the best results has been adopted for the Experiment III.
III	The area, the maximum euclidean distance and shape of the five discontinuities which have been described in section 6.3 have been evaluated five times. Prior to each evaluation, the samples have been prepared with the PT chemicals.

CHAPTER 7

RESULTS, ANALYSIS AND DISCUSSION

In the previous chapter, several experiments have been proposed. Firstly, a methodology for setting the angle α and distance C has been suggested as an attempt to optimize the image quality in inspection. Secondly, a procedure for selecting the most suitable threshold value for segmentation based on probability of detection curves (POD) has been written, specifying meticulously the steps for tracing these graphics. At the end, the basis for an analysis of measurements of area, maximum euclidean distance and classification of indications contained in diverse samples has been introduced.

This chapter aims at presenting the results of the experiments mentioned previously. The setting of the illumination angle and distance between the specimen and ultraviolet light source, the plot of probability of detection curves for determining the capability and reliability of the developed system and the measurement of area, maximum euclidean distance and classification of shape of indications have been conducted, evaluating the samples and proposed system. Graphics, figures, tables of measurements, precision uncertainties have provided relevant information for an analysis of the obtained results. The performance of the developed system has been discussed, emphasizing critically positive and negative aspects of the developed system.

This chapter has been organized as follows: In sections 7.1 and 7.2, the influence in the image quality of the angle α and the distance C has been analyzed. Based on an evaluation of the impact of these parameters, a configuration for the remaining experiments has been chosen. In section 7.3, the probability of detection curves have been presented, quantifying the capability and reliability of the developed system. In section 7.4, the system performance related to the measurement of the area, maximum euclidean distance and shape classification of indications has been exposed. At the end, in section 7.5, the results have been discussed.

7.1 Analysis of the influence of the illumination angle in image acquisition

After acquiring images with α varying from 10°to 75°, it is possible to conclude that as large as the angle is, more brightness is added to the image, once more ultraviolet light power is provided to the inspected surface. In figure 7.1, an image of the coarse sensitivity test panel acquired with C and α set respectively to 30 centimeters and 75°has been depicted. This picture and the remaining images of the coarse sensitivity test panel with α adjusted to 75°and 65 °and C=30 centimeters have presented excessive glare on its center (as exposed in the area inscribed in the red rectangle of figure 7.1), blurring this zone, compromising the overall image resolution. The images of the coarse panel with C equal to 30 centimeters and α positioned to 45°, 25°and 10°which have been shown in figures 7.2, 7.3 and 7.4 respectively have obtained a more homogeneous brightness distribution. The images of the coarse crack sensitivity panel with α set to 25°and 10°are darker than the ones which have been acquired with larger angles.

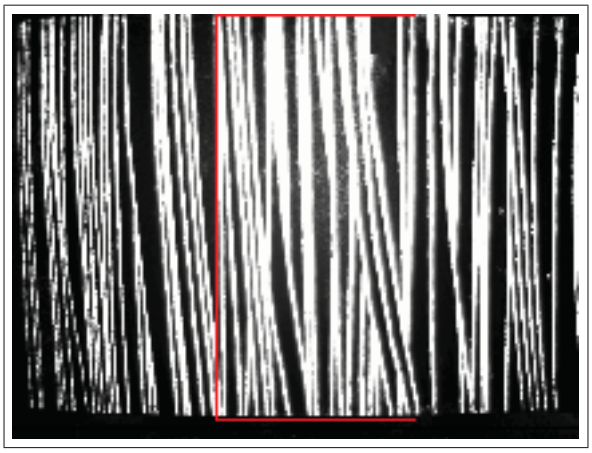

Figure 7.1 Image of the coarse sensitivity test panel that has been acquired through *IDS*. The angle α and C have been set to 75°and 30 centimeters respectively.

Furthermore, the lack of UV light power compromises the detection as well. For instance, regarding the fine sensitivity test panel, once its discontinuities entrap less liquid penetrant, more light power is mandatory for the seeability of indications. The figures 7.5 and 7.6 whose images have been acquired with α set to 25°and 10°respectively contain indications with low brightness. In figures 7.7 and 7.8 (whose images have been obtained with α set to 65°and 45°), even tough the light source has not provided enough power for the perfect indication's observation,

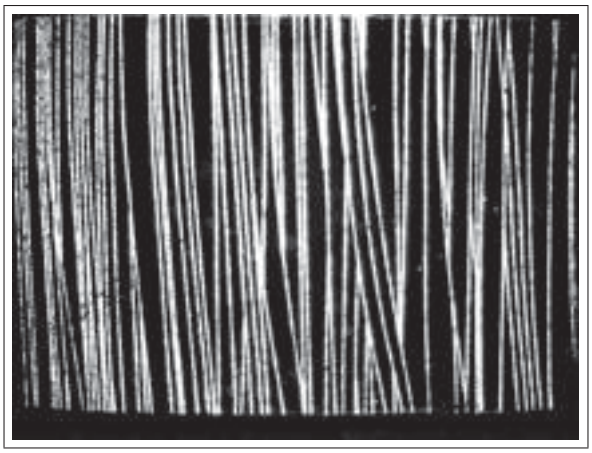

Figure 7.2 Image of the coarse sensitivity test panel that has been acquired through *IDS*. The angle α and C have been set to 45°and 30 centimeters respectively.

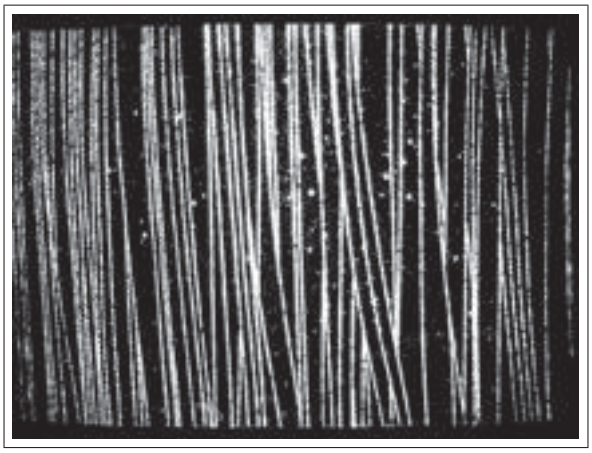

Figure 7.3 Image of the coarse sensitivity test panel that has been acquired through *IDS*. The angle α and C have been set to 25°and 30 centimeters respectively.

the image quality is better. The images of the medium sensitivity test panel which have been exposed in figures 7.9 and 7.10 have illustrated indications with intermediate level of brightness when compared with images that have been captured of the fine and coarse sensitivity panels according to the corresponding angle.

After acquiring images with different α configurations, setting it to 45 °seems to be the best choice. This adjustment has avoided the excessive glare in medium and coarse crack panels and has obtained the third best indication brightness in the fine test panels.

Figure 7.4 Image of the coarse sensitivity test panel that has been acquired through *IDS*. The angle α and C have been set to 10°and 30 centimeters respectively.

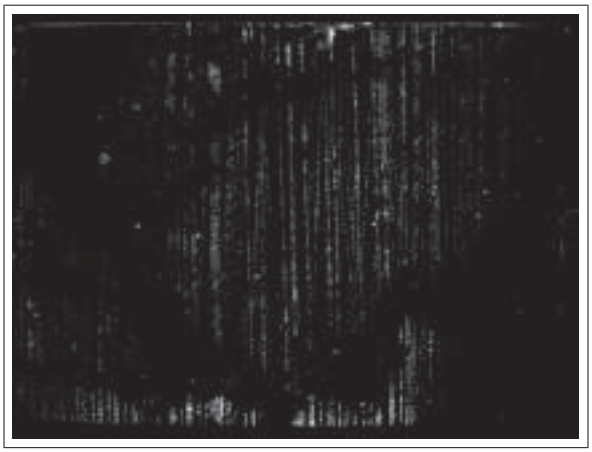

Figure 7.5 Image of the fine sensitivity test panel that has been acquired through *IDS*. The angle α and C have been set to 25°and 30 centimeters respectively.

7.2 Analysis of the influence of the distance C in image acquisition

After evaluating the influence of the angle α in image acquisition, the distance from the sample to the UV lamp *C* has been analyzed in terms of impact on the image quality. With α set to 45°, images of the coarse, medium and fine sensitivity test panels have been exposed in the previous section with C equal to 30 centimeters. In order to complete the analysis of the influence of the distance C, images with different settings of C have been acquired and discussed. The angle α has been adjusted to 45°in all remaining acquisitions.

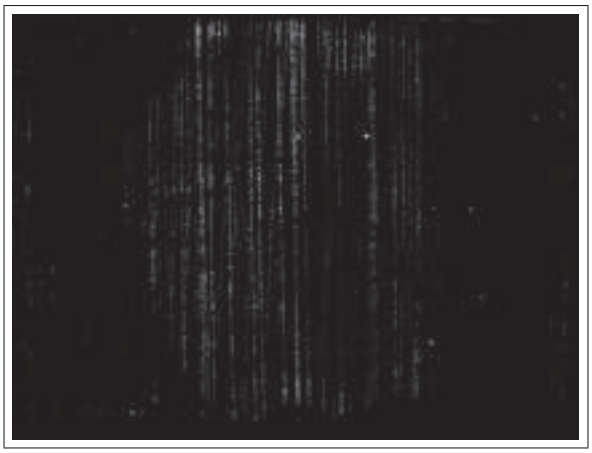

Figure 7.6 Image of the fine sensitivity test panel that has been acquired through *IDS*. The angle α and C have been set to 10°and 30 centimeters respectively.

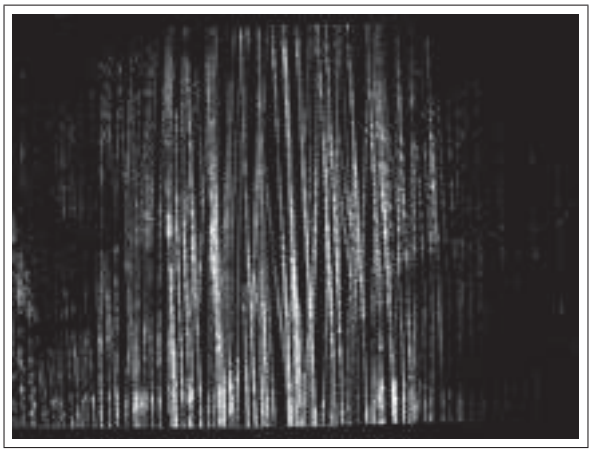

Figure 7.7 Image of the fine sensitivity test panel that has been acquired through *IDS*. The angle α and C have been set to 65°and 30 centimeters respectively.

When the ultraviolet lamp has been positioned very close to the coarse and medium sensitivity test panels (e.g. C=10 or 20 centimeters), the images have presented excessive glare on its center as illustrated in figures 7.11 7.14. With C equal to 30, 40 and 50 centimeters (as exposed in figures 7.2, 7.15, 7.12 and 7.13 respectively), the images have not obtained extreme brightness regions.

In the images of the fine test panel, indications have been observed in a larger area with C set to 40 centimeters and 50 centimeters (figures 7.16 and 7.17) in comparison with the ones captured with C equal to 30 (see figure 7.8), 20 and 10 (see figure 7.18) centimeters. This

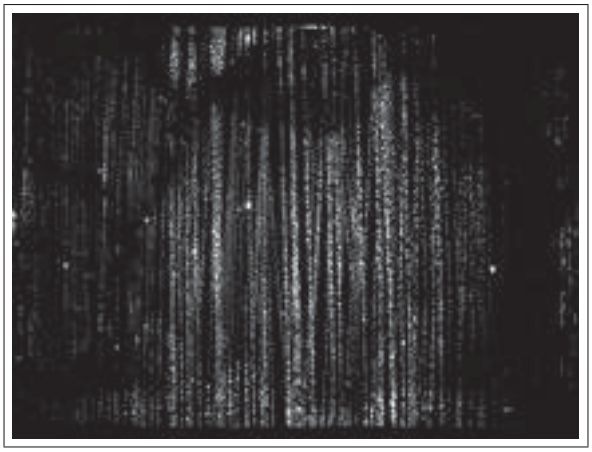

Figure 7.8 Image of the fine sensitivity test panel that has been acquired through *IDS*. The angle α and C have been set to 45°and 30 centimeters respectively.

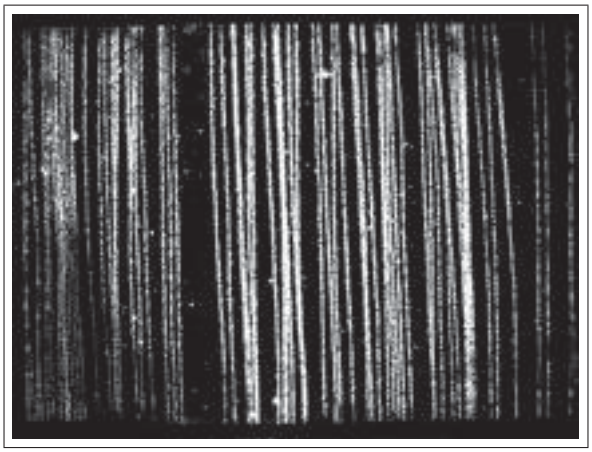

Figure 7.9 Image of the medium sensitivity test panel that has been acquired through *IDS*. The angle α and C have been set to 25°and 30 centimeters respectively.

has happened, because the ultraviolet lamp provides a divergent beam. As farther as the lamp has been positioned, more spread the light has been, illuminating a larger surface area of the panels, reducing the irradiance. The ultraviolet light power on image center has been decreased as long as the distance C has been increased. It is possible to realize it, just comparing figures 7.16, 7.17 and 7.18). When C has been adjusted to 40 centimeters, the incident UV light has been diverged moderately and has not resulted in excessive glare during the illumination of the coarse sensitivity panel. A considerable number of cracks in the medium and fine sensitivity test panel have been observed with these configurations. Therefore, regarding all acquired images that have been exposed in this section, we have considered the images with C set to 40

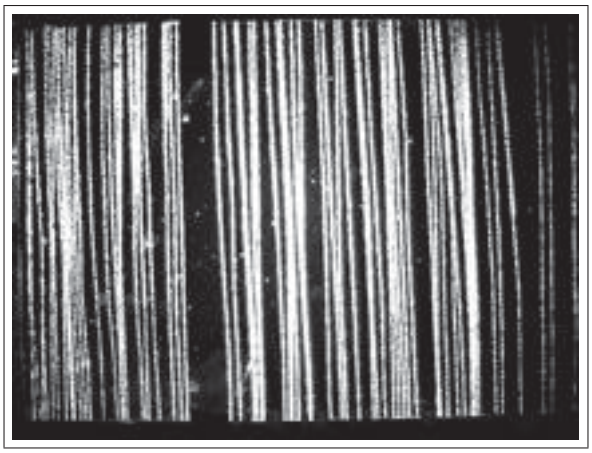

Figure 7.10 Image of the medium sensitivity test panel that has been acquired through *IDS*. The angle α and C have been set to 75°and 30 centimeters respectively.

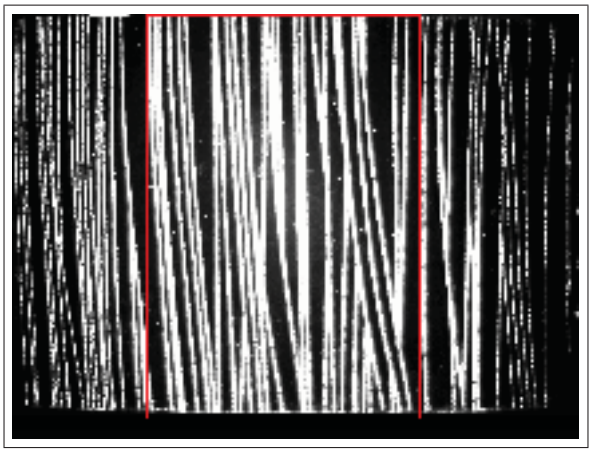

Figure 7.11 Image of the coarse sensitivity test panel that has been acquired through *IDS*. The angle α and C have been set to 45°and 10 centimeters respectively.

centimeters the most suitable for the detection. For the remaining experiments of this work, the UV lamp has been positioned 40 centimeters from the specimen in an inclination of 45°.

7.3 Probability of Detection Curves of the Detection System

After presenting and analyzing diverse images with different angles α and distances C, in the previous section, we have agreed that the best configuration of these parameters contained α =45°and C=40 centimeters. Regarding that the proposed detection algorithm employs the thresholding in a filtered image followed by boundary extraction, tracing histograms prior to select the best threshold value is highly recommended. Figures 7.19, 7.20 and 7.21 are the

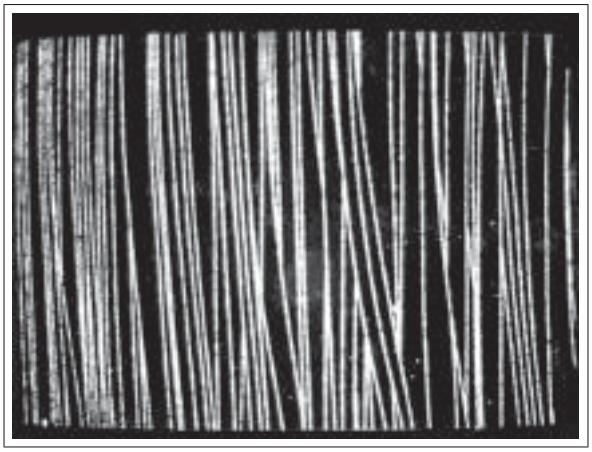

Figure 7.12 Image of the coarse sensitivity test panel that have been acquired through *IDS*. The angle α and C have been set to 45°and 40 centimeters respectively.

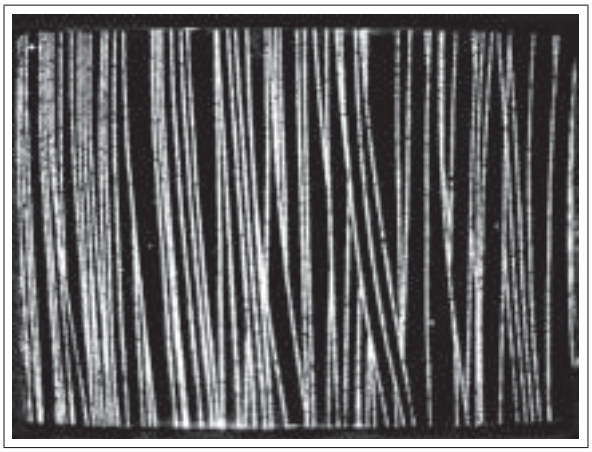

Figure 7.13 Image of the coarse sensitivity test panel that has been acquired through *IDS*. The angle α and C have been set to 45°and 50 centimeters respectively.

corresponding filtered images of the figures 7.12, 7.15 and 7.16 respectively. Figures 7.22, 7.23 and 7.24 contain the filtered image histograms. Figures 7.25, 7.26 and 7.27 contain the magnified histograms of figures 7.22, 7.23 and 7.24.

In the histogram of the figure 7.22, the distribution of pixels have presented two peaks: I) in the graylevel 0 and II) in the graylevel 255. The former represents the rate of the pixels contained in the background. The latter whose percentage is much lower (2%) depicts the amount of the indication pixels contained in the image. The histogram in figure 7.23 identically have illustrated two peaks in the same graylevels. However, regarding that the corresponding image

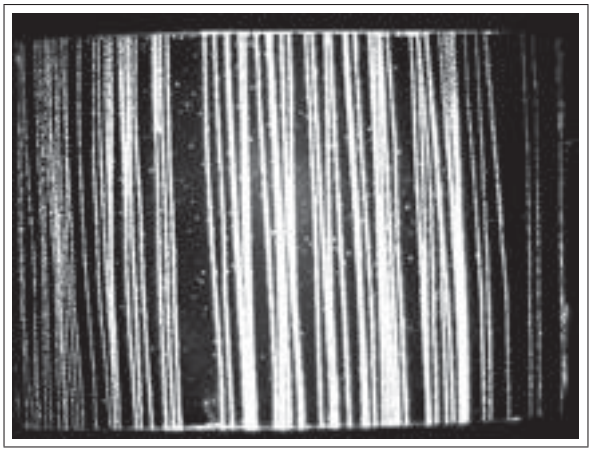

Figure 7.14 Image of the medium sensitivity test panel that has been acquired through *IDS*. The angle α and C have been set to 45°and 10 centimeters respectively.

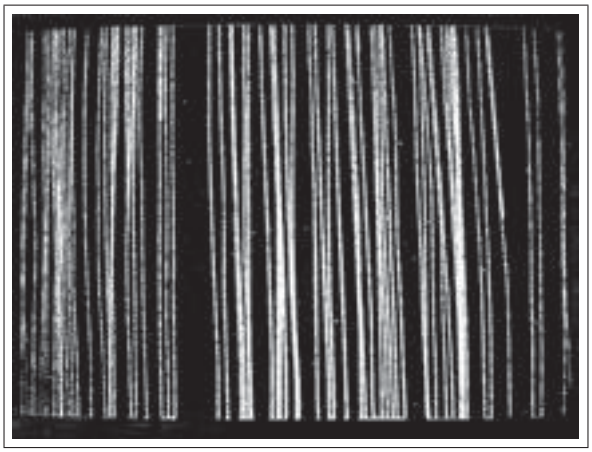

Figure 7.15 Image of the medium sensitivity test panel that has been acquired through *IDS*. The angle α and C have been set to 45°and 40 centimeters respectively.

is darker, due to smaller amount of penetrant entrapped into discontinuities, in graylevels 0 and 255, respectively higher and lower percentage of pixels have been obtained. The figure 7.24 which depicts the last exposed histogram in this work has demonstrated an unique peak of 61.84% for the background pixels. The figures 7.22 and 7.23 have indicated that the threshold for segmenting the indications must be set between graylevels 0 and 255. The histogram in figure 7.24 only have demonstrated that the indication's brightness is distributed over all possible pixel intensities, not having a clear separation between indications and background. Although not all histograms of test panels are exposed in this chapter, with α=45°and $C = 40cm$, the remaining graphics have presented almost identical behaviour.

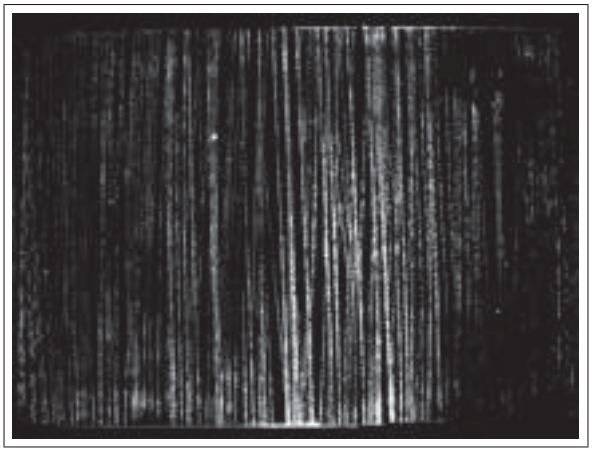

Figure 7.16 Image of the fine sensitivity test panel that has been acquired through *IDS*. The angle α and C have been set to 45°and 40 centimeters respectively.

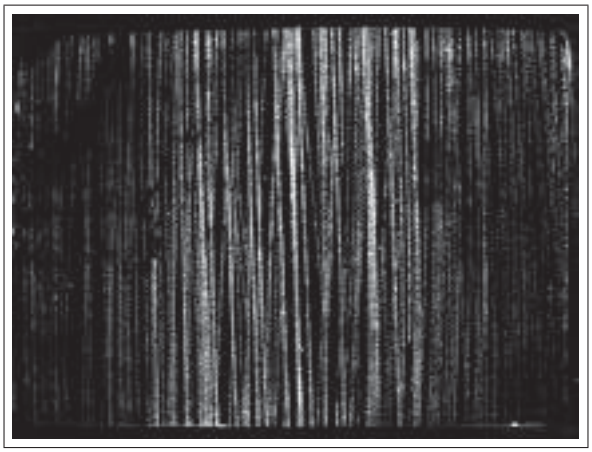

Figure 7.17 Image of the fine sensitivity test panel that has been acquired through *IDS*. The angle α and C have been set to 45°and 50 centimeters respectively.

Based on these histograms, three probability of detection curves POD(%)X Depth(microns) have been traced. The first with segmentation threshold set to 70; the second, to 150; and the third, to 200. The four images of each sensitivity test panel which have been acquired with α and C respectively adjusted to 45°and 40 centimeters have been used for the POD curve tracing. With the segmentation threshold set to 70, 150 and 200, we computed the probability of detections as shown in tables 7.1, 7.2 and 7.3. The corresponding POD curves are plotted respectively in figures 7.28, 7.29 and 7.30.

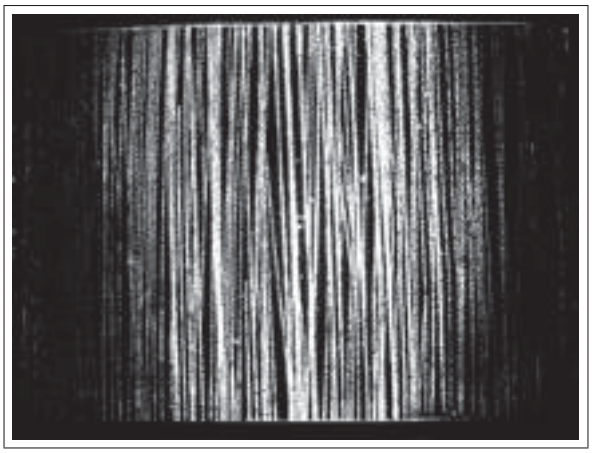

Figure 7.18 Image of the fine sensitivity test panel that has been acquired through *IDS*. The angle α and C has been set to 45°and 10 centimeters respectively.

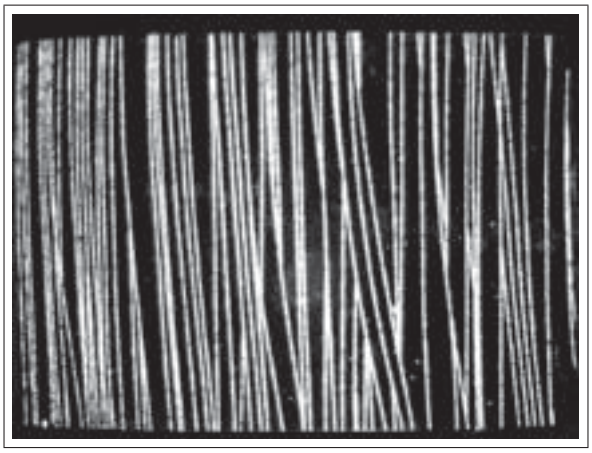

Figure 7.19 Image that illustrates the effect of the convolution of a weighted averaging mask to the image in figure 7.12

Among these POD graphics, the curve with the threshold set to 70 has obtained the highest probability of detection rates. All cracks from the coarse and medium sensitivity test panels

Table 7.1 Probabilities of detection obtained with each inspected panel with the threshold set to 70

Depth (microns)	**Probabilities of Detection**				
-	**1**	**2**	**3**	**4**	**Average**
10.8	11.8	21.2	17.7	10.6	15.3
21.6	100.0	100.0	100.0	81.8	95.5
50.2	100.0	100.0	100.0	100.0	100.0

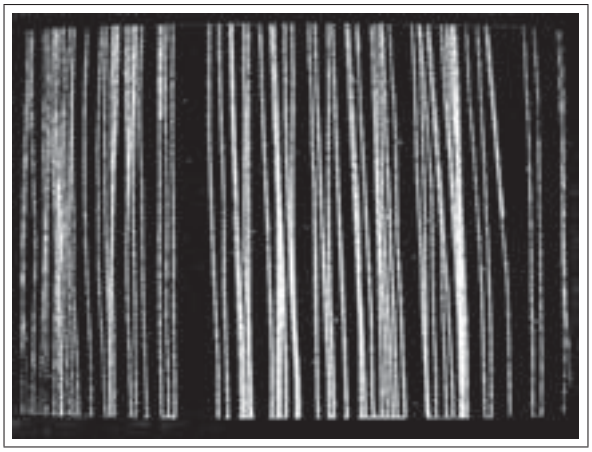

Figure 7.20 Image that illustrates the effect of the convolution of a weighted averaging mask to the image in figure 7.15

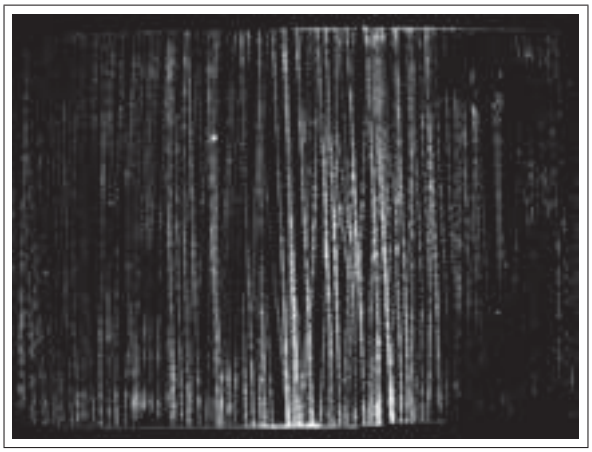

Figure 7.21 Image that illustrates the effect of the convolution of a weighted averaging mask to the image in figure 7.16

have been detected with this setting. Low average POD rate has been reached for the fine sensitivity test panel. Adjusting the threshold to 150, not all cracks in all inspections have been

Table 7.2 Probabilities of detection obtained with each inspected panel with the threshold set to 150

Depth (microns)	**Probabilities of Detection**				
-	**1**	**2**	**3**	**4**	**Average**
10.8	7.1	3.5	4.7	2.4	4.4
21.6	90.9	81.8	78.8	84.8	84.1
50.2	93.3	100.0	100.0	100.0	98.3

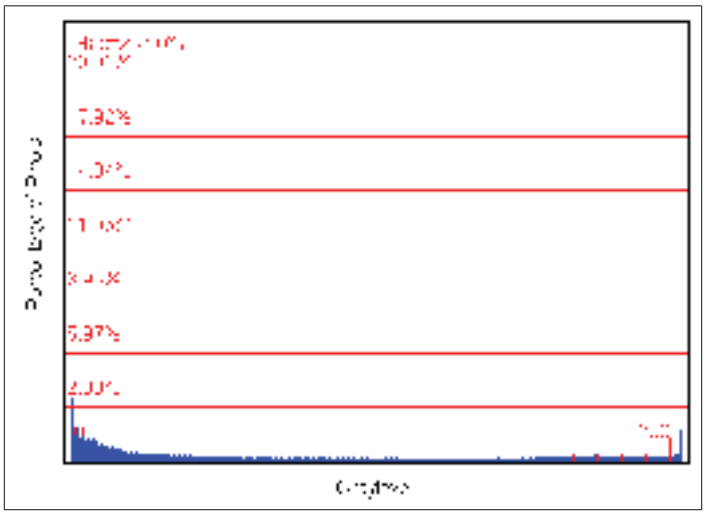

Figure 7.22 Histogram that has been traced based on the filtered image demonstrated figure 7.19

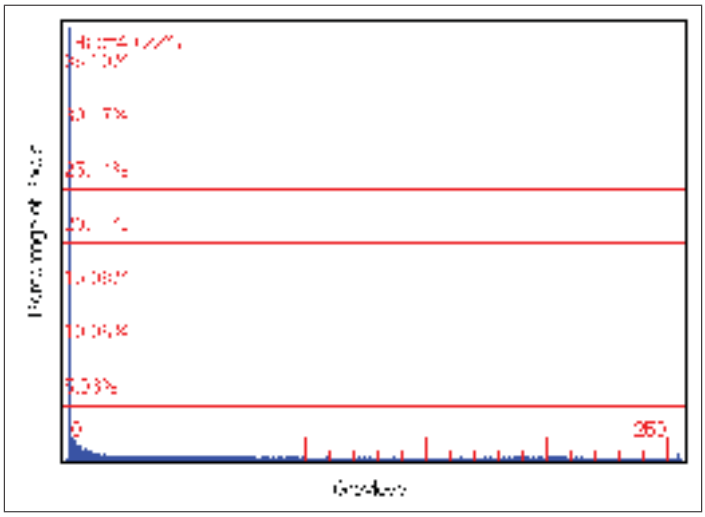

Figure 7.23 Histogram that has been traced based on the filtered image demonstrated in figure 7.20

Table 7.3 Probabilities of detection obtained with each inspected panel with the threshold set to 200

Depth (microns)	**Probabilities of Detection**				
-	**1**	**2**	**3**	**4**	**Average**
10.8	1.2	0.0	0.0	0.0	0.3
21.6	60.6	60.6	75.8	69.7	66.7
50.2	86.7	93.3	100.0	86.7	91.7

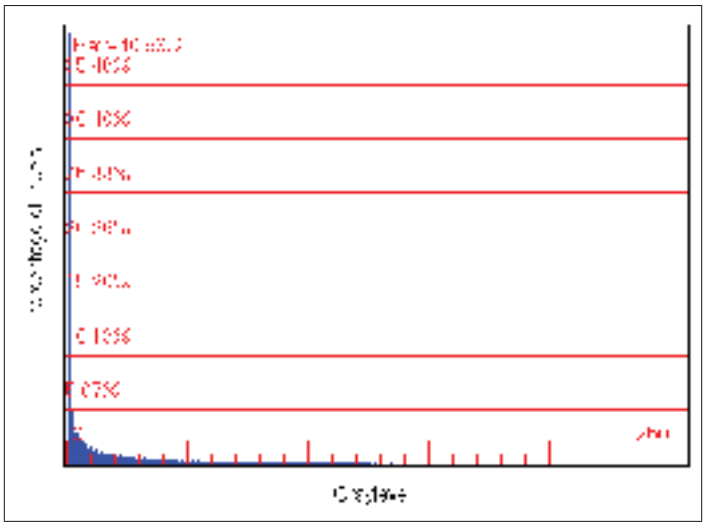

Figure 7.24 Histogram that has been traced based on the filtered image demonstrated in figure 7.21

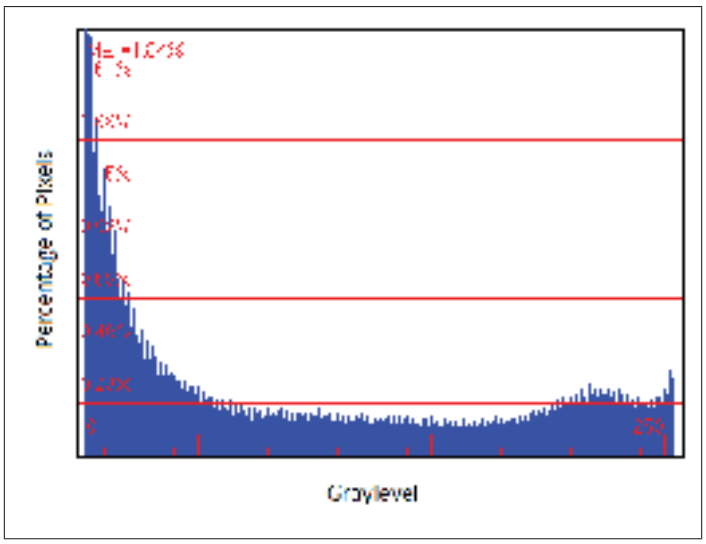

Figure 7.25 Magnified histogram that has been traced based on the filtered image in figure 7.19

discerned in the coarse and medium crack panels. Nonetheless, satisfactory values have been achieved. The inspection of the fine sensitivity test panel with this threshold has had a very poor performance. The setting of the threshold to 200 has resulted in even worse probabilities of detection.

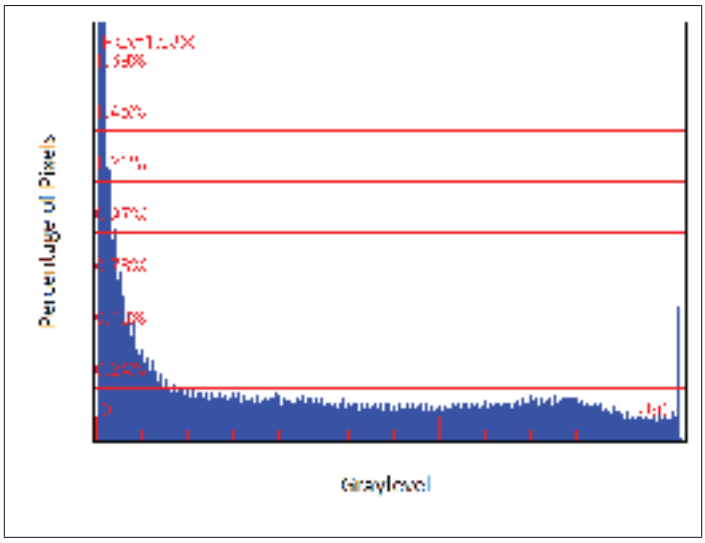

Figure 7.26 Magnified histogram that has been traced based on the filtered image in figure 7.20

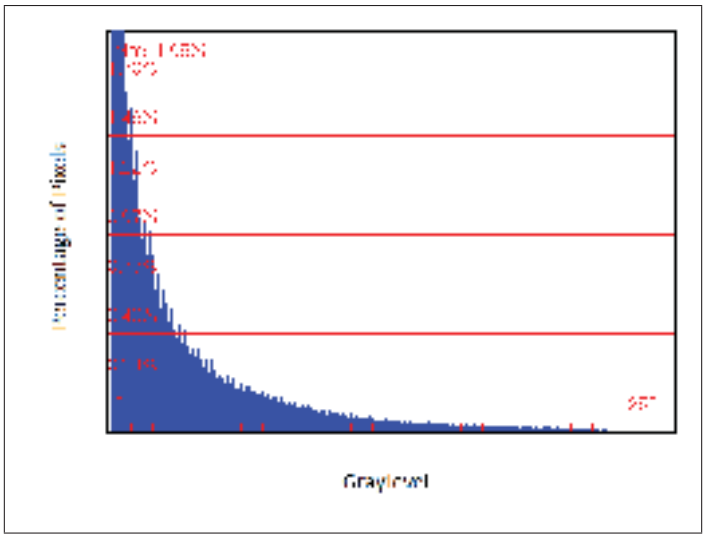

Figure 7.27 Magnified histogram that has been traced based on the filtered image in figure 7.21

7.4 Measurement of Maximum Euclidean Distance, Area and Classifying Shapes of Indications

In the previous section, three POD curves based on three different thresholds have been illustrated. Regarding that the curve with the segmentation threshold set to 70 has obtained the better results, we have adopted 70 as value for the experiments exposed in this section. As

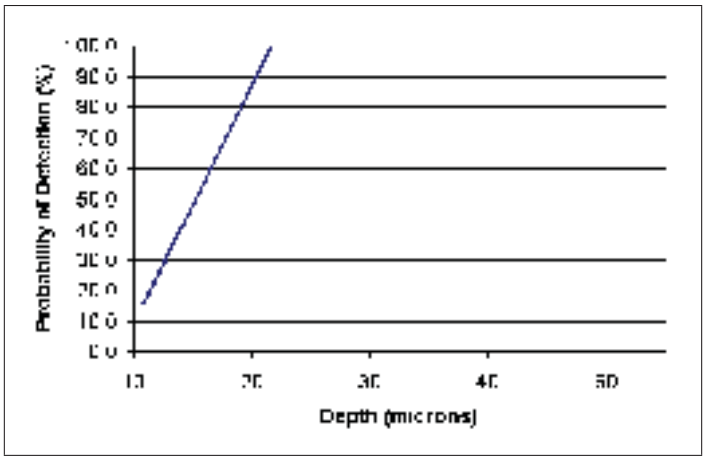

Figure 7.28 Probability of detection curve obtained with the threshold set to 70

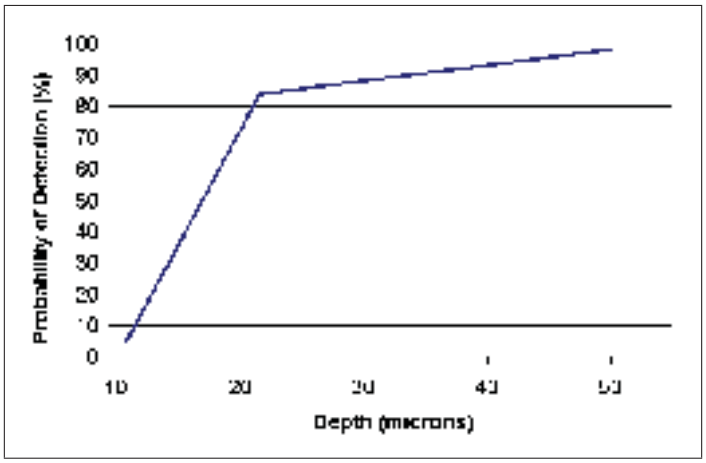

Figure 7.29 Probability of detection curve obtained with the threshold set to 150

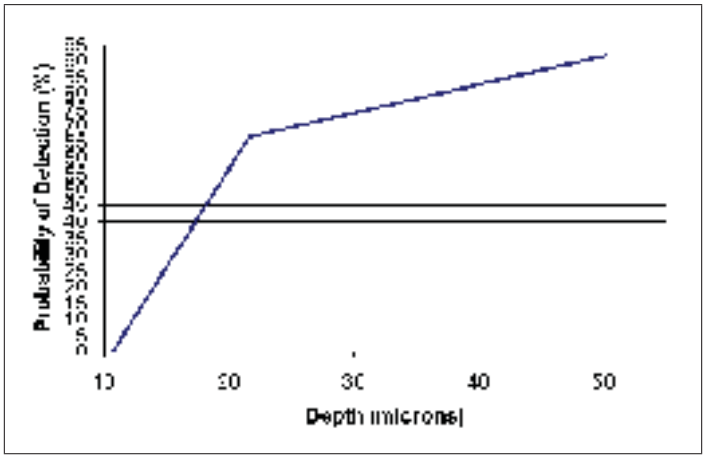

Figure 7.30 Probability of detection curve obtained with the threshold set to 200

an attempt to evaluate the ability of the system to measure the area and maximum euclidean distance of indications in millimeters and to classify their shapes, the samples which have been described in section 6.3 have been analyzed through the software exposed in subsection 6.1.1. Figure 7.31 contains the five acquired images of each discontinuity which have been obtained running the *Procedure I*. The corresponding images which have resulted from executing the *Procedure II* followed by *Procedure III* are illustrated in figure 7.32. Per acquired image, the measurements of area, maximum euclidean distance and shape classification of indications are exposed in tables 7.4, 7.5 and 7.6. Note that precision uncertainty specified in tables 7.5 and 7.6 is calculated, using the student method, with a 90% confidence interval.

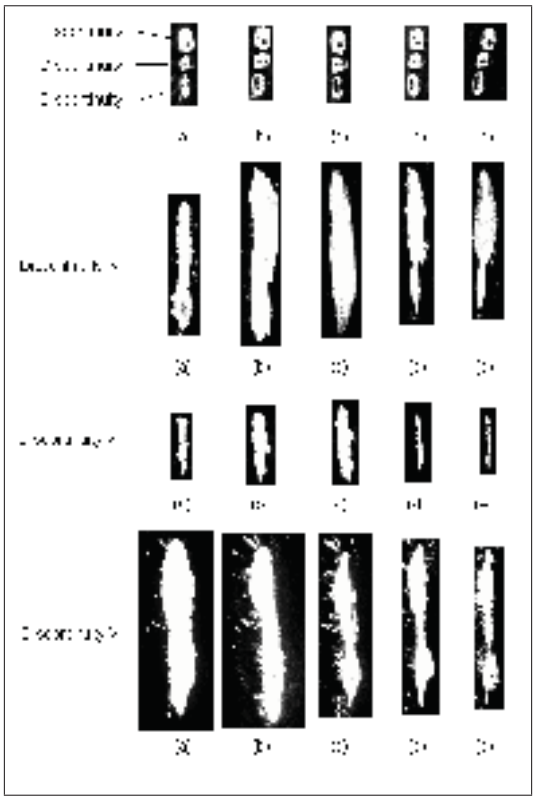

Figure 7.31 Images of the samples described in section 6.3 that have been acquired through *IDS*

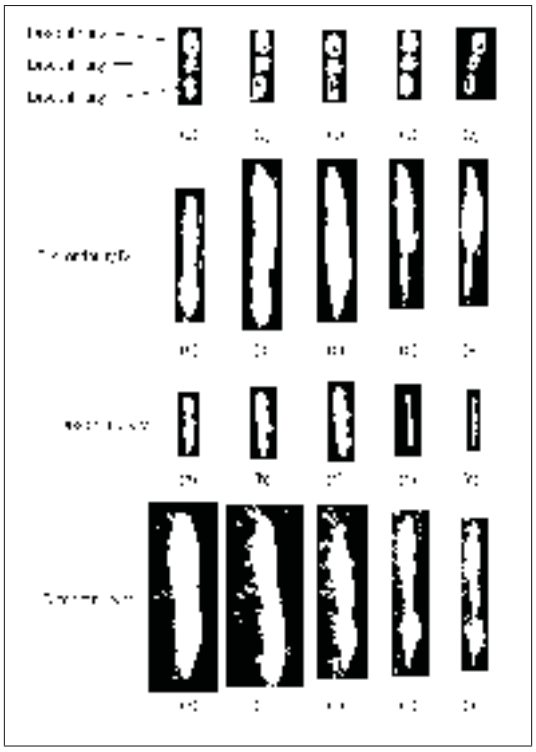

Figure 7.32 Images that have been obtained after running the Procedures II and III with the ones in figure 7.31

Table 7.4 Shape Classification Table. L and R stand for linear and rounded respectively. The classifications (a),...,(e) are related to the images (a),...,(e) in figures 7.31 and 7.32

-	**Classification**				
Discontinuity	(a)	(b)	(c)	(d)	(e)
I	R	R	R	R	R
II	R	R	R	R	R
III	L	L	L	L	L
IV	L	L	L	L	L
V	L	L	L	L	L
VI	L	L	L	L	L

7.5 Discussion

In chapter 6, experiments related to the setting of parameters α and C, the tracing of a POD curve and the measurement of area, maximum euclidean distance and shape classification of

Table 7.5 Area in mm^2 obtained with the threshold set to 70. The abbreviations Avg., Disc., S.D. and P.U. stand for respectively Average, Discontinuity, Standard Deviation and Precision Uncertainty calculated with 90% of level of confidence. The measurements (a), (b),...,(e) are related to the images (a), (b),...,(e) in figures 7.31 and 7.32

Disc.	**Measurements** (mm^2)						S.D.(mm^2)	P.U.(mm^2)	P.U.(%)
-	(a)	(b)	(c)	(d)	(e)	Avg	-	-	-
I	10.34	9.45	8.85	9.17	7.49	9.06	1.04	0.99	10.95
II	4.51	6.55	6.05	6.00	4.37	5.49	0.99	0.94	17.16
III	6.41	7.25	5.28	7.37	5.04	6.27	1.08	1.03	16.44
IV	52.93	104.13	86.45	52.91	53.79	70.04	23.88	22.77	32.51
V	13.94	22.51	25.55	7.73	5.73	15.09	8.77	8.36	55.40
VI	127.17	126.98	87.12	69.56	58.07	93.78	32.11	30.61	32.64

Table 7.6 Maximum euclidean length in *mm* obtained with the threshold set to 70. The abbreviations Avg., Disc., S.D. and P.U. stand for respectively Average, Discontinuity, Standard Deviation and Precision Uncertainty calculated with 90% of level of confidence. The measurements (a),...,(e) are related to the images (a),...,(e) in figures 7.31 and 7.32

Disc.	**Measurements** (*mm*)						S.D.(*mm*)	P.U.(*mm*)	P.U.(%)
-	(a)	(b)	(c)	(d)	(e)	Avg	-	-	-
I	4.41	4.13	4.23	4.04	3.83	4.13	0.21	0.20	4.95
II	2.66	3.41	2.99	2.91	2.88	2.97	0.27	0.26	8.78
III	4.44	4.23	4.02	4.21	4.05	4.19	0.17	0.16	3.77
IV	22.03	28.66	26.68	24.05	22.78	24.84	2.77	2.64	10.63
V	9.78	11.19	12.47	9.16	8.53	10.23	1.6	1.52	14.88
VI	29.2	32.04	25.9	26.8	25.25	27.84	2.79	2.66	9.54

indications have been proposed. In the previous sections, the results of those experiments have been demonstrated. In this section, the obtained results have been discussed.

Concerning the selection of the angle α and the distance C, the image quality in terms of how defined the indications have been displayed per parameter setting has been the most important factor taken into account. For adjusting them, a subjective evaluation has been conducted. The system with α and C set respectively to 45°and 40 centimeters has obtained the best quality images. This configuration has been adopted for performing the subsequent experiments.

According to Tracy and Moore (2001) for the evaluation of the capability and reliability of the system, the probability of detection curves are the best tool. Regarding that the segmentation procedure employs thresholding, the impact of its adjustment has been verified. Using the segmentation threshold set to 70, the capability of the system has achieved 21.6 microns with 100% of reliability. Adjusting it to 150, the capability has only reached 50.2 microns with 98.3% of reliability. Setting it to 200, the same capability has been obtained with a worse reliability. Based on these results, assigning it to 70 has resulted in the best performance. The values which have been employed for tracing the probability of detection curves have been selected based on the histograms in figures 7.22 and 7.23. These graphics exhibit peaks too widely spread. If they would have presented the intensity peaks of the background and indications distinguished by a smaller range of pixels (e. g. the peak of the background pixels around 40 graylevel and the peak of the indication pixels around 120 graylevel), it would have been feasible to choose the segmentation threshold more precisely. Nonetheless, the obtained separation has indicated that there is a good contrast between the background and indications in images which have been acquired from the coarse and medium sensitivity test panel. Regarding that the histogram in figure 7.24 has only illustrated one peak, the same assumption is not valid for the filtered images of the fine sensitivity test panel.

Furthermore, the performance in measurement of area, maximum euclidean distance and shape classification of indications has been verified in this chapter. Observing the table 7.6, with the exception of *Discontinuity V*, values either equal or below 10% of the precision uncertainties of the maximum euclidean distance have been obtained. It demonstrates that low variability has been obtained in most of these measurements. A precision uncertainty of 14.88%, which has been calculated for the *Discontinuity V*, is not the ideal value, but it is still a good result. On the other hand, analyzing table 7.5, half of the samples (*Discontinuity IV, Discontinuity V and Discontinuity VI*) have obtained precision uncertainties above 30% for the inspections of area. Only the measurements of the *Discontinuity I* have resulted in 10%. Regarding the classification of the indication's shape that has been exposed in table 7.4, very good results have been achieved. All linear indications have been correctly classified. Among the rounded

ones, only the *Discontinuity III* has been identified as linear by *IDS*. Nonetheless, observing the figures 7.31 and 7.32, the maximum euclidean distance of the indication is 3 times greater than the width in all images. Therefore, even though it is rounded, due to the presented length and width, the indication has been correctly regarded as linear.

All variability in measurements, especially high (e.g. in cases that the precision uncertainties are above 30%), is due to pre/post-cleaning, penetrant/developer/emulsifier applications which have been conducted manually. In other words, the amount of penetrant that has been entrapped into discontinuities, the concentration of developer that has been applied differs among chemical applications. This is the main explanation for the variation in area and maximum euclidean distance in the experiments.

CONCLUSION

This dissertation has been focused on the development of image acquisition and processing approaches for automating the inspection in FPI. Towards the building of the system, our efforts have been mostly concentrated on: i)optimizing the illumination angle α and distance from the ultraviolet lamp to the specimen C in an attempt to acquire the most suitable image; ii) developing a feature extraction algorithm which calculates the maximum euclidean distance, area and classifies the shape of indications; iii) conducting experiments for evaluating the overall system performance.

After conducting experiments for optimizing α in image acquisition, varying it from 10°to 75°, it is possible to conclude that as long as this angle has been increased, more brightness has been added. This has happened, because, setting it to 65°and 75°, more ultraviolet light power has been provided to the specimen than adjusting it to 45°, 25°and 10°. The most suitable images, in our evaluation, have been obtained with 45°. This adjustment has avoided the excessive glare in coarse sensitivity test panel and the lack of ultraviolet light power in fine sensitivity test panel. Unfortunately, inclinations greater than 75°could not have been evaluated, due to shade caused by the interception of the ultraviolet rays by the camera. Adjusting α smaller than 10°has resulted in very poor incident ultraviolet light power, not being regarded for the parameter optimization.

The impact of the adjustment of the distance C in acquisition has been evaluated as well for the illumination parameter optimization. It is possible to infer that positioning the ultraviolet lamp very close to the coarse and medium sensitivity test panels (e.g. C=10 or 20 centimeters) has resulted in images with excessive glare on its center and lack of light power on the other sides. Setting this distance to 30, 40 and 50 centimeters, the brightness has been more homogeneously distributed, illuminating a larger surface area of the panels. These diverse light power distributions are consequences of the divergent beam provided by the UV lamp. As farther as it has been placed, more spread and uniform the illumination has been, reducing the UV irradiance. Adjusting the light source to 40 centimeters, the incident UV radiation has been

moderately spread, the images of the coarse sensitivity test panel have not presented extreme brightness, the cracks have been properly observed in inspections of the medium sensitivity test panel and suitable UV light intensity has been supplied for the observation of indications in fine sensitivity test panel. Therefore, in our evaluation, the most adequate configuration has been obtained with α and C set respectively to 45°and 40 centimeters.

Selecting the most suitable illumination parameters is extremely important in detection, measurement and classification of indications. However, the instrument which performs these tasks is a software that has been developed for this project. It acquires images, filters them, segments relevant objects and extracts features for data analysis. Regarding that the adopted segmentation procedure employs thresholding in filtered images, intensity distributions must be verified for choosing the best segmentation threshold value. The histograms provide this information. They have been traced for this purpose based on filtered images of the sensitivity test panels. Two intensity peaks have been illustrated in the graphics of the coarse and medium sensitivity test panels in this work: One around graylevel 0; and a second around intensity 255. This separation has demonstrated that there has had a good contrast between the background and indications in the filtered images of these panels. On the other hand, the represented intensity peaks have been too widely separated, being difficult to define a small range of intensities for segmenting the indication pixels. Therefore, the histograms have provided only an overview of the distribution of pixels, demonstrating that the segmentation threshold must be adjusted within 0 and 255 graylevel. Due to this reason, values such as 70, 150 and 200 (graylevels between 0 and 255) have been chosen for the plotting curves POD (%) X Depth (microns). The threshold whose POD curve has obtained the best capability and reliability has been adopted for the remaining experiments of this project. Furthermore, considering that the histogram in figure 7.24 has only depicted one peak, the same observations are not valid for the filtered images of the fine sensitivity test panels.

The probability of detection curves POD(%)X Depth(microns) have been traced for the evaluation of the capability and reliability of the system. The former represents the smallest discontinuity that can be detected and the latter is the corresponding probability of detection. By

adjusting the segmentation threshold to 70 the best results have been obtained. More representative curves would have been plotted, in case a greater number of sensitivity test panels have been inspected for this experiment.

The automated detection that has been developed for this project presents several advantages when compared to manual process. For instance, an inspector using a calliper can easily measure the maximum euclidean distance and classify the shape in inspection. However, for the correct verification, the calliper must be handled and positioned by him/her in parallel with the indication being evaluated. Otherwise, a wrong measurement is being performed. In addition, the area, depending on the geometry, is not easily measured with this instrument. On the other hand, using the system IDS, the measurement is not compromised by these inconvenients. It performs non-contact evaluations and the area, maximum euclidean distance and shape are easily obtained. The speed of the process is increased allowing better performance. The system is capable to, only in the inspection stage, eliminate inconvenients inherent to human inspectors such as lack of vision acuity, attitude and motivation.

In spite of all mentioned advantages, the automation of FPI presents disadvantages as well. Automated systems may become obsolete, if manufacturing/maintenance specifications are modified. In other words, this system has been developed for detecting indications with a minimum depth in workpieces with certain roughness. In case these requirements are altered, the current configuration ($\alpha = 45^{\circ}$, $C = 40cm$ and segmentation threshold=70), depending on the level of the change, may not be suitable anymore for the inspection.

The developed system has demonstrated the ability to detect open to surface indications with a capability of 21.6 microns of depth with 100% of reliability. It has classified correctly their shapes either as linear (if the maximum euclidean distance is three times greater the width) or as rounded (otherwise). Excellent performance has been achieved, in the measurements of maximum euclidean distance in millimeters. High variability has been obtained in the inspection of area. The lack of control in penetrant/developer application, pre/post cleaning has been the main cause for the variation in the experiments, not being related to the inspection stage itself.

Automating the whole specimen preparation process may drastically increase the repeatability. Therefore, the system *IDS* is capable to approve/reject workpieces based on features such as maximum euclidean distance, area and shape of indications.

Future Works

The results obtained in the dissertation were encouraging for the full automation of the fluorescent penetrant inspection. Nonetheless, several aspects which are capable to contribute for the development of a complete mechanized FPI system were not emphasized. Therefore, guidelines for future investigation include:

- Developing automated systems for precleaning, postcleaning, drying, excess removal, applying liquid penetrant and developer in order to improve the overall sensitivity, reliability and repeatability of FPI;
- Evaluating other image acquisition approaches such as (i) using a single photodetector and (ii) utilizing an array of photodetectors disposed in a line ;
- Changing the current illumination concept. Ultraviolet lasers comprise coherent radiation which may provide a more homogeneous UV light distribution;
- Measuring the capability of the system with a curve probability of detection (%) X discontinuity length. In this project, only the capability related to the discontinuity depth was evaluated. A better evaluation of the system performance would have been conducted, in case of assessment of the discontinuity length impact in detection.

BIBLIOGRAPHY

Adair, T., D. Wehener, M. Kindrew, H. Winter, and B. MacCracken, 1998. Automated fluorescent penetrant inspection (fpi) system is triple a. *SAE Conference Proceedings*, number 329, pages 141–172.

Alburger, J., 1966. Fluorescent brightness measurement. *Materials Evaluation*, 24(11):624–630.

American Society for Materials, 2002a. *ASM Handbook*, volume 16, Machining. American Society for Materials.

American Society for Materials, 2002b. *ASM Handbook*, volume 17, Nondestructive Evaluation and Quality Control. American Society for Materials.

American Society for Materials, 2002c. *ASM Handbook*, volume 6, Welding, Brazing and Soldering. American Society for Materials.

American Society for Materials, 2010a. *ASM Handbook*, volume 14A, Metalworking: Bulk Forming. American Society for Materials.

American Society for Materials, 2010b. *ASM Handbook*, volume 15, Casting. American Society for Materials.

American Society for Nondestructive Testing, 1981. *ASNT Continuing Education in Nondestructive Testing (Materials and Processes for NDT Technology)*. American Society for Nondestructive Testing.

Armstrong, C., 1986. High defect-resolution capability from a computer-controlled fluorescent penetrant processing and viewing system. *Materials Evaluation*, 44(12):1426–1429.

Betz, C., 1963. *Principles of Penetrants*. Magnaflux Corporation.

Brasche, L., R. Lopez, D. Eisenmann, and K. Griffiths, February 2009. Engineering studies for fluorescent penetrant inspection with focus on developer application methods. *Insight*, 51(2):88–91.

Bray, D. and R. Stanley, 1997. *Nondestructive evaluation: a tool in design manufacturing and service*. CRC Press.

Burkel, R., 1990. Automated fluorescent penetrant inspection of aircraft engine structures. *Materials Evaluation*, 48(8):978–982.

Callister Jr, W., 2007. *Materials Science and Engineering: An Introduction*. John Wiley & Sons, Inc.

Campbell, W. and R. McMaster, 1967. Derivation of penetrant-developer resolution. *Materials Evaluation*, 25(5):126–128.

Canadian Institute for NDE, 2010. *Liquid Penetrant: Levels 1 and 2*. Canadian Institute for NDE.

Glaskov, Y., 1989. The question of evaluation of the wettability of liquids for penetrant inspection. *Defektoskopiya -The Soviet Journal of Nondestructive Testing*, (11):801–806.

Glaskov, Y. and E. Bruevich, 1985. Determination of the whiteness of developers for the penetrant flaw inspection. *Defektoskopiya -The Soviet Journal of Nondestructive Testing*, 21(4):76–81.

Gonzalez, R. and R. Woods, 2008. *Digital Image Processing*. Prentice-Hall, Inc.

Graham, B., May 1967. Mechanisms contributing to fluorescence and visibility of penetrants. *Proceedings of the Fifth International Conference of Nondestructive Testing*, pages 225–233.

Grills, R., 2001. Probability of Detection - An NDT Solution. *Materials Evaluation*.

Larson, B., January 2002. Study of Factors Affecting the Sensitivity of Liquid Penetrant Inspections: Review of Literature Published from 1970 to 1998, FAA Technical Report Number DOT/FAA/AR-01/95, Office of Aviation Research.

McMaster *et al.*, R., 1982. *Nondestructive Testing Handbook*, volume 2, Liquid Penetrant Testing. American Society for Nondestructive Testing.

Migoun, N., P. Prokhorenko, A. Gnusin, M. Stadhaus, and H. Thomas, 2002. On the reliability of quantitative evaluation of penetrant systems quality. *Review of Quantitative Nondestructive Evaluation*, 21:1991–1996.

NDT Resource Center, 2010. Ndt on-line. Available at http://www.ndt-ed.org.

Robinson, S. and J. Schmidt, 1984. Fluorescent penetrant sensitivity and removability - what the eye can see, a fluorometer can measure. *Materials Evaluation*, 42(8):1029–1034.

Rummel, W., January 1998. Probability of detection as a quantitative measure of nondestructive testing end-to-end process capabilities. *Materials Evaluation*.

Sekerin, A. and A. Kornev, 1997. Effect of flaw-detection operations on the efficiency of product inspection with use of liquid penetrants. *Russian Journal of Nondestructive Testing*, 33(4):239–244.

Sherwin, A., March 1974. Establishing liquid penetrant dwell modes. *Materials Evaluation*, 32(3):63–67.

Shull, P. J., 2002. *Nondestructive Evaluation - Theory. Techniques and Applications*. CRC Press.

Tracy, N. and P. Moore, 2001. *Liquid Penetrant Testing (Nondestructive Testing Handbook)*, volume 2. American Society for Nondestructive Testing.

Vaerman, J., November 1985. Fluorescent penetrant inspection process, automatic method fo sensitivity quantification. *Proceedings of 11th World Conference on Nondestructive testing*, volume III, pages 1920–1927.

Vasquez, I., December 1997. Fluorescent penetrant inspection system performance test using known defect standards. *Materials Evaluation*, pages 1319–1322.

Vasquez, I., February 2002. The use of known discontinuity standards. *Materials Evaluation*, pages 142–145.